Experimental Tests of the Standard Model in $e^+e^- \rightarrow f\bar{f}$ at the Z Resonance

Joachim Mnich[‡]

III. Physikalisches Institut, RWTH Aachen
D-52056 Aachen, Germany

and

CERN-PPE
CH-1211 Geneva 23, Switzerland

Abstract

During the first six years of operation in the vicinity of the Z pole the four LEP experiments ALEPH, DELPHI, L3 and OPAL have collected approximately 14 million decays of the Z into hadrons and charged leptons. These data allow the precise determination of many parameters and stringent tests of the Standard Model of electroweak interactions. Among the outstanding results are the precise determination of the Z mass, $m_Z = 91\,188.4 \pm 2.2$ MeV, the measurement of its total and partial decay widths to per mille accuracy and the definite conclusion that there are three different types of light neutrinos in the universe. From the measured asymmetries at LEP and SLC the effective weak mixing angle is derived to be $\sin^2\bar{\vartheta}_W = 0.2314 \pm 0.0003$. The data support the concept of lepton universality and the axial-vector and vector coupling constants of charged leptons are determined to $\bar{g}_A^\ell = -0.5011 \pm 0.0004$ and $\bar{g}_V^\ell = -0.0380 \pm 0.0007$. Electroweak observables studied at the Z resonance are found to be in agreement with the Standard Model and from a common fit the mass of the top quark can be derived to be $m_t = 181\,^{+8}_{-9}\,^{+17}_{-20}(m_H)$ GeV. This Standard Model prediction is now confirmed by the recent direct observation and mass measurement of the top quark in $p\bar{p}$ experiments.

[‡]Supported by the German Bundesministerium für Bildung, Wissenschaft, Forschung und Technologie

Contents

1 Introduction

A great success of theoretical and experimental physics of the last decades is the unification of electromagnetic and weak interactions. This can be compared to the development of Maxwell's equations in the last century which provide a common theoretical description of electric and magnetic phenomena. As Maxwell's theory predicted electromagnetic waves which were subsequently experimentally confirmed the unified description of electromagnetic and weak interactions postulated the existence of heavy gauge bosons, $W^{\pm}$ and Z.

The Standard Model of electroweak interactions has been developed by S.L. Glashow, A. Salam and S. Weinberg [1], hence sometimes called GSW model. It describes neutral and charged current weak interactions by the exchange of Z and $W^{\pm}$ bosons. Weak interactions of quarks are complicated by the fact that the gauge bosons couple to mixtures of the quark mass eigenstates [2]. Only charged current interactions can mediate transitions between different fermion flavors. The suppression of flavor changing neutral current interactions is achieved by the introduction of the GIM mechanism [3]. This remarkable ingredient of the Standard Model led to the postulation of the charm quark which has been discovered subsequently [4].

Important discoveries such as the observation of the neutral currents in neutrino-electron scattering [5] and the discovery of the $W^{\pm}$ and Z in proton-antiproton collisions [6] supported the Standard Model experimentally. During the last about 15 years significant contributions to the understanding of the neutral current sector of the Standard Model are provided by e^+e^- annihilation experiments. The interference of the photon and Z boson exchange, first observed in the scattering of polarized electrons from deuterium [7], has been confirmed by the measurements of forward-backward asymmetries in $e^+e^- \rightarrow f\bar{f}$ at PETRA and PEP [8, 9].

With the advent of the SLC [10] and LEP [11] e^+e^- accelerators experimental results on the neutral current sector of the Standard Model are dominated by the experiments performed at these facilities. Z bosons are copiously produced in a very clean experimental environment enabling the determination of electroweak observables with unprecedented precision. From the measurements of the total cross sections $e^+e^- \rightarrow f\bar{f}$ one of the fundamental input parameter of the Standard Model, the mass of the Z, is obtained very precisely. The total and partial decay widths of the Z deduced from these measurements allow the unambiguous determination of the number of light neutrino families in the universe. Adding the observed lepton forward-backward asymmetries and the tau polarization measurements allows the experiments to determine coupling constants of the Z to charged leptons. Comparing these couplings among the three fermion generations tests one of the cornerstones of the Standard Model: the concept of lepton universality.

All measurements must be compared to theoretical predictions including radiative corrections. The experiments are sensitive to higher order effects and therefore test the theory at the level of its quantum structure. A striking example for the quality of the comparison of measurements with the theory is that one can deduce a quite precise value for the mass of the top quark which in the past has been too heavy to be produced and detected in collision experiments. Now the top quark has finally been observed in $p\bar{p}$ collision experiments [12, 13] and it has indeed the mass predicted from the measurements at LEP and SLC. This is a major triumph for the predictive power of the Standard Model. It opens a window for further investigations concerning the existence and the mass of the Higgs boson [14] which in the Standard Model explains the masses of the gauge bosons and the fermions.

The Standard Model of electroweak interactions as well as Quantum Chromodynamics (QCD) [15], the theory of strong interactions among quarks and gluons, describe very successfully the observed phenomena among elementary particles at energies up to $\mathcal{O}(100\ \mathrm{GeV})$. However, the Standard Model does not address many unanswered questions like the large number of free parameters and the missing connection of electroweak and strong interactions, and eventually gravitation. It is therefore generally believed that the Standard Model is not the ultimate theory. This motivates the development of theories which contain the Standard Model as low energy manifestation of an underlying symmetry solving the apparent arbitrariness of the Standard Model. Many of these extensions such as SU(5) [16], Supersymmetry [17] and Technicolour [18] are under discussion. The precision measurements of many observables, as well as the direct search for predicted particles, performed by the LEP experiments limit the variety of these models and give clues for the progress of elementary particle theory.

In this article the experimental results on neutral current electroweak parameters based on the data accumulated from 1989 to 1994 by the four LEP experiments are summarized. In total the experiments have observed about 14 million Z decays. Many of these recently obtained numbers are only preliminary, in particular the analysis of the 1993 and 1994 LEP runs is not yet finalized. The basis of the preliminary experimental results presented here is the summary performed by members of the LEP experiments for the 1995 summer conferences [19].

The measurements performed at LEP are compared and combined with experimental results on electroweak parameters obtained in other $\mathrm{e^+e^-}$ or $\mathrm{p\bar{p}}$ experiments like the measurement of polarization asymmetries, the measurement of the $\mathrm{W^\pm}$ mass or the search for the top quark. The implications of the currently available experimental information on postulated extensions of the theory are discussed as well as the prospects for improved accuracy expected for the future.

This article is organized as follows: After a brief introduction to the Standard Model of electroweak interactions emphasizing the features relevant for the neutral current reaction $\mathrm{e^+e^-} \rightarrow \mathrm{f\bar{f}}$ (section 2) radiative corrections are discussed in section 3. This is followed by a description of the LEP accelerator and the four detectors (section 4) installed at the ring concentrating on items important for the measurement of Z parameters. Results obtained from the measurements of total cross sections, the Z mass, the total and partial decay widths, are presented in section 5 and some conclusion which can be derived from these measurements are discussed (section 6). The experimental results obtained at LEP and SLD on various asymmetries (forward-backward asymmetry of leptons and heavy quarks, tau polarization and left-right asymmetry) are presented (section 7) and they are used (section 8) to derive the effective weak mixing angle and the coupling constants of leptons and quarks. In section 9 the electroweak observables are interpreted in the Standard Model framework to estimate the mass of the top quark and to derive a statement on the Higgs boson mass. Also, some consequences for models extending the Standard Model are discussed. An outlook for Standard Model tests possible in the future is given in section 10 before concluding in section 11.

2 The Standard Model of Electroweak Interactions

In this section the main features of the Standard Model are recalled. The discussion focuses on the properties most relevant for Z physics at LEP.

2.1 The Fermions

The current understanding of elementary particle physics is that fermions are the fundamental building blocks of matter. The fundamental fermions are subdivided into leptons and quarks. Quarks contrary to leptons do participate in strong interactions described by the theory of Quantum Chromodynamics (QCD). All fundamental fermions are pointlike objects which is experimentally verified down to distances of $\mathcal{O}(10^{-16}$ cm). There are three known generations of fermions with identical properties. Fermions of different generations are only distinguishable by their masses and not by their electroweak or strong interactions. Measuring and comparing the couplings of fermions thus is an important test of the theory.

Leptons			Quarks		
	Mass [MeV]	Charge [e]		Mass [MeV]	Charge [e]
ν_e	$< 5.1 \cdot 10^{-6}$	0	up u	$2-8$	$+2/3$
Electron e	0.511	-1	down d	$5-15$	$-1/3$
ν_μ	< 0.27	0	charm c	$1\,000-1\,600$	$+2/3$
Muon μ	105.7	-1	strange s	$100-300$	$-1/3$
ν_τ	< 31	0	top t	180 000	$+2/3$
Tau τ	1 777	-1	bottom b	$4\,100-4\,500$	$-1/3$

Table 1: Mass and electric charge of the fundamental fermions.

Table 1 summarizes the particles of the three generations with their measured masses and their electric charges in units of the absolute electron charge [20, 13]. For each fermion there is an antiparticle with the same mass but opposite electric charge. According to QCD each quark species exists in three different colours, the analogue of the electric charge in strong interactions. The masses of the light quarks cannot be determined unambiguously because of the non-perturbative behaviour of QCD at low energies.

The existence of the tau neutrino ν_τ can be inferred from studies of the tau decay [21]. The precision measurements at LEP and SLC require three different neutrino species (see sections 6.1 and 6.2). Though, the experimental proof that ν_τ is the weak isospin partner of the tau, for instance in the inverse tau decay $\nu_\tau e^- \to \tau^- \nu_e$, has not yet been accomplished.

Since the discovery of the b-quark experiments at e^+e^- and $p\bar{p}$ colliders are searching for the top quark. Until recently the conclusion was that its mass must be larger than 131 GeV [22]. The existence of the top quark is experimentally supported by the non-observation of flavor changing neutral currents in b-quark decays. And the determination of the electroweak couplings of the b-quark (see section 8.3) suggests indeed the existence of a weak isospin partner of the b-quark.

Now top quark production in $p\bar{p}$ collisions has been observed by the CDF and D0 collaborations [13] at the Tevatron. From these experiments a top quark mass of $m_{\mathrm{t}} = 180 \pm 12$ GeV is obtained which is in very good agreement with the expectation derived from LEP and SLC measurements of electroweak radiative corrections (see section 9.1).

The Standard Model does not predict the number of generations of fundamental fermions. The most convincing experimental determination of the number of neutrino generations has been performed by the LEP and SLC experiments. The measurement of the width of the Z decaying into invisible particles (see section 6.1) excludes the existence of a fourth neutrino species up to a mass $m_\nu \leq 45$ GeV. Independently, the number of light neutrino species is deduced from the relative abundance of ${}^4_2$He nuclei in the universe by cosmological arguments [23]. As the neutrinos are the lightest members of the known families this provides evidence that there are no more fermion generations than those of table 1.

The Standard Model of electroweak interactions is based on the invariance of the Lagrangian under local gauge transformations. Electroweak interactions among the fundamental fermions are described by gauge invariant transformations of the weak isospin $\mathrm{SU(2)_L}$ and the weak hypercharge U(1). The fundamental fermions carry the quantum numbers of the weak isospin T, with its third component T_3, and the weak hypercharge Y. The electric charge Q is related to the electroweak quantum numbers:

$$Q = T_3 + Y/2 \tag{1}$$

			Q	T	T_3	Y
$\begin{pmatrix} \nu_{\mathrm{e}} \\ \mathrm{e} \end{pmatrix}_L$	$\begin{pmatrix} \nu_\mu \\ \mu \end{pmatrix}_L$	$\begin{pmatrix} \nu_\tau \\ \tau \end{pmatrix}_L$	0 -1	$1/2$ $1/2$	$1/2$ $-1/2$	-1 -1
$\begin{pmatrix} \mathrm{u} \\ \mathrm{d}' \end{pmatrix}_L$	$\begin{pmatrix} \mathrm{c} \\ \mathrm{s}' \end{pmatrix}_L$	$\begin{pmatrix} \mathrm{t} \\ \mathrm{b}' \end{pmatrix}_L$	$2/3$ $-1/3$	$1/2$ $1/2$	$1/2$ $-1/2$	$1/3$ $1/3$
$\mathrm{e_R}$	μ_{R}	τ_{R}	-1	0	0	-2
$\mathrm{u_R}$	$\mathrm{c_R}$	$\mathrm{t_R}$	$2/3$	0	0	$4/3$
$\mathrm{d'_R}$	$\mathrm{s'_R}$	$\mathrm{b'_R}$	$-1/3$	0	0	$-2/3$

Table 2: Assignment of the electroweak quantum numbers T_3 and Y to the fundamental fermions.

The assignment of these quantum numbers is shown in table 2. The left-handed components of the fermions form isospin doublets and the right-handed components isospin singlets. The symbols d′, s′, b′ for the $T_3 = -1/2$ members of the quark doublets denote the eigenstates of weak interactions. They are obtained by a unitary transformation U, the Cabbibo-Kobayashi-Maskawa mixing matrix [2, 24], from the mass eigenstates:

$$\begin{pmatrix} \mathrm{d}' \\ \mathrm{s}' \\ \mathrm{b}' \end{pmatrix} = U \begin{pmatrix} \mathrm{d} \\ \mathrm{s} \\ \mathrm{b} \end{pmatrix} \tag{2}$$

Here neutrinos are assumed to be massless in agreement with experiment [25, 20]. Neutrinos are then defined as eigenstates of weak interactions and right handed neutrinos do not exist. However, the Standard Model does not require the neutrinos to be massless. In the general case of massive neutrinos the eigenstates of weak interactions have no defined mass and a unitary mixing matrix would relate the different eigenstates as in the case of the quarks [26].

2.2 The Bosons

The symmetry group $SU(2)_L \times U(1)$ is constructed from four generators. The three fields $\overrightarrow{W_\mu} = \left(W_\mu^1,\ W_\mu^2,\ W_\mu^3\right)$ are the generators of the weak isospin and B_μ denotes the generator of the weak hypercharge. The observable fields, the carriers of charged ($W^\pm$) and neutral (Z) weak currents and the photon of QED, are obtained from these basic generators by a linear transformation:

$$\begin{aligned} W_\mu^\pm &= \frac{1}{\sqrt{2}}\left(W_\mu^1 \mp i W_\mu^2\right) \\ Z_\mu &= W_\mu^3 \cos\vartheta_W - B_\mu \sin\vartheta_W \\ A_\mu &= W_\mu^3 \sin\vartheta_W + B_\mu \cos\vartheta_W \end{aligned} \tag{3}$$

This transformation introduces the weak mixing angle $\sin\vartheta_W$.

The observable fields acquire mass by the spontaneous symmetry breaking of $SU(2)_L \times U(1)$, the Higgs mechanism [14]. Spontaneous symmetry breaking is achieved by introducing a complex scalar isospin doublet in the theory

$$\Phi = \begin{pmatrix} \Phi^+ \\ \Phi^0 \end{pmatrix} = \begin{pmatrix} \Phi_1 + i\,\Phi_2 \\ \Phi_3 + i\,\Phi_4 \end{pmatrix} \tag{4}$$

with a non-vanishing vacuum expectation value $|\Phi^0|^2 = v^2/2 > 0$. Together with the $SU(2)_L$ and $U(1)$ coupling constants, g and g', the vacuum expectation value determines the masses of the gauge bosons:

$$\begin{aligned} m_W^2 &= g^2\,\frac{v^2}{4} \\ m_Z^2 &= \left(g^2 + g'^2\right)\frac{v^2}{4} \\ m_\gamma &= 0 \end{aligned} \tag{5}$$

The photon remains massless and the electric charge e is the only conserved quantum number.

The linear transformation of eq. 3 relates the coupling constants of $SU(2)_L$ and $U(1)$ to the electric charge e or the electromagnetic coupling constant $\alpha = e^2/4\pi$:

$$\begin{aligned} g &= \frac{e}{\sin\vartheta_W} \\ g' &= \frac{e}{\cos\vartheta_W} \end{aligned} \tag{6}$$

From eqs. 5 and 6 the weak mixing angle relates the masses of the heavy gauge bosons

$$\cos\vartheta_W = \frac{m_W}{m_Z} \tag{7}$$

which can be used as the defining relation of the weak mixing angle (see section 3.1).

The Higgs mechanism is also the source of the fermion masses. However, none of the particle masses is predicted and they remain free parameters of the Standard Model.

The introduction of the complex doublet (eq. 4) gives rise to four additional degrees of freedom. Three of these are the additional longitudinal polarization states of the three massive gauge bosons, $\mathrm{W}^{\pm}$ and Z. The fourth degree of freedom manifests itself in an additional particle, the neutral Higgs boson H^0. The mass of the Higgs boson, m_{H}, does not evolve from the theory and it is another free parameter which has to be determined experimentally.

Higgs boson self-coupling is proportional to the square of its mass and thus the mass of the Higgs is related to the scale to which perturbation theory is valid. From the unitary limit in the scattering of longitudinal polarized $\mathrm{W}^{\pm}$ and Z the Standard Model sets an upper bound for the Higgs mass [27]:

$$m_{\mathrm{H}} < 1000 \text{ GeV} \tag{8}$$

For higher Higgs masses perturbation theory breaks down. For more general Higgs representations eq. 8 represents a boundary for an average mass of the Higgs particles [28].

The discovery of the Higgs boson, or more generally the experimental verification of spontaneous symmetry breaking as the origin of the masses of the vector bosons represents the most important missing test of the Standard Model.

Experiments performed at LEP rule out the entire mass range [29]

$$0 \leq m_{\mathrm{H}} \leq 63.5 \text{ GeV} \qquad (95\%\text{C.L.}) \tag{9}$$

for the Higgs boson. Table 3 summarizes the experimentally determined masses and mass limits of the bosons [20, 30].

	Mass [GeV]	Charge [e]
$\mathrm{W}^{\pm}$	80.23 ± 0.18	± 1
Z	91.1884 ± 0.0022	0
γ	$< 3 \cdot 10^{-36}$	0
H^0	> 63.5	0

Table 3: Mass and electric charge of the gauge bosons.

The minimal Standard Model as outlined above contains only one complex scalar doublet. However, symmetry breaking can also be achieved by the introduction of more complicated structures. One defines the ρ parameter by the ratio of neutral to charged current coupling strength or equivalently as the deviation from the vector boson mass relation (eq. 7):

$$\rho = \frac{m_{\mathrm{W}}^2}{m_{\mathrm{Z}}^2 \cos^2\vartheta_{\mathrm{W}}} \tag{10}$$

The ρ parameter is unity in the Standard Model with one Higgs doublet and the introduction of further isospin doublets does not modify the ρ parameter. Deviations from $\rho = 1$ then can originate only from radiative corrections (see section 3.2).

2.3 Vector and axial-vector coupling constants

In the limit of massless fermions, i.e. unbroken $SU(2)_L$ symmetry, only left-handed fermions couple to the $W^\pm$ bosons. As a consequence charged current interactions can be decomposed in two parts of equal strength with transformation properties of a vector and an axial-vector, respectively. This is known as the V-A structure of weak interactions.

The weak neutral current is a linear superposition of the $SU(2)_L$ and $U(1)$ generators, the latter also acting on right-handed helicity states. The contribution of the vector and axial-vector part to the interactions is different and their relative strength, denoted by the vector and axial-vector coupling constants g_V and g_A, reflects the admixture of the $U(1)$ generator B_μ (see eq. 3):

$$\begin{aligned} g_V^f &= T_3^f - 2\,Q_f \sin^2\vartheta_W \\ g_A^f &= T_3^f \end{aligned} \tag{11}$$

The vector coupling of a fermion f to the Z depends on its electric charge Q_f. The values of g_V and g_A for the different fermions are summarized in table 4 using the weak mixing angle $\sin^2\vartheta_W = 0.226$ as derived from the boson masses (table 3).

Fermion	Q_f	g_V^f	g_A^f
$\nu_e,\ \nu_\mu,\ \nu_\tau$	0	1/2	1/2
e, μ, τ	−1	−0.048	−1/2
u, c, t	2/3	0.199	1/2
d, s, b	−1/3	−0.349	−1/2

Table 4: Assignment of the vector and axial-vector coupling constants of the fermions for $\sin^2\vartheta_W = 0.226$

In the Standard Model these coupling constants are universal for all generations. In particular, the equality of these coupling constants for the three charged leptons, referred to as lepton universality, has been verified with high accuracy at LEP (see section 8.2).

From eq. 11 the relative couplings of the Z to left- and right-handed fermions, g_L and g_R, are obtained:

$$\begin{aligned} g_L^f &= g_V^f + g_A^f = 2\,T_3^f - 2\,Q_f \sin^2\vartheta_W \\ g_R^f &= g_V^f - g_A^f = -2\,Q_f \sin^2\vartheta_W \end{aligned} \tag{12}$$

2.4 The reaction $e^+e^- \to f\bar{f}$ in lowest order

Electron-positron annihilation into a fermion-antifermion pair is described in lowest order by the exchange of a photon and a Z boson (see figure 1)[1]. Due to the smallness of the electron mass the exchange of a Higgs boson does not contribute significantly and is neglected here. The two diagrams lead to three terms in the cross section corresponding to the exchange of a photon, a Z boson and the interference

[1] The t-channel contribution to the process $e^+e^- \to e^+e^-$ is not considered here.

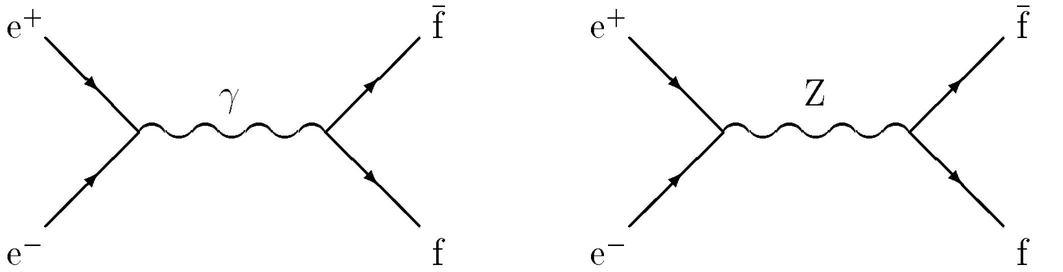

Figure 1: Electron-positron annihilation into a fermion-antifermion pair in lowest order mediated by the exchange of a photon or a Z boson.

of both with their individual contributions depending on the center-of-mass energy. For massless fermions and summing over all helicity states the cross section as a function of the scattering angle Θ, the angle between the incoming electron e^- and the outgoing fermion f, can be written as:

$$\begin{aligned}
\frac{d\sigma_f}{d\cos\Theta} &= N_c^f \frac{\pi\alpha^2}{2\,s}\Big\{Q_f^2\,(1+\cos^2\Theta) && (\gamma \text{ exchange}) \\
&\quad - Q_f\Big[2\,g_V^e g_V^f (1+\cos^2\Theta) + 4\,g_A^e g_A^f \cos\Theta\Big]\,\Re\{\chi\} && (\text{Interference}) \\
&\quad + \Big(\Big[(g_V^e)^2+(g_A^e)^2\Big]\Big[(g_V^f)^2+(g_A^f)^2\Big](1+\cos^2\Theta) \\
&\qquad\qquad + 8\,g_V^e g_A^e g_V^f g_A^f \cos\Theta\Big)|\chi|^2\Big\} && (\text{Z exchange})
\end{aligned}$$

$$N_c^f = \begin{cases} 1 \text{ for leptons} \\ 3 \text{ for quarks} \end{cases}$$

$$\chi = \frac{1}{4\,\sin^2\vartheta_W\cos^2\vartheta_W}\,\frac{s}{s-m_Z^2+i\,\Gamma_Z\,m_Z} \tag{13}$$

The total width of the Z, Γ_Z, is the sum of the partial decay width into fermions:

$$\begin{aligned}
\Gamma_Z &= \sum_f \Gamma_f \qquad\qquad (m_f < m_Z/2) \\
\Gamma_f &= N_c^f\,\frac{\alpha\,m_Z}{12\,\sin^2\vartheta_W\cos^2\vartheta_W}\Big[(g_V^f)^2+(g_A^f)^2\Big]
\end{aligned} \tag{14}$$

The total cross section $e^+e^- \to f\bar{f}$ is found to be:

$$\begin{aligned}
\sigma_f &= \frac{4\,\pi\alpha^2}{3\,s}N_c^f\Big\{Q_f^2 \\
&\quad - 2\,Q_f\,g_V^e g_V^f\,\Re\{\chi\} \\
&\quad + \Big[(g_V^e)^2+(g_A^e)^2\Big]\Big[(g_V^f)^2+(g_A^f)^2\Big]|\chi|^2\Big\}
\end{aligned} \tag{15}$$

Again, the second term is the interference of the photon with the vector part of

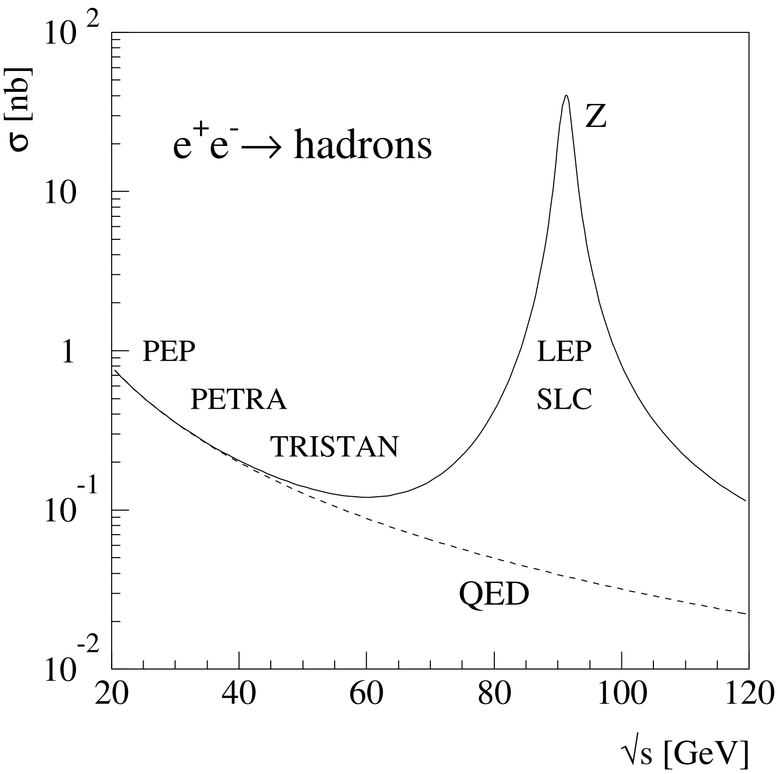

Figure 2: Lowest order cross section for $e^+e^- \to$ hadrons as a function of the center-of-mass energy.

the Z exchange. Figure 2 shows the total cross section for $e^+e^- \to$ hadrons as a function of the center-of-mass energy $\sqrt{s}$. One notices the enormous increase of the cross section at the Z pole as compared to the $1/s$ dependence of the pure photon exchange in QED. Indicated are the approximate energy ranges of e^+e^- accelerators. The effect of the Z on the total cross section is small for the previous generation of e^+e^- accelerators PEP, PETRA and TRISTAN. For the experiments performed at LEP and SLC at the Z resonance the cross section $e^+e^- \to$ hadrons is about thousand times larger than the cross section from photon exchange.

For $\sqrt{s} = m_Z$, where the interference term vanishes and the photon contribution is very small, the lowest order cross section can be written as:

$$\begin{aligned} \sigma_f(\sqrt{s} = m_Z) &\approx \frac{12\,\pi}{m_Z^2}\,\frac{\Gamma_e\Gamma_f}{\Gamma_Z^2} \\ &= \frac{12\,\pi}{m_Z^2}\,BR\,(Z \to e^+e^-)\cdot BR\,(Z \to f\bar{f}) \end{aligned} \tag{16}$$

The peak cross section is thus the product of the branching ratios of the Z decaying into the initial and the final state fermions times a dimensional factor. At the peak the cross section takes its maximum value which is physically possible without violating the unitary limit [31]. The branching ratios as calculated from the lowest order formula (eq. 14) are given in table 5. About 20% of the Z bosons decay into

	$BR = \Gamma_{\rm f}/\Gamma_{\rm Z}$
e, μ, τ	3.5%
$\nu_{\rm e}$, ν_μ, ν_τ	7%
hadrons ($= \sum_{\rm q} {\rm q\bar{q}}$)	69%

Table 5: Lowest order branching ratios of the Z

neutrinos and are thus not detected[2].

Most of the Z bosons decay into hadrons. The ratio of the hadronic to leptonic width

$$R_\ell = \frac{\Gamma_{\rm had}}{\Gamma_\ell} \approx \frac{\sigma_{\rm had}}{\sigma_\ell} \qquad (\ell = {\rm e},\ \mu,\ \tau) \tag{17}$$

at the Z is $R_\ell \approx 20$ which is much larger than at lower energies, e.g. at PETRA and PEP, where the ratio of the cross sections is given by the squares of the electric charges:

$$R_\ell = \frac{\sigma_{\rm had}}{\sigma_\ell} = N_c \sum_{\rm q} Q_{\rm q}^2 = \frac{11}{3}\ . \tag{18}$$

Also, the cross section ratio for u-type and d-type quarks at $\sqrt{s} = m_{\rm Z}$

$$R_{\rm u} = \Gamma_{\rm u}/\Gamma_{\rm d} \approx 0.78 \tag{19}$$

differs from the ratio at lower energies $R_{\rm u} = (Q_{\rm u}/Q_{\rm d})^2 = 4$. This leads to a different quark composition in hadronic Z decays. At LEP more b-quarks than u-quarks are produced.

The terms proportional to $\cos\Theta$ in the differential cross section (eq. 13) lead to a difference in the number of fermions produced in the forward (N_F) and backward (N_B) hemispheres. The forward-backward asymmetry $A_{\rm FB}$ is thus defined as:

$$\begin{aligned} A_{\rm FB} &= \frac{N_F - N_B}{N_F + N_B} \\ N_F &= \int_0^1 \frac{\partial\sigma}{\partial\cos\Theta}\,{\rm d}\cos\Theta \\ N_B &= \int_{-1}^0 \frac{\partial\sigma}{\partial\cos\Theta}\,{\rm d}\cos\Theta \end{aligned} \tag{20}$$

From integration of eq. 13 the forward-backward asymmetry in lowest order for the process $\rm e^+e^- \to f\bar{f}$ is obtained:

$$\begin{aligned} A_{\rm FB}^{\rm f}(s) &= \frac{3}{8}\,\frac{-4\,Q_{\rm f}\,g_A^{\rm e} g_A^{\rm f}\,\Re\{\chi\} + 8\,g_A^{\rm e} g_V^{\rm e} g_A^{\rm f} g_V^{\rm f}\,|\chi|^2}{Q_{\rm f}^2 - 2\,Q_{\rm f}\,g_V^{\rm e} g_V^{\rm f}\,\Re\{\chi\} + [(g_A^{\rm e})^2 + (g_V^{\rm e})^2]\,[(g_A^{\rm f})^2 + (g_V^{\rm f})^2]\,|\chi|^2} \\ A_{\rm FB}^{\rm f}(\sqrt{s} = m_{\rm Z}) &= 3\,\frac{g_{\rm V}^{\rm e}\,g_{\rm A}^{\rm e}}{(g_{\rm V}^{\rm e})^2 + (g_{\rm A}^{\rm e})^2}\,\frac{g_{\rm V}^{\rm f}\,g_{\rm A}^{\rm f}}{(g_{\rm V}^{\rm f})^2 + (g_{\rm A}^{\rm f})^2} \end{aligned} \tag{21}$$

For the example of $\rm e^+e^- \to \mu^+\mu^-$ the dependence of $A_{\rm FB}$ on the center-of-mass energy is shown in figure 3. The cause of the forward-backward asymmetry is

[2]With the exception of $\rm e^+e^- \to \nu\bar{\nu}\gamma$ events (see section 6.2).

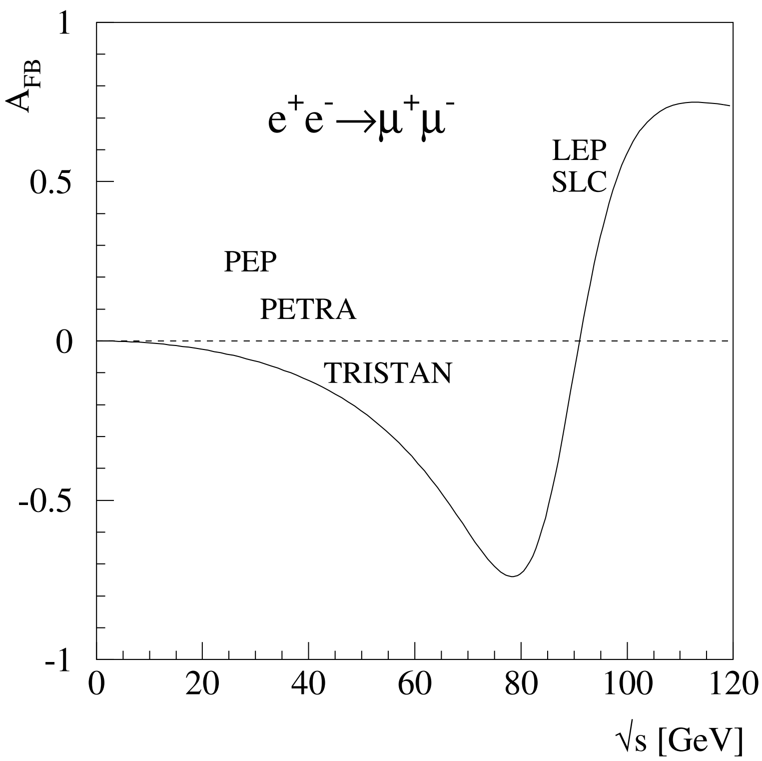

Figure 3: Lowest order forward-backward asymmetry in $e^+e^- \to \mu^+\mu^-$ as a function of the center-of-mass energy.

the superposition of vector and axial-vector currents. Thus, the interference of the photon with the axial-vector component of the Z gives rise to a large asymmetry already at energies well below the Z. The interference of photon and Z has been observed at experiments performed at PEP, PETRA and TRISTAN through the forward-backward asymmetry. At the Z pole the vector and the axial-vector parts of the Z determine the asymmetry. As the relative strength of the vector coupling of the Z to the charged leptons is small (see table 4) the observed asymmetry for $e^+e^- \to \mu^+\mu^-$ and $e^+e^- \to \tau^+\tau^-$ on the peak is small.

2.5 Helicities in $e^+e^- \to f\bar{f}$ at the Z pole

The cross section $e^+e^- \to f\bar{f}$ is composed of four helicity configurations (figure 4). For $\sqrt{s} = m_Z$ and neglecting the photon exchange the cross section for each of the four configurations can be expressed in terms of the couplings of the Z to the left- and right-handed fermion states:

$$
\begin{aligned}
\frac{d\sigma_{ll}}{d\cos\Theta} &\propto (g_L^e)^2 (g_L^f)^2 \,(1+\cos\Theta)^2 \\
\frac{d\sigma_{lr}}{d\cos\Theta} &\propto (g_L^e)^2 (g_R^f)^2 \,(1-\cos\Theta)^2 \\
\frac{d\sigma_{rr}}{d\cos\Theta} &\propto (g_R^e)^2 (g_R^f)^2 \,(1+\cos\Theta)^2
\end{aligned}
$$

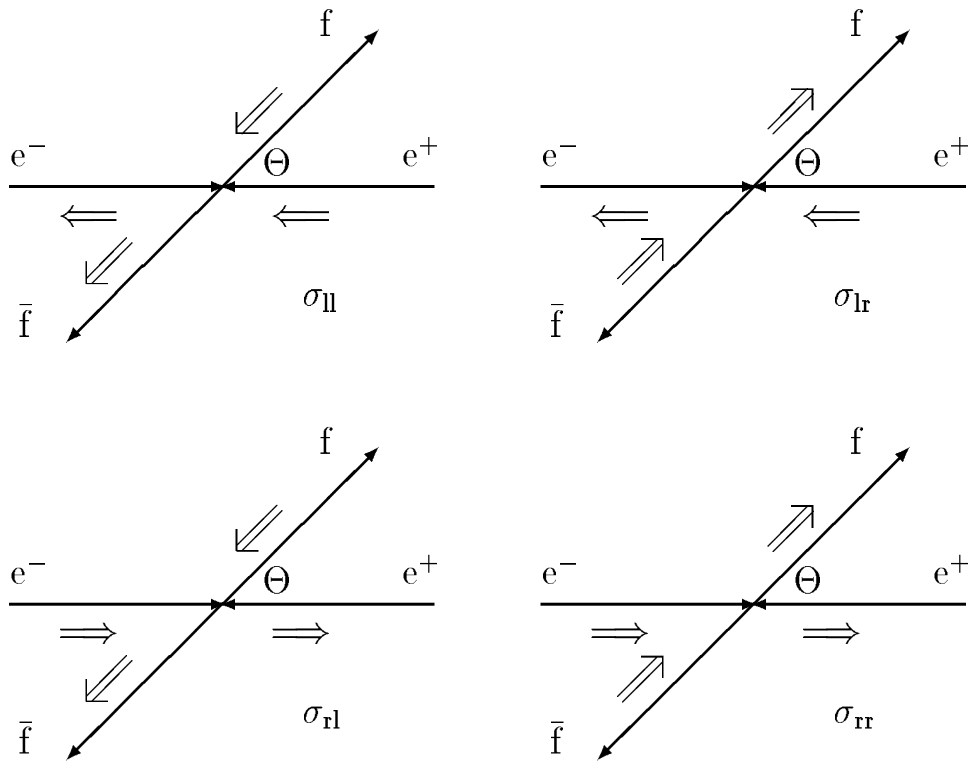

Figure 4: The four helicity configurations in $e^+e^- \to f\bar{f}$.

$$\frac{d\sigma_{rl}}{d\cos\Theta} \quad \propto \quad (g_R^e)^2 (g_L^f)^2 \, (1 - \cos\Theta)^2 \tag{22}$$

The dependence on the scattering angle is readily obtained from angular momentum conservation.

This can be transformed in a set of linearly independent cross sections which are experimentally better accessible:

$$\begin{aligned}
\sigma_{tot} &= \sigma_{ll} + \sigma_{lr} + \sigma_{rr} + \sigma_{rl} && \text{(total cross section)} \\
\sigma_{pol} &= \sigma_{ll} - \sigma_{lr} - \sigma_{rr} + \sigma_{rl} && \text{(final state polarization)} \\
\sigma_{LR} &= \sigma_{ll} + \sigma_{lr} - \sigma_{rr} - \sigma_{rl} && \text{(initial state polarization)} \\
\sigma_{FB} &= \sigma_{ll} - \sigma_{lr} + \sigma_{rr} - \sigma_{rl} && \text{(forward} - \text{backward)}
\end{aligned} \tag{23}$$

These are the total cross section and the differences in cross section for left- and right-handed electrons, the production of left- and right-handed final state fermions and for fermions scattered in the forward and backward hemisphere. Normalizing to the total cross section one obtains the well known asymmetries and their dependence on the coupling constants for $\sqrt{s} = m_Z$:

$$\begin{aligned}
\sigma_{tot} &\propto [(g_V^e)^2 + (g_A^e)^2]\,[(g_V^f)^2 + (g_A^f)^2] \\
\mathcal{P}_f &= -\frac{\sigma_{pol}}{\sigma_{tot}} = -A_f \\
A_{LR} &= \frac{\sigma_{LR}}{\sigma_{tot}} = A_e \\
A_{FB} &= \frac{3}{4}\frac{\sigma_{FB}}{\sigma_{tot}} = \frac{3}{4} A_e A_f
\end{aligned}$$

$$\text{with } \mathrm{A_f} \equiv 2\,\frac{g_V^f\, g_A^f}{(g_V^f)^2 + (g_A^f)^2} \tag{24}$$

The sign in the definition of $\mathcal{P}_\mathrm{f}$ reflects that historically polarization asymmetries are defined as cross section differences of right- to left-handed states. Since A_FB is defined as the relative difference of forward to backward scattered fermions (eq. 20) a dilution factor of 3/4 arises from the integration of the $(1 \pm \cos\Theta)$ terms in eq. 22.

The parity violation of neutral current weak interactions, first observed in scattering of polarized electrons on deuterium [7], is contained in the quantity A_f which on the Z resonance can be directly observed in the initial and final state polarization asymmetries.

The total cross section σ_tot and the forward-backward asymmetry A_FB can be measured for all charged lepton flavors, heavy quarks and, inclusively, for all five quark flavors. The polarization of the final state fermion is observable only in the reaction $\mathrm{e^+e^-} \to \tau^+\tau^-$ where $\mathcal{P}_\tau$ is inferred from the energy spectra of the decay products of the tau (see section 7.4). For the measurement of A_LR all Z decays into hadrons and charged leptons can be used. However, it requires the longitudinal polarization of the incoming electrons in $\mathrm{e^+e^-}$ collisions which for time being has only been achieved for the favourable conditions of the SLC collider [32].

The cross section differences of left- and right-handed fermions in the initial and final state, σ_LR and σ_pol defined in eq. 23, can be measured as a function of the scattering angle Θ. This way one defines

$$A_\mathrm{FB}^\mathrm{pol} = \frac{1}{\sigma_\mathrm{tot}}\left[\int_0^1 \frac{\partial\sigma_\mathrm{pol}}{\partial\cos\Theta}\,\mathrm{d}\cos\Theta - \int_{-1}^0 \frac{\partial\sigma_\mathrm{pol}}{\partial\cos\Theta}\,\mathrm{d}\cos\Theta\right] \tag{25}$$

and

$$A_\mathrm{FB}^\mathrm{LR} = \frac{1}{\sigma_\mathrm{tot}}\left[\int_0^1 \frac{\partial\sigma_\mathrm{LR}}{\partial\cos\Theta}\,\mathrm{d}\cos\Theta - \int_{-1}^0 \frac{\partial\sigma_\mathrm{LR}}{\partial\cos\Theta}\,\mathrm{d}\cos\Theta\right]. \tag{26}$$

As a consequence of helicity conservation at the $\mathrm{Zf\bar{f}}$ vertices the measurement of the angular dependence of the final state polarization asymmetry provides information on the couplings of the initial state electrons and vice versa:

$$\begin{aligned} A_\mathrm{FB}^\mathrm{pol} &= \frac{3}{4}\,A_\mathrm{e} \\ A_\mathrm{FB}^\mathrm{LR} &= \frac{3}{4}\,A_\mathrm{f} \end{aligned} \tag{27}$$

Thus, the measurement of the tau polarization as function of $\cos\Theta$ yields a measurement of the electron couplings. And $A_\mathrm{FB}^\mathrm{LR}$, for instance of heavy quarks identified in $\mathrm{e^+e^-} \to$ hadrons events, measures the polarization of the final state and thus provides experimental information about the coupling constants of these quarks to the Z.

3 Radiative corrections in $e^+e^- \to f\bar{f}$

3.1 The Standard Model parameters

As outlined in section 2 the Standard Model has several input parameters which are not predicted by the model and which must be determined by experiment. A commonly used set of these input parameter is the on-shell renormalization scheme [33]:

α, m_Z, m_W

m_H, fermion masses

α_s, CKM matrix

Given the QED coupling constant $\alpha = e^2/4\pi$ and the two vector boson masses all observables in $e^+e^- \to f\bar{f}$ reactions can be calculated in lowest order. In fact, only these three parameters enter in the Standard Model formulae given in the previous section. In particular, the weak mixing angle is defined by the ratio of the $W^\pm$ and Z mass (eq. 7).

To incorporate mass effects and higher order diagrams in the calculations the masses of all fermions are required. Corrections to the massive gauge boson propagators, as well as Higgs production cross section, depend on the mass of the Higgs boson m_H. In hadronic final states the strong coupling constant α_s enters through QCD radiative corrections. The Cabbibo-Kobayashi-Maskawa (CKM) matrix relates the electroweak and mass eigenstates of quarks. However, quark mixing is not important for total hadronic cross sections in neutral current interactions considered here.

These parameters are all known by now, except the mass of the still undiscovered Higgs boson. In Standard Model calculations of electroweak observables assumptions about m_H based on experimental and theoretical limits have to be made. The mass of the top quark plays an important role in precise Standard Model calculation and its value has only recently been determined.

The QED coupling constant α is measured at low momentum transfer (Thomson scattering limit) for instance with the Quantum Hall effect or in $g-2$ experiments [34, 20] with very high precision:

$$\alpha^{-1} = 137.035\,989\,5(61) \tag{28}$$

Also the mass of the Z is now precisely determined by the experiments at LEP (see section 5.3) and does not introduce any sizeable uncertainty in Standard Model calculations.

However, the $W^\pm$ mass is only known to a relative precision of $\Delta m_W/m_W = 2\cdot 10^{-3}$. This is not adequate for the measurements performed at LEP which are of similar or sometimes even better accuracy. In Standard Model calculations this parameter is therefore replaced by the Fermi coupling constant G_F determined from the muon lifetime τ_μ [35]:

$$\begin{aligned} \frac{1}{\tau_\mu} &= \frac{G_F^2}{192\,\pi^3}\, m_\mu^5 \left(1 - 8\,\frac{m_e^2}{m_\mu^2}\right)\left(1 + \frac{3}{5}\,\frac{m_e^2}{m_W^2} + \delta_{QED}\right) \\ \delta_{QED} &= \frac{\alpha}{2\,\pi}\left(\frac{25}{4} - \pi^2\right) \end{aligned} \tag{29}$$

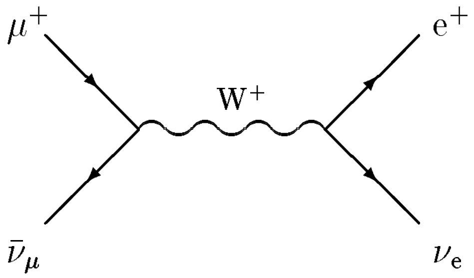

Figure 5: Muon decay in lowest order.

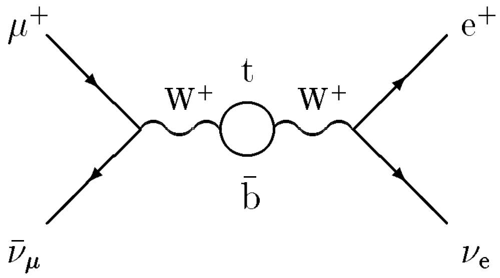

Figure 6: $\mathrm{W}^\pm$ vacuum polarization involving the top quark.

The experimental result $\tau_\mu = 2.197\,03 \pm 0.000\,04$ μs yields [20]

$$G_\mathrm{F} = 1.166\,39(2) \cdot 10^{-5} \text{ GeV}^{-2}. \tag{30}$$

Mass effects and photonic corrections, δ_QED, to the lowest order diagram of the muon decay (figure 5) are taken into account in the definition of G_F. Other higher order corrections, in particular the vacuum polarization of the $\mathrm{W}^\pm$ as shown in figure 6, are contained in the definition of the physical mass m_W but are not accounted for in eq. 29 where G_F is defined. The relation between m_W and G_F thus contains a term Δr describing the electroweak radiative corrections [36]:

$$\frac{G_\mathrm{F}}{\sqrt{2}} = \frac{\pi\,\alpha}{2}\,\frac{1}{m_\mathrm{W}^2 \sin^2\vartheta_\mathrm{W}}\,\frac{1}{1-\Delta r} \tag{31}$$

It can be split into QED corrections due to the running of the QED coupling constant $\Delta\alpha$ (see section 3.3) and pure weak corrections Δr_w [37, 38]:

$$\Delta r = \Delta\alpha - \Delta r_\mathrm{w} + \Delta r_\mathrm{rem} \tag{32}$$

The remaining corrections Δr_rem are smaller than the main contributions discussed below but nevertheless numerically important [39]. They are included in the Standard Model calculations performed later in this article.

3.2 Weak radiative corrections

The main cause of the weak radiative corrections Δr_w is the $\mathrm{W}^\pm$ vacuum polarization diagram shown in figure 6. The contribution of this kind of diagrams is proportional to the difference of the squared masses of the two fermions. Thus, the by far most important diagram is the virtual decay of the $\mathrm{W}^\pm$ into a top and bottom quark which gives rise to large corrections due to the mass difference in this isospin doublet.

Weak isospin symmetry breaking by fermion doublets with large mass splitting modifies the ρ-parameter [40] which is unity in lowest order (see section 2.2). The leading contribution is quadratic in m_t:

$$\begin{aligned} \bar{\rho} &= 1 + \Delta\rho \\ \Delta\rho_\mathrm{t} &= \frac{3\,G_F}{8\,\pi^2\sqrt{2}}\,m_\mathrm{t}^2 + \ldots \end{aligned} \tag{33}$$

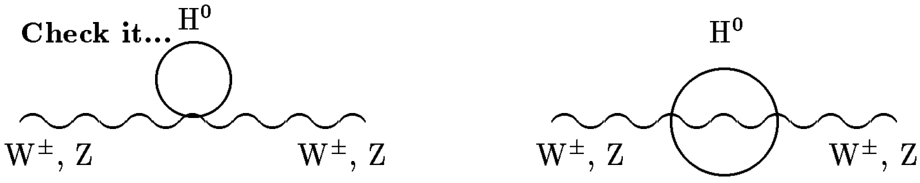

Figure 7: Vacuum polarization of $W^{\pm}$ and Z from the Higgs boson.

The weak radiative corrections can be expressed in terms of $\Delta\rho$:

$$\Delta r_{\rm w} = \frac{\cos^2\vartheta_{\rm W}}{\sin^2\vartheta_{\rm W}}\,\Delta\rho \tag{34}$$

As will be shown below the effect of the top quark mass is large and the precision measurements at LEP of the Z widths and the asymmetries can be used to constrain $m_{\rm t}$ in the Standard Model. Testing the Standard Model at LEP and SLC consist in comparing the $m_{\rm t}$ values derived from different observables at the Z and comparing $m_{\rm t}$ to the direct measurement which is now available. In addition, the top quark mass inferred from LEP measurements can be expressed in terms of a $W^{\pm}$ mass value which can be compared to the direct measurement of $m_{\rm W}$ at $\rm p\bar{p}$ colliders.

There are other weak radiative corrections present in the $W^{\pm}$ as well as in the Z exchange, for instance vertex corrections and box diagrams. In general, these corrections are small and do not give rise to large $m_{\rm t}^2$ dependent terms. Of particular interest are weak radiative corrections from virtual exchange of a Higgs boson. Since the coupling of the Higgs is proportional to the mass of the particle only diagrams where the Higgs couples to the heavy gauge bosons matter. The purely bosonic vacuum polarization, depicted in figure 7, gives contributions to the ρ-parameter which depend only logarithmically on the Higgs boson mass [39]:

$$\Delta\rho_{\rm Higgs} = \frac{3\sqrt{2}\,G_{\rm F}\,m_{\rm W}^2}{16\,\pi^2}\,\frac{\sin^2\vartheta_{\rm W}}{\cos^2\vartheta_{\rm W}}\left(\ln\frac{m_{\rm H}^2}{m_{\rm W}^2}-\frac{5}{6}\right) \tag{35}$$

As a result the dependence of Standard Model predictions on the unknown Higgs mass is much smaller than on $m_{\rm t}$.

It is convenient to introduce the effective couplings, $\bar{g}_{\rm A}$ and $\bar{g}_{\rm V}$, and the effective weak mixing angle $\sin^2\bar{\vartheta}_{\rm W}$ which are related to the lowest order couplings by the ρ-parameter [41]:

$$\begin{aligned}
\bar{g}_{\rm A}^{\rm f} &= g_{\rm A}^{\rm f}\,\sqrt{\bar{\rho}_{\rm f}} \\
\bar{g}_{\rm V}^{\rm f} &= g_{\rm A}^{\rm f}\,\sqrt{\bar{\rho}_{\rm f}}\,(1-4\,|Q_{\rm f}|\,\sin^2\bar{\vartheta}_{\rm W}) \\
\sin^2\bar{\vartheta}_{\rm W}^{\rm f} &= (1+\frac{\cos^2\vartheta_{\rm W}}{\sin^2\vartheta_{\rm W}}\Delta\bar{\rho}_{\rm f}+\ldots)\,\sin^2\vartheta_{\rm W}
\end{aligned} \tag{36}$$

In principle, the effective couplings are different for the fermions because of the flavor dependent corrections to the $\rm Zf\bar{f}$ vertex resulting in slightly different $\bar{\rho}_{\rm f} = 1 + \Delta\bar{\rho}_{\rm f}$

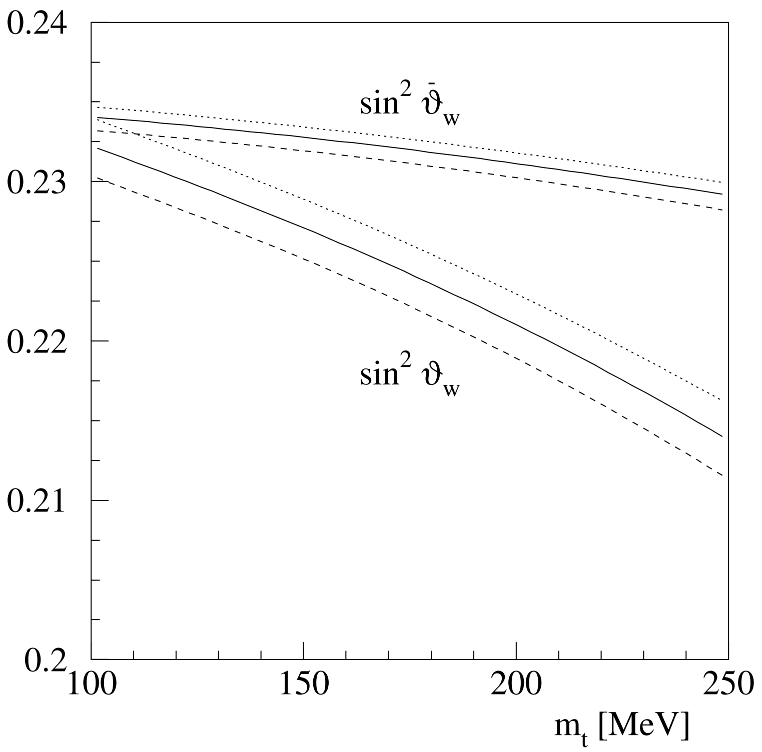

Figure 8: Comparison of the relation between the weak mixing angle defined as $\sin^2\vartheta_W \equiv 1 - m_W^2/m_Z^2$ and the effective weak mixing angle $\sin^2\bar{\vartheta}_W$ and the top quark mass m_t (for $m_H = 300$ GeV). The broken (dotted) lines show the shift of the central value for $m_H = 60$ (1000) GeV.

values. However, with the exception of the $Zb\bar{b}$ vertex the differences are small compared to the current experimental error on these quantities. Experimental values of $\sin^2\bar{\vartheta}_W$ obtained from different decays $Z \to f\bar{f}$ ($f \neq b$) can be compared directly (see section 8.1).

As can be seen from eq. 36 the bulk of the radiative corrections is absorbed in the definition of the weak mixing angle. Replacing $\sin^2\vartheta_W$ by $\sin^2\bar{\vartheta}_W$ in eq. 31 results in a different relation between $\sin^2\bar{\vartheta}_W$ and $\Delta\rho$ or, equivalently, m_t. Figure 8 compares the dependence on the top quark mass for the two definitions of the weak mixing angle calculated from eq. 31 with complete treatment of electroweak radiative corrections[3].

The advantage of $\sin^2\bar{\vartheta}_W$ and the effective coupling constants is that they are closely related to the observables at the Z resonance. For instance, the partial decay width of the Z into a fermion-antifermion pair, including radiative corrections, can be written similarly to the lowest order formula (Improved Born-approximation) [41]:

$$\begin{aligned} \Gamma_f &= N_c^f \frac{G_F\, m_Z^3}{6\,\pi\,\sqrt{2}} \left[\left(\bar{g}_A^f\right)^2 + \left(\bar{g}_V^f\right)^2 \right] \\ &\quad + \text{ QED and QCD corrections} \end{aligned} \tag{37}$$

[3]Using the ZFITTER program (see section 3.6).

In this section the weak radiative corrections, or the effects leading to $\Delta\rho$, originating from Standard Model effects are outlined. The interpretation of observables like Γ_ℓ or $\sin^2\bar{\vartheta}_{\mathrm{W}}$ in terms of m_{t} or m_{H} thus implies the validity of the Standard Model and that there are no other causes changing the effective couplings of the fermions to the Z. Possible additional effects could be a fourth generation of fermions with large mass splitting as in the top-bottom quark doublet or an additional gauge group with a heavy boson Z'. Also, particles predicted by Supersymmetry would modify the ρ-parameter obtained from measurements at the Z resonance [42].

The interpretation of direct experimental observables (total cross sections, asymmetries) in terms of physical parameters is done in steps of increasing level of assumptions about the underlying theory. The extraction of Z parameters (mass and widths) can be done in a way which relies only on the validity of QED[4] and without assuming that weak radiative corrections originate from known Standard Model processes and particles only. Also, the effective couplings $\bar{g}_{\mathrm{V}}$ and $\bar{g}_{\mathrm{A}}$, and thus $\sin^2\bar{\vartheta}_{\mathrm{W}}$, can be obtained from the measured asymmetries, corrected only for QED effects (see section 8). This is often called 'model independent' just because it allows the comparison of these derived quantities with the Standard Model without restricting them to their Standard Model expectations.

Using these results to constrain parameters like m_{t} depends on the validity of the Standard Model and ignores possible contributions to the observed cross sections and asymmetries from physics not described by the Standard Model.

3.3 The running of the QED coupling constant α

The QED corrections $\Delta\alpha$ in eq. 32 arise from the running of the QED coupling constant α from its definition at low momentum transfer ($Q^2 \to 0$) to the scale of the heavy gauge bosons:

$$\alpha(m_{\mathrm{Z}}) = \frac{\alpha}{1-\Delta\alpha}. \tag{38}$$

This can be pictured as the change in the electron charge e when approaching it from large distances. The determination of $\alpha(m_{\mathrm{Z}})$ requires the calculation of the self energy of the photon (see figure 9). The contributions to $\Delta\alpha$ for light ($m_{\mathrm{f}} \ll m_{\mathrm{Z}}$) and heavy, i.e. the top quark, fermions are [43]:

$$\begin{aligned} \Delta\alpha_{\mathrm{f}} &= \frac{\alpha}{3\pi} Q_{\mathrm{f}}^2 N_c^{\mathrm{f}} \left[\ln\left(\frac{m_{\mathrm{Z}}}{m_{\mathrm{f}}}\right)^2 - \frac{5}{3}\right] && \text{for } \mathrm{m_f} \ll \mathrm{m_Z} \\ \Delta\alpha_{\mathrm{t}} &= \frac{\alpha}{3\pi}\frac{4}{15}\left(\frac{m_{\mathrm{Z}}}{m_{\mathrm{t}}}\right)^2 \to 0 && \text{for } \mathrm{m_t} \gg \mathrm{m_Z}. \end{aligned} \tag{39}$$

The numerical results for the leptons are summarized in table 6.

	$\mathrm{e^+e^-}$	$\mu^+\mu^-$	$\tau^+\tau^-$	$\sum_{\mathrm{e},\mu,\tau}$
$\Delta\alpha$	0.01743	0.00918	0.00481	0.03142

Table 6: Contributions to $\Delta\alpha$ from charged leptons

[4] This does not fully hold for the determination of m_{Z} (see discussion in section 5.1).

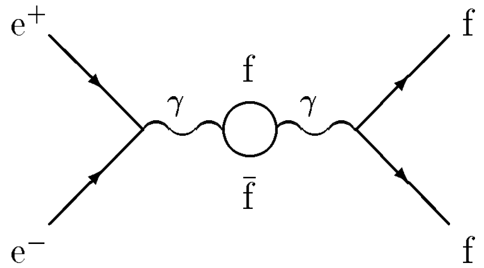

Figure 9: Photon vacuum polarization.

Here the contribution of the top quark is small but the five other, lighter quark flavors pose a problem since their masses are not well defined. The total contribution of the light quarks can be evaluated using experimental cross sections for $e^+e^- \rightarrow$ hadrons at low energies [44, 45] to be

$$\Delta\alpha_q = 0.0280 \pm 0.0007 \qquad (q = u, d, c, s, b) \tag{40}$$

where the error reflects the experimental uncertainty of the cross section measurements. The result for the QED coupling constant at the Z mass

$$\begin{aligned} \Delta\alpha &= 0.0594 \pm 0.0007 \qquad \text{or} \\ \alpha(m_Z)^{-1} &= 128.896 \pm 0.090 \end{aligned} \tag{41}$$

differs by about 6% from its definition at low momentum transfer which is very large compared to the precision of electroweak observables at LEP.

The relative error $\Delta\alpha(m_Z)/\alpha(m_Z) = \pm 7 \cdot 10^{-4}$ translates to an uncertainty in the Standard Model calculation of the effective weak mixing angle $\Delta \sin^2\bar{\vartheta}_W = \pm 0.00023$. This corresponds to $\Delta m_t = \pm 4$ GeV on the top mass as determined from the measurements of Z parameter at LEP.

It should be noted that other calculations of $\alpha(m_Z)$ which either use also the measured hadronic cross sections below the Z pole [46] or attempt to partially calculate the hadronic contribution to $\Delta\alpha$ from QCD [47] lead to results which differ by up to twice the error given in eq. 40. Hence, using these results instead of eq. 41 shifts the mass of the top quark derived from the measurement of electroweak radiative corrections (see section 9.1) by up to 9 GeV. See reference [44] for a comparison of determinations of $\alpha(m_Z)$. Improved measurements leading to a better understanding of the total cross section $e^+e^- \rightarrow$ hadrons at low energies are hence very important to reduce this uncertainty in future precision tests of the Standard Model.

3.4 QED radiative corrections in $e^+e^- \rightarrow f\bar{f}$

Besides the running of the QED coupling constant α discussed above there are other higher order QED processes contributing to $e^+e^- \rightarrow f\bar{f}$. These corrections are due to higher order diagrams with additional real or virtual photons. Two examples, initial state bremsstrahlung and corrections to the $Zf\bar{f}$ vertex, are depicted in figure 10.

In particular, the presence of initial state bremsstrahlung has a huge impact on the cross section. Around the Z resonance its effect can be understood qualitatively

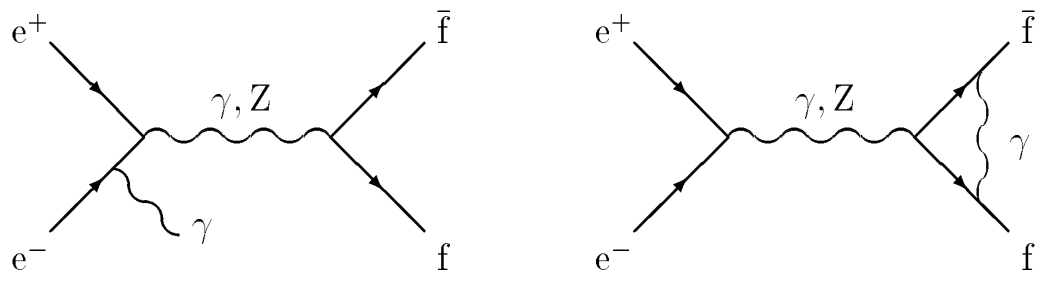

Figure 10: Examples of higher order QED processes in $e^+e^- \to f\bar{f}$.

by considering that the radiated photon removes some fraction of the center-of-mass energy, $\sqrt{s}$, such that the production of the Z takes place at a reduced effective energy, $\sqrt{s'}$, where the cross section is different.

Figure 11 shows the effect of QED radiative corrections. The total cross section $e^+e^- \to$ hadrons in lowest order is compared to the full calculation which includes contributions up to order $\mathcal{O}(\alpha^2)$, i.e. up to two additional photons. The higher order QED diagrams lead to [48]

- a reduction of the peak cross section to 74%,
- an energy shift of the peak cross section by $\Delta\sqrt{s} = 112$ MeV
- and to an asymmetric cross section curve below and above the Z pole.

The effect of these three items on the extraction of the partial widths, the mass and the total width of the Z is large compared to the experimental error achieved. Therefore, QED corrections up to $\mathcal{O}(\alpha^2)$ must be taken into account. The uncertainty due to omitted $\mathcal{O}(\alpha^3)$ and higher terms in the calculations introduced in the experimental determination of the Z parameters is estimated to be small compared to the current experimental accuracy [49].

Figure 12 compares the lowest order forward-backward asymmetry (eq. 21) to the $\mathcal{O}(\alpha^2)$ calculation for $e^+e^- \to \mu^+\mu^-$. The large difference can be understood by the effect of initial state bremsstrahlung. For a fraction of the events part of the energy is radiated away by a photon. The muon pair is then actually produced at an effective center-of-mass energy $\sqrt{s'} < \sqrt{s}$ where the cross section and the asymmetry are different.

The size of the QED corrections depends on the experimental cuts used to select the events. For instance, a tight cut on the acolinearity angle ξ effectively limits the maximum energy of the bremsstrahlung photon. This reduces the impact of initial state bremsstrahlung and the asymmetry gets closer to the lowest order calculation (figure 12).

Again, the QED radiative corrections are large compared to the experimental error achieved by the experiments. As a numerical example for $\sqrt{s} = m_Z$ the asymmetry expected for typical experimental cuts ($\xi < 15°$, $p_\mu > 2$ GeV) in $e^+e^- \to \mu^+\mu^-$ is $A_{FB} = -0.0001$ whereas in the improved Born-approximation one finds $A^0_{FB} = 0.0155$ (see section 7.2).

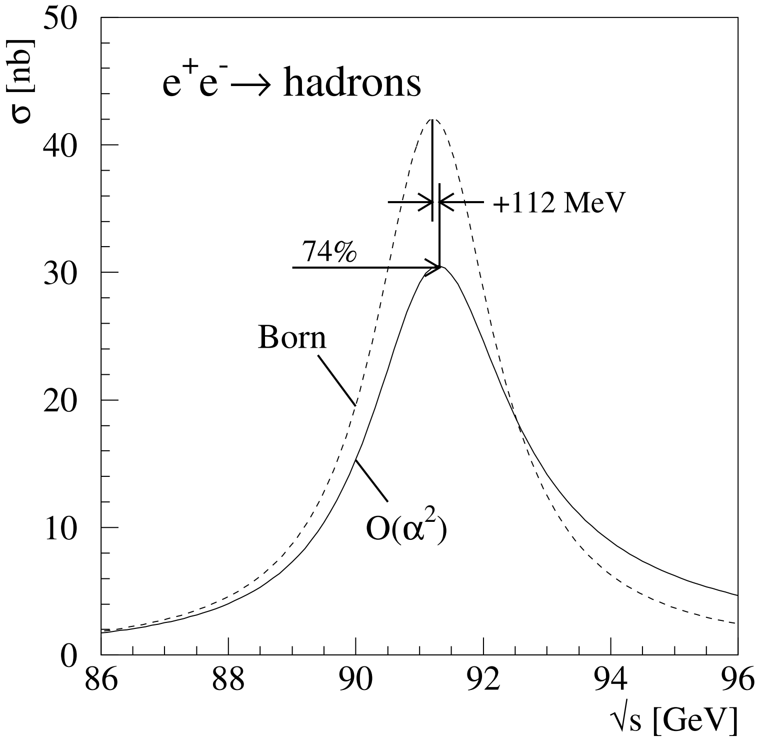

Figure 11: The cross section $e^+e^- \to$ hadrons including $\mathcal{O}(\alpha^2)$ corrections (solid line) compared to the lowest order cross section (broken line) at the Z resonance.

3.5 QCD radiative corrections in $e^+e^- \to$ hadrons

Apart from the higher order QED effects discussed above the cross section $e^+e^- \to$ hadrons is also modified by QCD corrections. They consist of gluons exchanged between or radiated from the quarks in the final state in a similar way as additional photons lead to QED radiative corrections (figure 13).

The radiation of gluons alters the event shape of hadronic Z decays. The rate of these '3-jet' events depends on the strong coupling constant α_s which provides an excellent way to measure its value at the mass of the Z [50, 51]. In this article α_s denotes the value of the strong coupling which it acquires at the Z mass $\alpha_s \equiv \alpha_s(m_Z)$.

Apart from modifying the shape of hadronic Z decays the hadronic decay width and thus the total cross sections $e^+e^- \to$ hadrons is modified by QCD corrections as a function of α_s. As the hadronic width contributes to about 70% to the total width the latter also depends on these corrections and thus indirectly all cross sections at the Z pole. In section 6.3 the precision measurements of total cross sections at LEP are used to extract the strong coupling constant α_s and to compare it to other determinations.

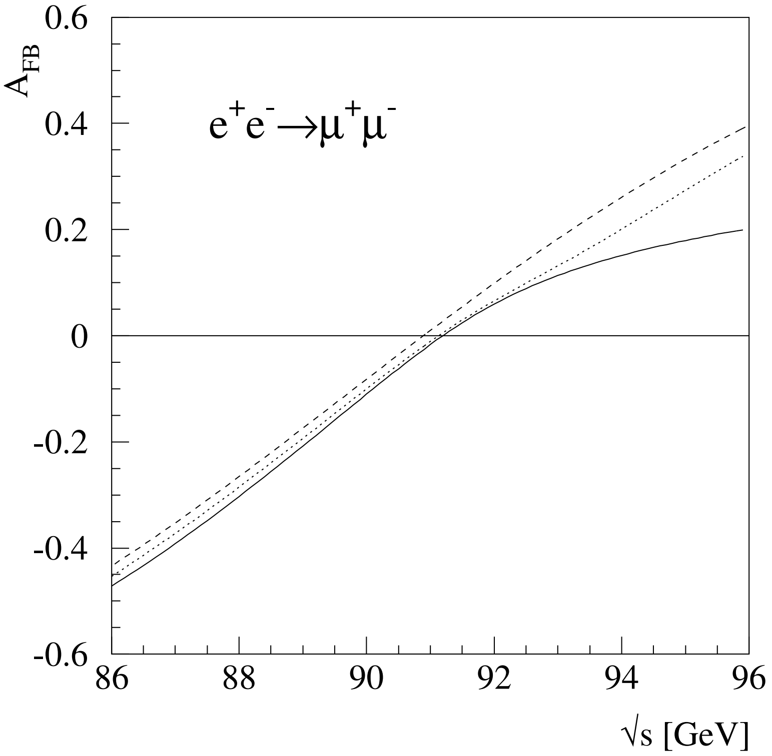

Figure 12: Forward-backward asymmetry in $e^+e^- \rightarrow \mu^+\mu^-$ including $\mathcal{O}(\alpha^2)$ corrections for an acolinearity $\xi \leq 15^\circ$ (solid line) and $\xi \leq 2^\circ$ (dotted line) compared to the lowest order (broken line).

3.6 Monte Carlo programs and analytical calculations

The precise measurements of cross sections and asymmetries requires a very good knowledge of the acceptance, selection efficiency and background contributions for a given reaction $e^+e^- \rightarrow f\bar{f}$. As discussed above cut dependent QED radiative corrections are large compared to the experimental precision and hence must be accounted for. Several groups of theoreticians have developed tools such as Monte Carlo generators which allow the exact simulation of experimental cuts and fast analytical calculations where only simple kinematical cuts can be accounted for in the integrations. The latter are necessary to be able to determine electroweak parameters from the measurements in an iterative fitting procedure.

To determine experimental acceptances and efficiencies in $e^+e^- \rightarrow$ hadrons the Monte Carlo generators HERWIG [52] and JETSET [53] are commonly used by the LEP experiments. These two programs treat the fragmentation of quarks and gluons into hadrons observed in the detectors in different ways. The production of muon and tau pairs is simulated by the KORALZ [54] program. The additional contributions for the t-channel and s-t interference in $e^+e^- \rightarrow e^+e^-$ is accounted for in the Monte Carlo generators and semi-analytical calculations ALIBABA [55], BHAGENE3 [56], UNIBAB [57] and TOPAZ0 [58]. For the simulation of detector response the experiments use the program GEANT [59] adopted to the particular

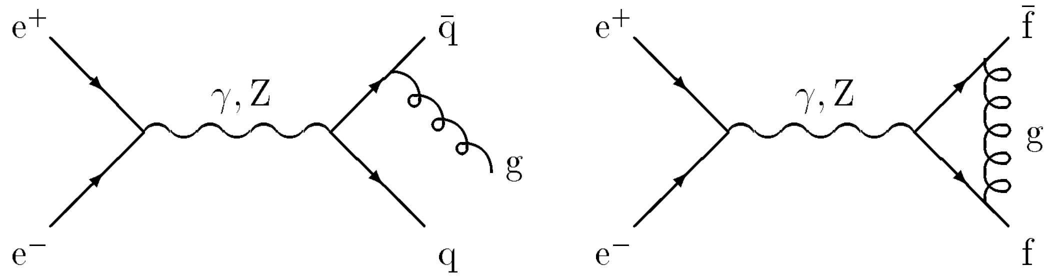

Figure 13: Examples of higher order QCD processes in $e^+e^- \to$ hadrons.

experimental setup. Hadronic shower simulation is done using GHEISHA [60].

For the calculation of the accepted cross section in the luminosity monitors the programs BHLUMI [61] and BABAMC [62] are available where the latter is mainly used to calculate the contribution from the γ–Z interference at small scattering angles. Until recently the accuracy of the BHLUMI $e^+e^- \to e^+e^-$ cross section calculation in the angular region used to determine the luminosity was estimated to be $\Delta\sigma_{e^+e^-}/\sigma_{e^+e^-} = 2.5 \cdot 10^{-3}$. This number arises from missing higher order contributions and the numerical precision of the computer program. This theoretical uncertainty is larger than the typical experimental error of the luminosity measurement of about $1 \cdot 10^{-3}$ achieved by the LEP detectors in 1993 (see section 4.3). It leads to an error common to all four LEP experiments limiting the experimental precision on the invisible width $\Gamma_{\rm inv}$ (see section 6.1). Now improved second-order Monte Carlo calculations implemented in the computer program BHLUMI 4.01 [63] are available. This improves the theoretical accuracy of the luminosity determination to $1.6 \cdot 10^{-3}$ and hence largely reduces the experimental precision on the hadronic pole cross section and the invisible width. Further work on calculation of additional QED corrections and improvements of the numerical accuracy of the computer codes is going on which in future should reduce the theoretical error to the level of the experimental error or below.

Analytical calculations of cross sections and asymmetries in $e^+e^- \to f\bar{f}$ including higher order corrections are necessary to compare to the experimental measurements and to extract electroweak parameters. The two programs ZFITTER [64] (DELPHI, L3, OPAL) and MIZA [65] (ALEPH) are used by the experiments. These programs allow the calculation of cross sections and asymmetries with some experimental cuts applied. ZFITTER includes electroweak radiative corrections to $\mathcal{O}(\alpha)$ and a common exponentiation of initial- and final-state bremsstrahlung. The corrections $\mathcal{O}(\alpha^2)$ are taken into account in the leading-log approximation and include the production of photon and fermion pairs in the initial state. Furthermore, the $\mathcal{O}(\alpha)$ and $\mathcal{O}(\alpha^2)$ corrections are supplemented with the $\mathcal{O}(\alpha\alpha_s m_t^2/m_W^2)$ and $\mathcal{O}(\alpha^2 m_t^4/m_W^4)$ from top quark insertions in the gauge boson self energies and in the $Zb\bar{b}$ vertex. In the case of the b-quark asymmetries, the $\mathcal{O}(\alpha\alpha_s m_t^2/m_W^2)$ corrections of the $Zb\bar{b}$ vertex are not included as they are not yet available. QCD corrections in final states with quarks are considered up to $\mathcal{O}(\alpha_s^3)$. The t-channel contribution and the s–t interference in $e^+e^- \to e^+e^-$ is calculated with ALIBABA or TOPAZ0 and added to the s-channel calculation of ZFITTER.

ZFITTER allows the calculation of cross sections and asymmetries from a Breit-Wigner ansatz of the resonance and the effective couplings of the fermions. Alternatively, all calculations can be done in the Standard Model framework using the input parameters described in section 3.1.

The electroweak parameters are determined in a χ^2 fit using the MINUIT program [66]. The χ^2 is derived from the measurements, their errors including the correlations and the analytical calculation.

If not stated otherwise, throughout this article Standard Model calculations are performed using the program ZFITTER 4.9. The input parameters used are summarized in eq. 42 with their values and errors or the range of variation:

$$\begin{aligned} m_{\mathrm{Z}} &= 91\,188 \pm 2 \text{ MeV} \\ m_{\mathrm{t}} &= 175 \text{ GeV} \qquad (100,\ 250 \text{ GeV}) \\ m_{\mathrm{H}} &= 300 \text{ GeV} \qquad (60,\ 1000 \text{ GeV}) \\ 1/\alpha(m_{\mathrm{Z}}) &= 128.90 \pm 0.09 \\ \alpha_{\mathrm{s}} &= 0.123 \pm 0.006\,. \end{aligned} \tag{42}$$

This particular choice is motivated by the discussion in the previous sections and by the experimental results discussed below. The only reason for selecting $m_{\mathrm{H}} =$ 300 GeV as the central value for the Higgs mass is that due to the logarithmic dependence of observables on m_{H} the two boundaries lead to approximately symmetric shifts around the central value.

4 The LEP storage ring and the four experiments

4.1 The Large Electron Positron Collider LEP

The Large Electron Positron collider LEP at CERN [11, 67] is situated in a tunnel of 27 km circumference on both sides of the border between France and Switzerland (see figure 14). It was commissioned in 1989 and has been very successfully operated ever since. The main components of the collider are

- eight bending sections of 2840 m length each, with in total 3304 dipole magnets. At 45 GeV beam energy, the required field is 0.048 T,
- eight straight sections, four of which house the experiments ALEPH [68], DELPHI [69], L3 [70] and OPAL [71]. On both sides of each experiment, the beam is focussed with superconducting quadrupole magnets, increasing the luminosity,
- two straight sections containing the radio frequency cavities with a total power of 16 MW, to accelerate the beam from injection energy to collision energy and to replace the energy lost by synchrotron radiation on each turn,
- the existing accelerators PS and SPS, which are used as part of the injection system in addition to the linear accelerator LIL and an accumulation ring to enhance the positron intensity.

At the beginning of each LEP fill, positrons and electrons are injected at an energy of 20 GeV. After ramping to collision energies, the beam lifetime is usually

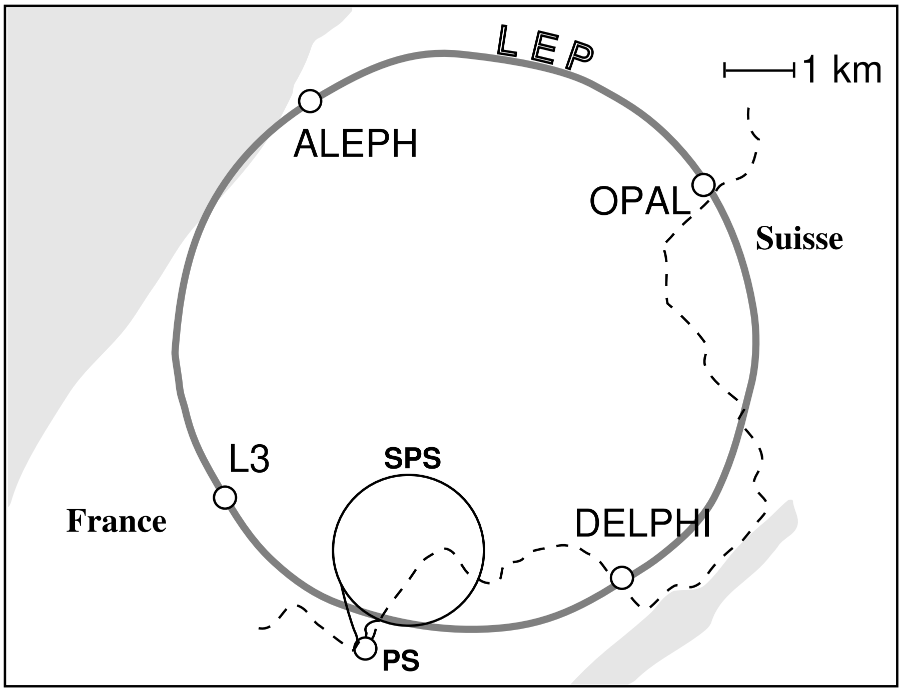

Figure 14: The LEP collider at CERN.

of the order of 20 hours at a typical total current of more than 3 mA. The typical instantaneous luminosity delivered to the experiments in 1994 was $15 \cdot 10^{30}$ cm^{-2}s^{-1}.

In agreement with the originally proposed schedule of LEP, the collider has so far been run at energies at the Z resonance. Figure 15 shows the history of integrated luminosity delivered to the experiments for the five running periods 1990 – 1994. As can be seen from this figure the integrated luminosity has been continuously increased such that by the end of 1994 LEP has delivered more than 150 pb^{-1} to each experiment. From the end of 1992 onwards LEP was mostly operating with eight electron bunches colliding with eight positron bunches (Pretzel scheme [72, 73]).

After the initial run in 1989 and the first measurement of the Z mass and width at LEP two scans of the Z resonance were performed in 1990 and 1991 with about 60% of the luminosity taken on the peak and the rest at six energy points approximately ± 1, ± 2 and $\pm$ 3 GeV off the peak. These runs led to a precise determination of the mass and the total width of the Z boson [74, 75, 76].

In 1992 data were only taken on the peak. The main benefits of these data are the high statistics measurements of lepton cross sections and asymmetries which significantly improved the precision of the ratio of hadronic to leptonic partial width, R_ℓ, and of the coupling constants, $\bar{g}_{\mathrm{A}}$ and $\bar{g}_{\mathrm{V}}$, of charged leptons [77].

In 1993 another scan of the Z resonance curve was performed. Out of the total of 40 pb^{-1} delivered to each experiment half of this luminosity was taken at two energy points approximately 2 GeV below and above the Z pole which quadrupled the total number of events at $\sqrt{s} \neq m_{\mathrm{Z}}$ collected by the experiments. Together with the better determination of the LEP beam energies (see section 4.2) this leads to a

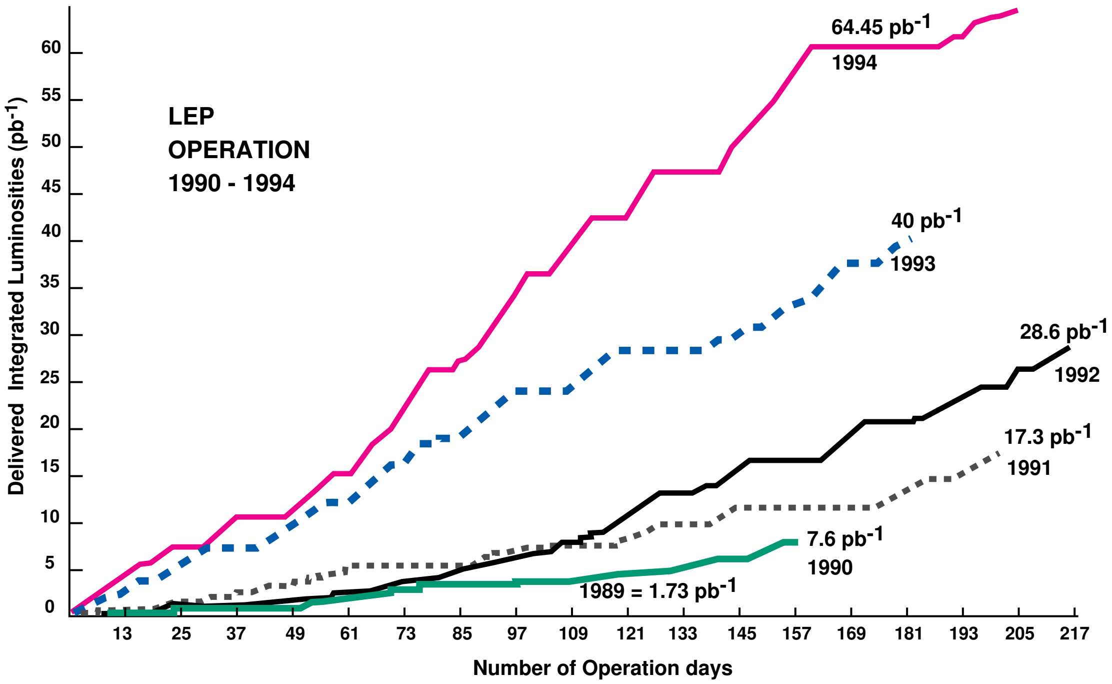

Figure 15: The integrated luminosity delivered by the LEP collider to each of the experiments for the five running periods 1990 – 1994.

reduction of the error of m_Z and Γ_Z by a factor of three and two, respectively, and significant improvements in many other electroweak parameters.

A high luminosity run providing 60 pb^{-1} per experiment at $\sqrt{s} = m_Z$ was carried out in 1994. At this moment preliminary results of these data are only partially available.

It is foreseen to further increase the luminosity of LEP by increasing the number of circulating bunches (Bunch-Train scheme [78, 79]) in 1995. This will be exploited to scan again the Z resonance to further improve the precision on m_Z and Γ_Z. Also, a pilot run at $\sqrt{s} \approx 140$ GeV is planned. This will conclude the LEP I program before in 1996 after installation of additional superconductive cavities the $e^+e^- \rightarrow W^+W^-$ threshold will be crossed (LEP II).

4.2 Calibration of the LEP beam energy

An important ingredient for the determination of the mass and the total width is the precise knowledge of the LEP beam energy. Several techniques [80, 81, 82] have been employed to measure it, the most precise being the one using resonant spin depolarization. This technique was successfully established at $\sqrt{s} \approx 93$ GeV in late 1991 during the scan of the Z resonance and a precision of $\Delta E_b/E_b = 5.7 \cdot 10^{-5}$ in the absolute beam energy scale was achieved.

The beam energy measurement by resonant depolarization is based on the fact that in e^+e^- storage rings like LEP transverse polarization of the circulating particles can build up, known as the Sokolov-Ternov effect [83]. With a small, but finite, probability synchrotron radiation flips the spin vector of the electron. This spin flip probability is asymmetric since the electron spin tends to align with the direction of the magnetic field in the dipole magnets.

However, there are competing effects which randomize the spin direction and thus depolarize the beam. Among these are synchrotron and betatron oscillations, imperfections of the magnetic field and electromagnetic interactions between the particle bunches squeezed at the collision points to optimize the luminosity. For this reason at LEP significant transversal polarization has only been achieved so far under special operation conditions, and up to the end of 1993, with only one particle type (electrons or positrons) circulating in the machine.

Once polarized the spin vector of the electrons precesses around the $\vec{B}$ field created by the dipole magnets. From the general Thomas-BMT equation [84] one derives the relation between the particle energy and the of number spin precessions per revolution around the storage ring, the spin tune ν_{s}:

$$\nu_{\mathrm{s}} = \frac{g_{\mathrm{e}} - 2}{2\, m_{\mathrm{e}}} \cdot E_{\mathrm{b}} = \frac{E_{\mathrm{b}}}{440.6486(1)\ \mathrm{MeV}} \tag{43}$$

Here g_{e} denotes the factor parametrizing the anomalous magnetic moment of the electron.

The spin tune and hence the beam energy can be measured by depolarizing with an external high frequency magnet creating a local field perpendicular to the initial polarization vector. At each passage it rotates the particle spin a bit and if its frequency matches the fractional part of the spin tune the rotations add up coherently. At this resonance condition the transversal polarization is destroyed, or even inverted, which is measured using a Compton polarimeter [85, 86]. The integral part of the spin tune is readily obtained from the dipole currents.

The spin tune ν_{s} must not be close to an integer value to avoid rapid depolarization by small imperfections of the dipole field. In practice suitable points for precise energy calibration are separated by $\Delta\nu_{\mathrm{s}} = \pm 1$, i.e. by ± 0.88 GeV in center-of-mass energy.

The method of resonant depolarization has an intrinsic accuracy of better than 0.2 MeV on the beam energy [87]. As the depolarization measurement cannot be done with colliding beams the center-of-mass energy in luminosity runs must be obtained from extrapolation of dedicated calibration runs. The uncertainty introduced by this extrapolation is the main contribution to the absolute scale error.

In 1991 the energy calibrations have been performed at one energy and they have to be transported to the other scan points using magnetic measurements. The limited knowledge of non-linearities in the bending dipoles leads to a local extrapolation error which mainly affects the determination of the total width. Other possible uncertainties of the LEP machine (setting precision, reproducibility) have been studied in detail [81] and the combined effect on the mass and the total width for the 1990 and 1991 energy scans is found to be [75]:

$$\begin{aligned} \Delta m_{\mathrm{Z}} &= \pm 6.3\ \mathrm{MeV} \\ \Delta \Gamma_{\mathrm{Z}} &= \pm 4.5\ \mathrm{MeV}. \end{aligned} \tag{44}$$

The method of resonant depolarization has been further developed in 1993 [86] where the electron beam could be transversely polarized above and below the Z pole at energies $\sqrt{s} \approx m_Z \pm 1.8$ GeV. This results in a better determination of the energy difference of the two points and hence in a reduced error on the measurement of the total width Γ_Z. Also, improved monitoring of beam energy changing parameters (temperatures, radio frequency etc.) and frequent calibration runs, usually performed right after a luminosity run, lead to a further reduction in the uncertainty of the absolute beam energy. In total, 24 calibrations of the energy were performed at the end of luminosity runs in the course of the energy scan in 1993. The resulting contribution to the error on the Z mass and total width is estimated to be [88][5]

$$\begin{aligned} \Delta m_Z &= \pm 1.4 \text{ MeV} \\ \Delta \Gamma_Z &= \pm 1.5 \text{ MeV}. \end{aligned} \tag{45}$$

The values obtained for the absolute beam energy calibration for the various LEP runs are summarized in table 7.

period	$\Delta E_b/E_b$ $[10^{-5}]$	center-of-mass energy
1990	29	m_Z, $m_Z \pm$ 1, 2, 3 GeV
before Aug. 14, 1991	20	m_Z
after Aug. 14, 1991	5.7	m_Z, $m_Z \pm$ 1, 2, 3 GeV
1992	20	m_Z
before June 27, 1993	20	m_Z
after June 27, 1993	1.5	m_Z, $m_Z \pm 2$ GeV
1994	4	m_Z

Table 7: Precision achieved for the absolute LEP beam energy 1990 – 94. The result for 1994 is preliminary. The approximate center-of-mass energies of the LEP runs are also indicated.

As can be seen from figure 12 the leptonic forward-backward asymmetries vary steeply around the Z pole[6]:

$$\left.\frac{\mathrm{dA_{FB}}}{\mathrm{dE}}\right|_{E=m_Z} = \frac{0.0088}{100 \text{ MeV}} \ . \tag{46}$$

When determining electroweak couplings from these asymmetries an uncertainty in the center-of-mass energy thus translates into an effective error on these couplings. Expressed in terms of the lowest order pole forward-backward asymmetry A^0_{FB} (see appendix A) and using the numbers in table 7 weighted by the luminosity collected at the different periods the contribution to the error of A^0_{FB} is estimated to be

$$\Delta A^0_{\mathrm{FB}} = \pm 0.0005. \tag{47}$$

The experiments take care of LEP energy errors in their fitting procedures applied to the measured cross sections and asymmetries to extract the Z parameters. These

[5]The experiments estimate the contribution of the beam energy uncertainty to the m_Z and Γ_Z error comparing fits with and without including beam energy uncertainties. Typical results obtained are $\Delta m_Z = \pm 1.5$ MeV and $\Delta\Gamma_Z = \pm 1.7$ MeV consistent with eq. 45. In section 5 the latter set of errors is used to form the averages.

[6]For $e^+e^- \to e^+e^-$ this applies only for the s-channel contribution to A_{FB}.

errors are common to all experiments and have to be properly accounted for when averaging the results.

The energy distribution of electrons and positrons circulating in a e^+e^- storage ring has a finite width due to synchrotron oscillations. The width of this distribution depends on the machine parameters. From the observed length of the particle bunches in LEP one deduces an effective spread of the center-of-mass energy around its nominal value of [88]:

$$\Delta\sqrt{s} = 55 \pm 5 \text{ MeV} \qquad (1993). \tag{48}$$

This distribution is assumed to be gaussian. The experiments observe a convolution of cross sections at energies scattering around a central value. The modification of the observed cross section, as compared to the one expected for a fixed energy, is proportional to the second derivative of the cross section with respect to the center-of-mass energy. The main effect is that the observed total cross section at the Z pole is lowered by 0.16% which in case of the hadronic cross section represents a sizeable correction. On the wings of the resonance the convoluted cross section is slightly higher than the one at the nominal energy. Since it does not scale with the cross section the beam energy spread has to be taken into account for the extraction of the Z parameters from the measured cross sections. The error given in eq. 48 translates to an uncertainty on Γ_Z of ± 1 MeV which has to be added to the error given in eq. 45. The additional error from this source on the Z mass is negligible.

4.3 The LEP experiments

The four LEP experiments ALEPH, DELPHI, L3 and OPAL are described in detail in references [68]–[71]. Here only a short overview on the most important experimental parameters for cross section measurements is given.

In table 8 the number of events used for cross section measurements by the experiments are listed. At the end of 1993 each experiment had collected about two million Z decays out of which about 200 000 are decays into charged lepton pairs. This ratio of observed hadronic to leptonic events is explained by the large branching ratio of the Z into hadrons (see table 5) and the fact that the experimental acceptance for hadronic events is generally larger than for lepton pairs.

	ALEPH	DELPHI	L3	OPAL
hadrons	1 771 k	1 730 k	1 748 k	1 833 k
leptons	215 k	177 k	159 k	228 k

Table 8: Event samples obtained in 1989–1993 used for cross section measurements by the four LEP experiments.

The cross sections and lepton forward-backward asymmetries obtained in 1989 – 1992 are already published (see references [89]–[100]). Details on experimental procedures and uncertainties can be found in these publications.

The 1993 data included in this article are still preliminary as the results on cross sections and forward-backward asymmetries are not final. In 1994 each of the experiments has collected approximately 1.5 million hadronic and 160 000 leptonic Z decays. Preliminary results from these data are only partially available and included in the fits where possible [19].

It should be noted that at the end of 1994 the LEP experiments have observed about $1.4 \cdot 10^7$ Z decays. The large number of accumulated events enables the experiments to study the detectors in great detail and to make full use of their capabilities. The experimental systematic errors on cross section measurements are small and similar for the four detectors. The error, excluding the contribution from luminosity, on the cross section $e^+e^- \rightarrow$ hadrons is typically 0.15% and for leptonic Z decays 0.3 – 0.5%, slightly higher for $e^+e^- \rightarrow \tau^+\tau^-$ due to the many different τ decay channels.

The experimental systematic error on the luminosity was typically 0.5% up to the end of 1992. With the improved luminosity monitors installed for the 1993 run (see for instance [101]) the experimental error achieved is of the order of 0.1%. In addition, there is a 0.16% contribution to the luminosity error common to all experiments which arises from the theoretical calculation of the low angle Bhabha scattering cross section [63].

A detailed comparison of the systematic errors on cross section and forward-backward asymmetry measurements can be found in reference [19, 102].

5 Results from the measurement of total cross sections at the Z resonance

5.1 Total cross sections at the Z resonance

The LEP experiments measure the total cross sections of four different reactions

$$
\begin{array}{ll}
e^+e^- \rightarrow \text{hadrons} & \qquad e^+e^- \rightarrow e^+e^- \\
e^+e^- \rightarrow \mu^+\mu^- & \qquad e^+e^- \rightarrow \tau^+\tau^-
\end{array}
$$

as a function of the center-of-mass energy. There are also cross section measurements of the reaction $e^+e^- \rightarrow \nu\bar{\nu}\gamma$ available which measures independently the invisible width of the Z and hence the number of light neutrino families (see section 6.2).

From the measurements of the total cross sections six quantities can be derived:

- the position of the peak yields the mass m_Z,
- the width of the curve yields the total width Γ_Z
- and the peak cross sections determine the partial widths of the Z decaying into hadrons Γ_{had}, electrons Γ_e, muons Γ_μ and taus Γ_τ (see eq. 16).

If lepton universality is assumed the leptonic cross sections are fitted to a common leptonic width Γ_ℓ and the number of fit parameters reduces to four.

The fit is performed using a Breit-Wigner ansatz. The total cross section as function of the center-of-mass energy is expressed in terms of mass, total and partial widths of the Z boson which are the free parameters of the fit. This way one does not imply Standard Model relations for these parameters and, in particular, the total width is not restricted by the sum of the partial decay widths into known particles. This ansatz describes the cross section by the subsequent formation and decay of a resonance $e^+e^- \to Z \to f\bar{f}$ [64]. The photon exchange as calculated from QED and the interference of the photon and the heavy boson are taken into account:

$$\begin{aligned}
\sigma^{\rm f}(s) &= \sigma^{\rm f}_{\rm Z} + \sigma^{\rm f}_{\gamma} + \sigma^{\rm f}_{\rm int} \\
\sigma^{\rm f}_{\rm Z} &= \frac{12\,\pi}{m_{\rm Z}^2}\,\Gamma_{\rm e}\Gamma_{\rm f}\,\frac{s}{(s-m_{\rm Z}^2)^2 + s^2\,\Gamma_{\rm Z}^2/m_{\rm Z}^2} \\
\sigma^{\rm f}_{\gamma} &= \frac{4\,\pi\alpha^2}{3\,s}\,Q_{\rm e}^2 Q_{\rm f}^2 N_c^{\rm f} \\
\sigma^{\rm f}_{\rm int} &= \frac{4\,\pi\alpha^2}{3}\,J_{\rm f}\,\frac{s-m_{\rm Z}^2}{(s-m_{\rm Z}^2)^2 + s^2\,\Gamma_{\rm Z}^2/m_{\rm Z}^2}\,.
\end{aligned} \tag{49}$$

QED radiative corrections are included by convoluting this cross section with radiator functions allowing also for experimental cuts on detector acceptance and photon phase space. QCD corrections and mass effects are accounted for. The two programs ZFITTER [64] (DELPHI, L3 and OPAL) and MIZA [65] (ALEPH) are used by the experiments.

The γ–Z interference cannot be expressed in terms of the free parameters $m_{\rm Z}$, $\Gamma_{\rm Z}$ and $\Gamma_{\rm f}$. Thus, it is usually expressed by the Standard Model equation

$$\begin{aligned}
J_{\rm f} &= \frac{G_{\rm F}\,m_{\rm Z}^2}{\sqrt{2}\pi\,\alpha}\,N_c^{\rm f}\,Q_{\rm e}Q_{\rm f}\,\bar{g}_{\rm V}^{\rm e}\bar{g}_{\rm V}^{\rm f} + \cdots \\
J_{\rm had} &= \sum_{\rm q} J_{\rm q} \qquad {\rm q} = {\rm u, d, s, c, b}
\end{aligned} \tag{50}$$

Even though $\sigma_{\rm int}$ is small around the Z pole it is important for the measurement of $m_{\rm Z}$. Fixing $J_{\rm f}$ to the Standard Model expectation implies some dependence of the extracted heavy boson mass on the validity of the Standard Model.

Because about 90% of the observed Z's decay into hadrons (see table 8) the hadronic cross sections dominate the results on the mass and the total width of the Z. Using $J_{\rm had}$ from the Standard Model prescribes the quark composition of hadronic Z decays and the coupling constants of quarks to the expected values. Experimentally, the couplings of the Z to quarks are not known for all flavors.

Alternatively, the hadronic interference term $J_{\rm had}$ can be left free as an additional parameter in the fit and determined from the total cross sections. However, as $\sigma_{\rm int}$ is small compared to $\sigma_{\rm Z}$ the precision on $J_{\rm had}$ is poor and a sizeable additional uncertainty is added to the mass measurement (see section 5.3).

A particular problem is the contribution from the t-channel photon exchange in $e^+e^- \to e^+e^-$. To minimize this effect the experiments limit their polar angle acceptance to the central region (typically $45° < \theta < 135°$) where the s-channel Z exchange dominates. The remaining contributions from t-channel and s–t interference are calculated using the ALIBABA [55], BHAGENE3 [56] and TOPAZ0 [58] programs to correct the observed cross sections.

As an example figure 16 shows the measured cross section $e^+e^- \to e^+e^-$ from the L3 experiment (data from 1990–92 [97]) in the angular range $44° < \theta < 136°$ as a function of the center-of-mass energy together with the result of the fit to all measured hadronic and leptonic cross sections. The individual contributions from the s- and t-channel exchange as well as their interference are shown separately. The

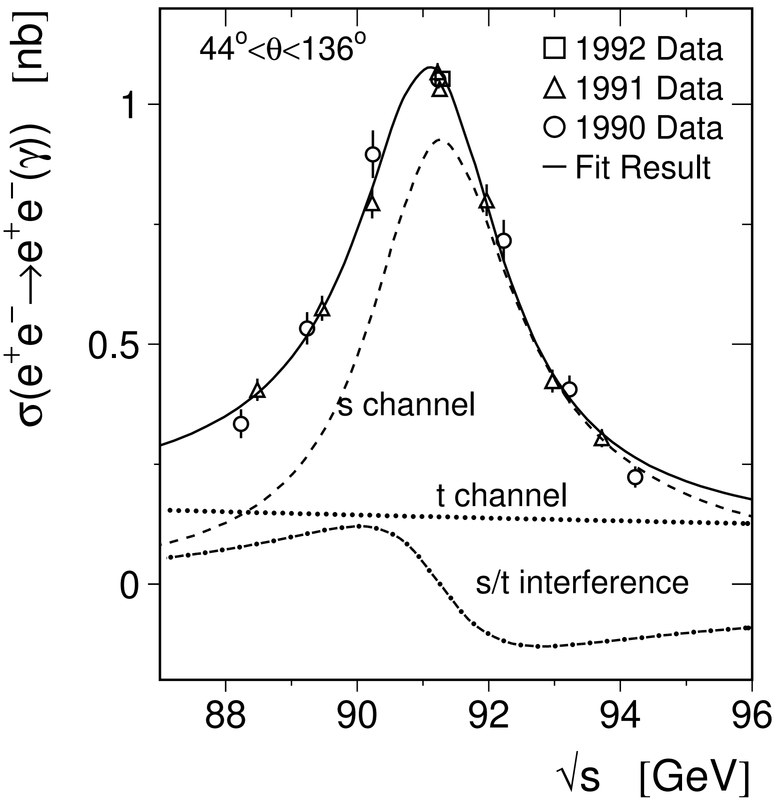

Figure 16: The cross section $e^+e^- \to e^+e^-$ at the Z resonance measured by the L3 experiment. The result of the fit is shown together with the individual contributions of the s- and t-channel (see text).

t-channel and the s–t interference are calculated with the ALIBABA program using the results of the fit in an iterative manner since the s–t interference contribution depends itself on the Z parameters and hence on the result of the fit.

Figure 17 shows the hadronic cross section as function of the center-of-mass energy obtained by the L3 experiment. The solid line is the result of the Breit-Wigner fit. The excellent agreement of data and fit can be seen from the bottom part of figure 17 where the ratio of measured cross section and the fit result is shown. The error bars indicate the statistical error of the data points. For better visibility the $\sqrt{s}$ values for the data sets on the Z peak are shifted slightly to the left and right.

One clearly notices the drastic improvement in statistics for $\sqrt{s} \neq m_Z$ achieved in the 1993 run. This is together with the improved LEP energy calibration the reason for the improvement of the mass and total width measurement compared to the previous scans. The data taken at the pole are split according to the LEP energy calibration periods given in table 7. The high statistics pole cross sections are in reasonable agreement among each other indicating a good control of the experimental apparatus during this long period of data taking.

The Z parameters discussed in this section can be derived from the measurements of total cross sections only. However, the results presented here are obtained from

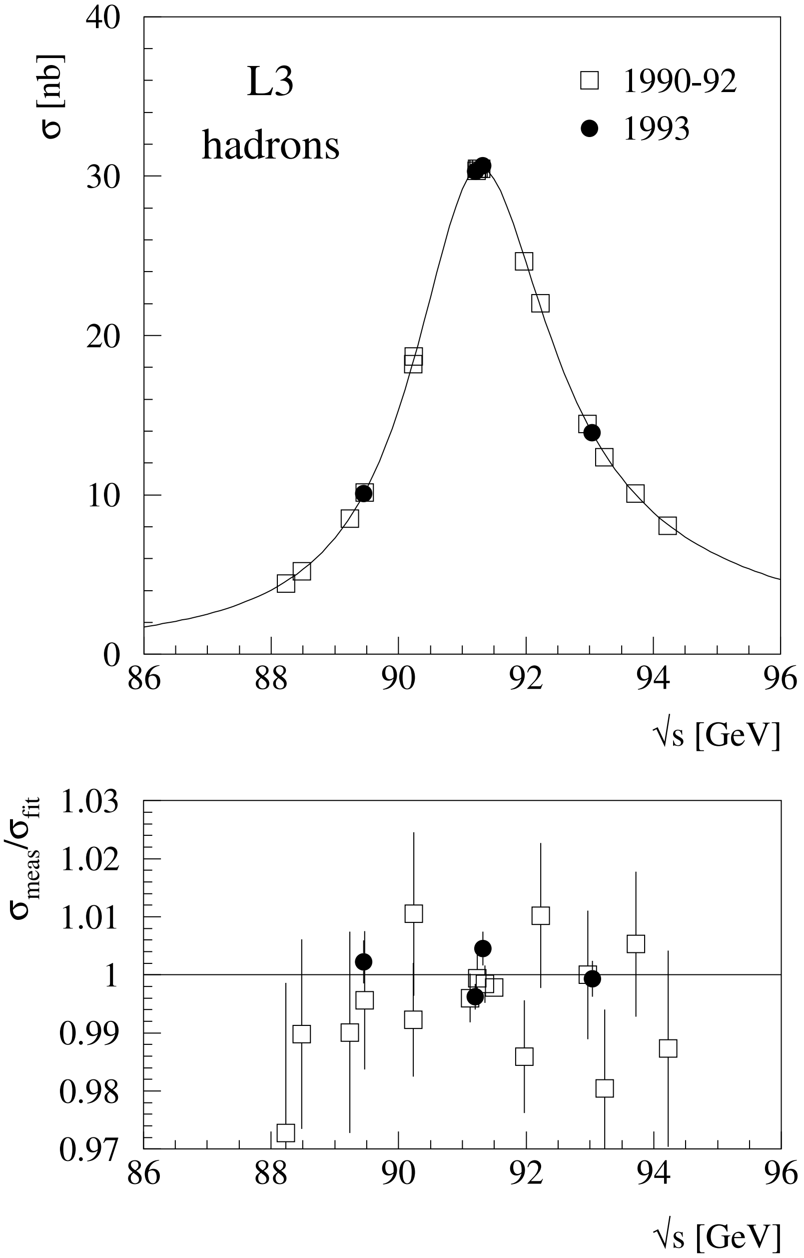

Figure 17: The cross section $e^+e^- \to$ hadrons at the Z resonance measured by the L3 experiment. The lower plot shows the ratio of the measured cross sections and the fit result together with the statistical error.

a common fit to total cross sections and lepton forward-backward asymmetries (see appendix A) which enables comparisons of the results among the experiments [77, 103]. The asymmetries add only little information to the mass and the widths and thus do not change significantly the results obtained from the total cross sections alone.

5.2 Definition of the Z mass and width

The ansatz of eq. 49 defines the Z mass m_Z and the total width Γ_Z as parameters of a Breit-Wigner resonance. This form arises from an ansatz for the Z propagator with an energy dependent imaginary part, i.e. an energy dependent width:

$$D_Z(s) = \frac{1}{s - m_Z^2 + i\, s\, \Gamma_Z / m_Z} \tag{51}$$

Such a propagator is motivated by quantum gauge theory in which the width is understood as the result of quantum corrections and therefore has a natural energy dependence [64]. The Z mass and total width quoted by the LEP experiments correspond to this definition.

There are other possible ways of defining these two parameters. The resonance can be described by a constant imaginary part of the Z propagator:

$$D_Z(s) = \frac{1}{s - \overline{m}_Z^2 + i\, \overline{m}_Z\, \overline{\Gamma}_Z} \tag{52}$$

Comparing the poles of eqs. 51 and 52 one finds that the two definitions of the mass and total width are related [104]:

$$\begin{array}{rclcl} \overline{m}_Z & = & m_Z\,(1 + \Gamma_Z/m_Z)^{-1/2} & \approx & m_Z - 34 \text{ MeV} \\ \overline{\Gamma}_Z & = & \Gamma_Z\,(1 + \Gamma_Z/m_Z)^{-1/2} & \approx & \Gamma_Z - 1 \text{ MeV} \end{array} \tag{53}$$

This definition is equivalent to starting from the energy dependent imaginary part in the propagator (eq. 51) and defining the mass as the real part of the pole in the complex s-plane:

$$s_0 = \overline{m}_Z^2 + i\, \overline{m}_Z\, \overline{\Gamma}_Z \tag{54}$$

Conventionally, the mass of an unstable particle is defined by the pole in the energy plane

$$s_0 = \left(\overline{m}'_Z - \frac{i}{2} \overline{\Gamma}'_Z \right)^2 \tag{55}$$

which leads to a slightly different shift compared to the definition of m_Z:

$$\overline{m}'_Z \;=\; m_Z \left[1 - \tfrac{3}{8}\,(\Gamma_Z/m_Z)^2 + \mathcal{O}\,(\Gamma_Z/m_Z)^4 \right] \;\approx\; m_Z - 25 \text{ MeV} \tag{56}$$

The issue of the Z mass definition is important as the differences of the various definitions are larger than the experimental error. The theoretical aspects of the different mass definitions are discussed in reference [105].

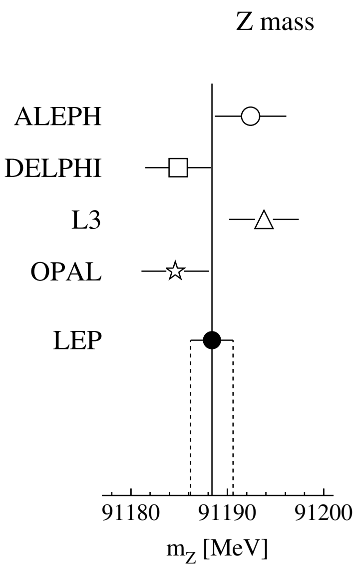

Figure 18: The mass of the Z as determined by the LEP experiments together with the combined result.

5.3 The mass of the Z boson

In figure 18 the values for the Z mass from the four LEP experiments and the combined result are compared. In this, and all similar plots following, the errors shown contain both the uncorrelated part and the part correlated among the experiments. The agreement among the experiments can be seen from the χ^2 value which is obtained from the uncorrelated part of the experimental errors as compared to the combined LEP value. In this example the χ^2 is 6.9 for three degrees of freedom.

Also shown in figure 18 is the combined LEP result for the Z mass

$$m_{\mathrm{Z}} = 91\,188.4 \pm 2.2 \text{ MeV} \tag{57}$$

together with the breakdown of the error in the uncorrelated and common part. In this case the common error is the LEP energy calibration uncertainty (eq. 45).

The mass of the Z is now known very precisely. The relative precision $\Delta m_{\mathrm{Z}}/m_{\mathrm{Z}} = 2.4 \cdot 10^{-5}$ has almost reached the precision of the Fermi constant as measured from the muon lifetime $\Delta G_{\mathrm{F}}/G_{\mathrm{F}} = 2 \cdot 10^{-5}$ [20].

As discussed above the hadronic interference term is fixed to the Standard Model value to obtain the result of eq. 57. Treating this term as a free parameter in the fit results in an additional uncertainty on the Z mass. The L3 experiment has determined J_{had} this way using their data of 1990–91 [106]. The additional error on m_{Z} is found to be:

$$\Delta m_{\mathrm{Z}} = \pm 9 \text{ MeV}. \tag{58}$$

The correlation of m_{Z} and the hadronic interference term J_{had} as obtained by the L3 experiment is shown in figure 19 [97]. The scan of the Z resonance in 1993 with only three different energy points does not improve the determination of J_{had}. From

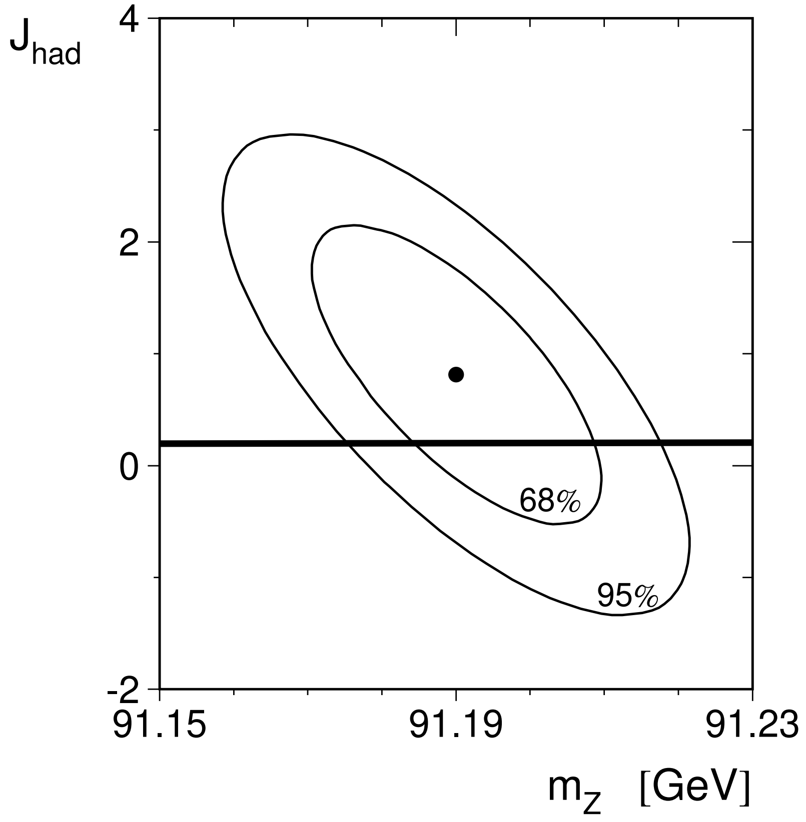

Figure 19: The correlation of the Z mass and the hadronic interference term J_{had} as obtained by the L3 experiment.

three hadron cross section measurements one can only derive m_Z, Γ_Z and Γ_{had} but not further constrain J_{had}. It would be desirable to improve the determination of the γ–Z interference from the data itself to cope with the improvements in the m_Z and Γ_Z measurements. This requires, however, a scan of the Z lineshape with more than only three energy points. The optimum sensitivity for the γ–Z interference is about 5 GeV above and below the Z peak [107, 108].

Alternatively, measurements of the hadronic cross section below the Z resonance can be added to improve the experimental precision on the hadronic interference term. The hadronic cross section measured by the TOPAZ collaboration at the TRISTAN collider ($\sqrt{s}$ = 57.77 GeV) used together with the data of the OPAL experiment (1989-91) yields for the hadronic interference term [109]

$$J_{\mathrm{had}} = 0.10 \pm 0.26 \qquad (59)$$

which is in good agreement with the Standard Model prediction $J_{\mathrm{had}}^{\mathrm{SM}} = 0.22 \pm 0.04$. The inclusion of low energy data significantly reduces the uncertainty on m_Z from the γ–Z interference (see also [110]).

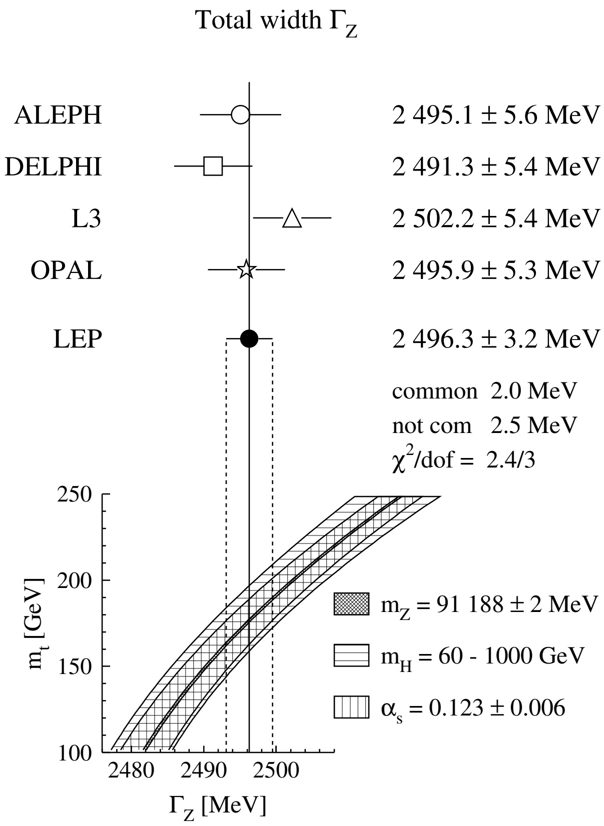

Figure 20: The total width of the Z determined by the LEP experiments together with the combined result and the Standard Model calculation.

5.4 The total width of the Z boson

The next quantity extracted from the measured cross sections is the total width Γ_Z. In figure 20 the results of the LEP experiments are summarized. The four experiments agree well and the combined value is

$$\Gamma_Z = 2\,496.3 \pm 3.2 \text{ MeV}. \tag{60}$$

The error contains a contribution of 2.0 MeV common to all experiments which is the quadratic sum of the LEP energy calibration and the uncertainty of the center-of-mass energy spread (see section 4.2).

At the bottom of figure 20 the LEP mean value for Γ_Z is compared to the Standard Model calculation. The width of the Z as a function of the top quark mass is obtained using the ZFITTER 4.9 [64] program. The hatched bands show the shift of the central value when varying the input parameters inside the limits given in eq. 42.

As can be seen from figure 20 the LEP measurement of Γ_Z is in very good agreement with the Standard Model prediction for top quark masses between 150 and 200 GeV.

It should be noted that the measurement of the total width like the measurement of the Z mass is not affected by uncertainties which scale with the cross section like, for instance, the experimental error in the luminosity measurement. On the other hand, a constant contribution to the cross section has a much larger impact on Γ_Z.

For example, an uncertainty of ± 15 pb in the determination of the non-resonant background in $e^+e^- \to$ hadrons, i.e. $0.5 \cdot 10^{-3}$ of the peak cross section, translates to an error in the total width of $\Delta\Gamma_Z \approx \pm 2$ MeV.

The energy dependence of the theoretical uncertainty in the luminosity measurement has been investigated in reference [111]. It is found that this does not contribute significantly to the error of Γ_Z or m_Z.

5.5 The partial widths into hadrons and charged leptons

The leptonic width is obtained by imposing lepton universality in the fit, i.e. forcing the decay widths into charged leptons to be the same apart from mass effects. The combined LEP value for the leptonic width is

$$\Gamma_\ell = 83.93 \pm\ 0.14 \text{ MeV}. \tag{61}$$

The error contains 0.10 MeV common to all four LEP experiments originating to about equal parts from the theoretical error of the luminosity measurement and the common error on the total width Γ_Z.

As the basic observable, the leptonic peak cross section, is proportional to $(\Gamma_\ell/\Gamma_Z)^2$ the precision on the leptonic width $\Delta\Gamma_\ell/\Gamma_\ell = 0.16\%$ contains a significant contribution from the knowledge of the total width $\Delta\Gamma_Z/\Gamma_Z = 0.13\%$. This part of the error cannot be reduced by further running at $\sqrt{s} = m_Z$ but only through an improved scan of the Z resonance with better LEP beam energy calibration.

In the same fit the hadronic width Γ_{had} of the Z is determined. The experiments find compatible numbers and the average value

$$\Gamma_{\text{had}} = 1744.8 \pm 3.0 \text{ MeV} \tag{62}$$

agrees well with the Standard Model.

Relaxing the condition of lepton universality the individual leptonic decay widths are determined from the fit. The measurements are all in very good agreement, even when taking into account that some fractions of the errors shown are correlated. After combining the experiments figure 21 shows that the individual partial widths into electrons, muons and taus agree to better than 0.5% among each other. This is a strong confirmation of lepton universality in weak neutral currents (see section 8.2).

An even more sensitive test of lepton universality is the comparison of the ratios of the hadronic and the individual leptonic decay widths. These quantities are essentially uncorrelated and they are found to be the same for the three charged leptons with a precision of 0.3% (see appendix A).

It should be noted that owing to the mass of the tau lepton the partial decay width of the Z into tau pairs Γ_τ is expected to be lower than the decay width into a massless charged lepton pair Γ_ℓ [41]

$$\Gamma_\tau \approx \Gamma_\ell \left(1 - 4\,\frac{m_\tau^2}{m_Z^2}\right)^{3/2} = \Gamma_\ell - 0.190 \text{ MeV}. \tag{63}$$

This mass correction is taken into account when obtaining the leptonic width in eq. 61.

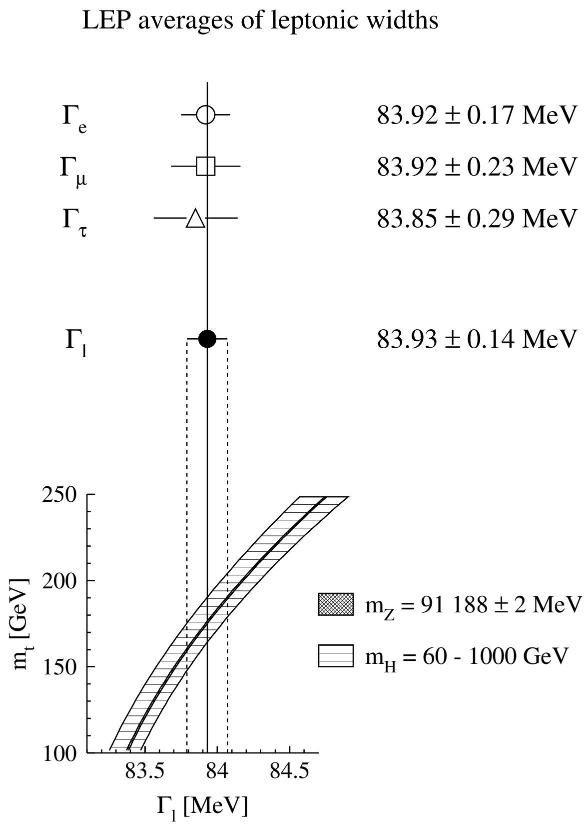

Figure 21: The combined LEP values for the partial widths of the Z into electrons, muons and taus. Also shown is the averaged leptonic decay width and the Standard Model calculation.

6 Results derived from the total and partial widths of the Z

6.1 The invisible width and the number of light neutrino families

From the measurement of the total and partial decay widths into hadrons and charged leptons the decay width of the Z into invisible particles is derived:

$$\Gamma_{\text{inv}} = \Gamma_Z - \Gamma_{\text{had}} - 3\,\Gamma_\ell. \tag{64}$$

Using the results of the five parameter fits (see appendix A) of the four experiments and the average LEP results obtained taking into account the correlations among the total and partial widths the numbers summarized in figure 22 are obtained. The experimental results are in good agreement and the mean value

$$\Gamma_{\text{inv}} = 499.9 \pm 2.5 \text{ MeV} \tag{65}$$

compares well to the Standard Model expectation for three generations of light neutrinos.

The part of the error common to all four experiments (1.8 MeV) is essentially due to the 0.16% error on the luminosity measurements caused by the current precision of

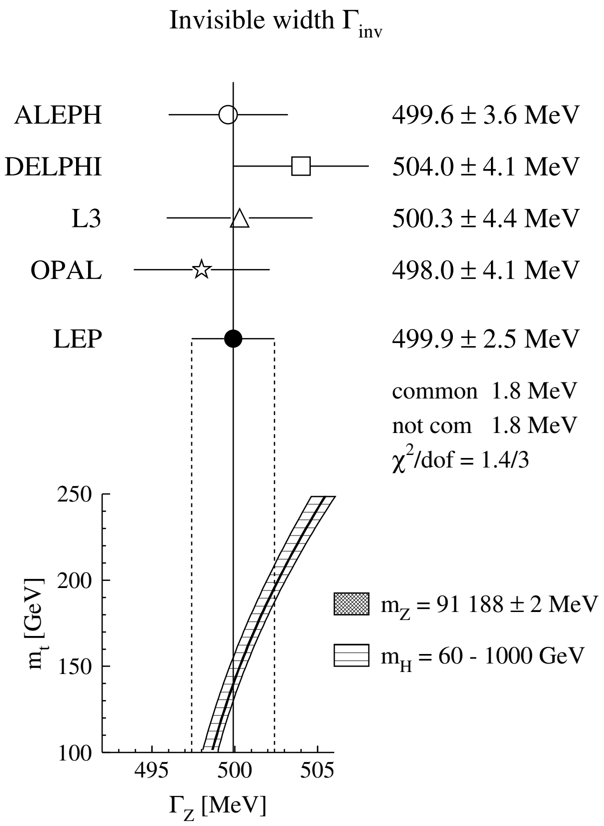

Figure 22: The decay width of the Z into invisible particles as determined from the total and partial decay widths into hadrons and charged leptons compared to the Standard Model calculation for three light neutrino generations.

the theoretical calculation of the small angle bhabha cross section (see section 3.6). The size of the effect on the error of $\Gamma_{\rm inv}$ is estimated following reference [112]. Further progress on the theoretical calculation of small angle Bhabha scattering is necessary to reduce the error on $\Gamma_{\rm inv}$ and to improve this very important test of the Standard Model [113].

The minimum partial width of the Z decaying into a neutrino-antineutrino pair, Γ_ν, allowed in the Standard Model is obtained for the smallest possible top quark mass ($m_{\rm t}$ = 156 GeV[7]) and the largest Higgs boson mass ($m_{\rm H}$ = 1 TeV) to $\Gamma_\nu^{\rm SM} >$ 166.6 MeV. Hence, the invisible width for three generations of light neutrinos is $\Gamma_{\rm inv}^{\rm SM} >$ 500.0 MeV which is well compatible with the experimental result of eq. 65. The precise measurement of $\Gamma_{\rm inv}$ can thus be used to set an upper limit of possible decays of the Z into other, non-observable particles:

$$\begin{aligned} \Gamma(\mathrm{Z} \to \mathrm{X_{inv}}) &< 5.0 \text{ MeV} \\ \text{or} \quad \mathrm{BR}(\mathrm{Z} \to \mathrm{X_{inv}}) &< 2.0 \cdot 10^{-3} \qquad (95\% \text{ C.L.}) \end{aligned} \tag{66}$$

Historically, the determination of $\Gamma_{\rm inv}$ is used to derive the number of light neutrino families N_ν. The first unambiguous determination that there are three and

[7]This is an estimated two standard deviation lower bound from eq. 109

only three light neutrino species has been achieved simultaneously by the five experiments at LEP [114]–[117] and SLC [118] from the measurement of the hadronic pole cross section using the first few thousands observed Z decays.

The result for $\Gamma_{\rm inv}$ can be converted into a number of light neutrino families:

$$N_\nu = \frac{\Gamma_{\rm inv}}{\Gamma_\nu} = \frac{\Gamma_{\rm inv}}{\Gamma_\ell}\left(\frac{\Gamma_\ell}{\Gamma_\nu}\right)^{\rm SM} \tag{67}$$

Using the ratio

$$\left(\frac{\Gamma_\ell}{\Gamma_\nu}\right)^{\rm SM} = 0.5021\,^{+0.0012}_{-0.0008}\,(m_{\rm t}, m_{\rm H}, \alpha(m_{\rm Z})) \tag{68}$$

from the Standard Model largely reduces the top mass dependence present in the calculation of the unmeasurable neutrino width Γ_ν since in the ratio of the widths the leading part of the $m_{\rm t}$ and $m_{\rm H}$ dependence cancels. The error given in eq. 68 is the remaining effect from varying $m_{\rm t}$, $m_{\rm H}$ and $\alpha(m_{\rm Z})$ in the limits given in eq. 42. It reduces even further to ± 0.0004 if the top quark mass is restricted to the result of the direct measurement (see eq. 109). The result

$$N_\nu = 2.990 \pm 0.015\,^{+0.008}_{-0.005}\,(m_{\rm t}, m_{\rm H}, \alpha(m_{\rm Z})) \tag{69}$$

firmly proves the presence of three standard neutrino families. The common theoretical uncertainty on the luminosity determination translates to $\Delta N_\nu = \pm 0.012$ and thus dominates the experimental error on the number of neutrino families.

6.2 Direct determination of the invisible width

Z decays into non-interacting particles, for instance neutrino pairs, can only be detected if one of the incoming electrons emits a bremsstrahlung photon with sufficiently large energy to pass the trigger and selection thresholds of the detectors. The study of events with only one photon and nothing else in the detector provides a possibility to determine in a direct way the partial width of the Z decaying into invisible particles $\Gamma_{\rm inv}$.

In the Standard Model the reaction $\rm e^+e^- \to \nu\bar{\nu}\gamma$ proceeds by the two diagrams depicted in figure 23: The s-channel exchange of a Z and the t-channel exchange of a $\rm W^\pm$ boson. Since the Z couples equally to all light neutrino species the contribution of the Z exchange is proportional to the number of neutrino families. In the LEP energy range around the Z pole (88 – 94 GeV) it accounts for $\geq 97\%$ of the total cross section $\rm e^+e^- \to \nu\bar{\nu}\gamma$ (for $N_\nu = 3$). The minimum photon energy required to detect a single photon event is typically $1 - 1.5$ GeV.

Figure 24 shows the measured cross section $\rm e^+e^- \to \nu\bar{\nu}\gamma$ for $E_\gamma \geq 1$ GeV as function of the center-of-mass energy obtained by the L3 experiment in the 1993 scan of the Z resonance. The measurement of the $\rm Z \to \nu\bar{\nu}$ lineshape is compared to Standard Model calculation for different numbers of neutrino generations and good agreement is found for $N_\nu = 3$.

The results obtained on $\Gamma_{\rm inv}$ and N_ν are summarized in table 9 and they are in good agreement with the results deduced from the measurements of the total Z width and the observable decays. Possibly correlated systematic errors are small [122] and thus the combined result can be obtained by simply averaging the individual

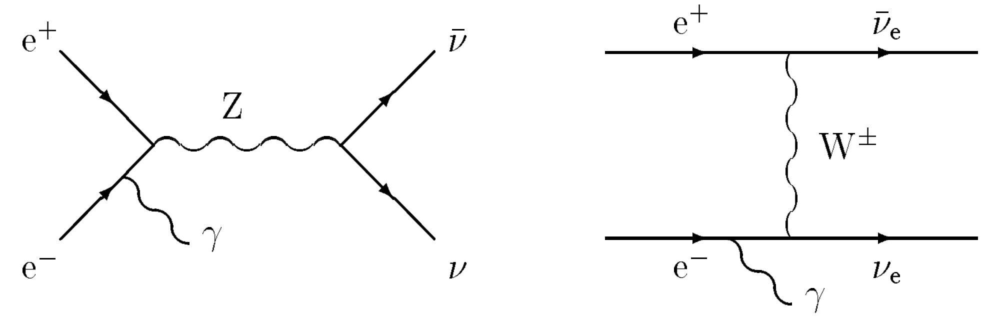

Figure 23: Feynman diagrams contributing to the reaction $e^+e^- \to \nu\bar{\nu}\gamma$.

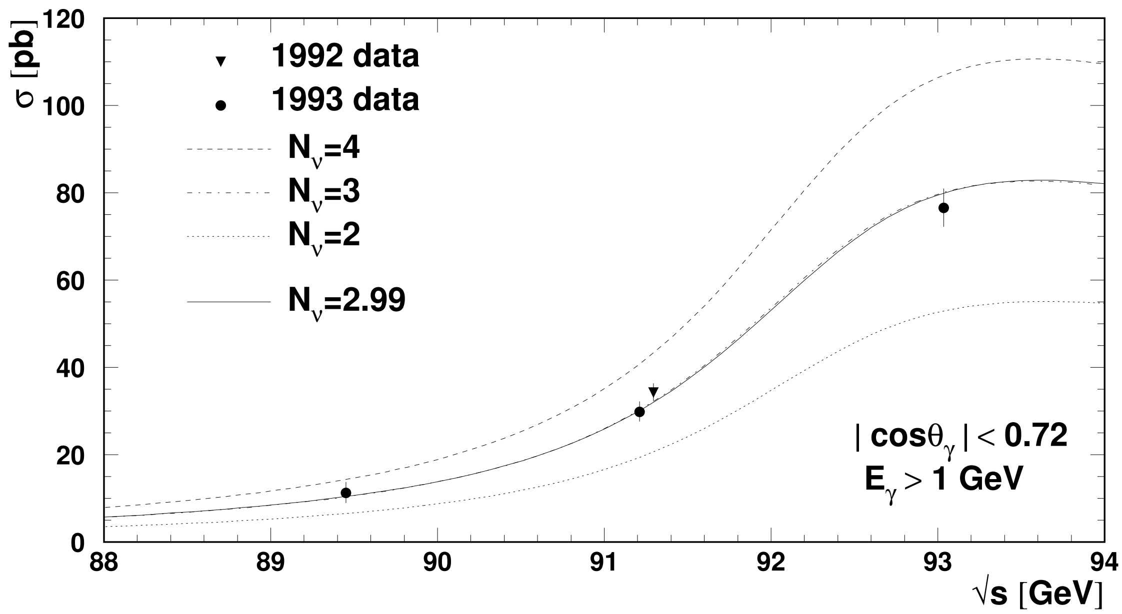

Figure 24: The cross section $e^+e^- \to \nu\bar{\nu}\gamma$ as a function of the center-of-mass energy as measured by the L3 experiment [119] compared to the Standard Model calculation for 2, 3 and 4 neutrino species.

	$\int\mathcal{L}\,\mathrm{dt}$ [pb^{-1}]	Γ_{inv} [MeV]	N_ν	ref.
ALEPH	15.7	$450 \pm 34 \pm 34$	$2.68 \pm 0.20 \pm 0.20$	[120]
L3	57.3	$503 \pm 15 \pm 13$	$3.01 \pm 0.09 \pm 0.08$	[119]
OPAL	40.5	$539 \pm 26 \pm 17$	$3.23 \pm 0.16 \pm 0.10$	[121]
Combined		507 ± 16	3.03 ± 0.10	

Table 9: Compilation of the results for Γ_{inv} and N_ν obtained from the direct measurement of $\mathrm{e^+e^-} \to \nu\bar{\nu}\gamma$.

numbers. Varying m_{t} and m_{H} in the usual limits does not contribute significantly to the error of N_ν at the current level of accuracy of this measurement. Yet, the study of $\mathrm{e^+e^-} \to \nu\bar{\nu}\gamma$ events alone clearly rules out the existence of a fourth generation of neutrinos in the Standard Model.

Eq. 64 provides an indirect determination of the invisible width as it relies on the assumption that events identified as hadronic and leptonic final states are indeed decays of the Z into hadrons or charged leptons, respectively, and not misinterpreted by the experimentors. The determination of Γ_{inv} from the measured cross section of single photon events thus is experimentally independent and an important consistency check for the determination of Z parameters performed at LEP. The observed agreement of the two results for Γ_{inv} (or N_ν) thus supports the measurements of the partial width presented in section 5.5. Note however, that when deriving the number of neutrino generations from the direct or indirect measurement of Γ_{inv} Standard Model couplings of the neutrinos to the Z have to be assumed in both cases.

6.3 Determination of the strong coupling constant α_{s} from the total hadronic cross section

Besides the determination of parameters of electroweak interactions precision measurements of total cross sections at the Z pole provide also a determination of the coupling constant of strong interactions α_{s}. As discussed in section 3.4 the presence of QCD radiative corrections in hadronic final states modifies apart from the shape of hadronic final states also the total cross section $\mathrm{e^+e^-} \to$ hadrons depending on the value of α_{s}.

The ratio of hadronic to leptonic width R_ℓ is, apart from small differences in the photon exchange contributing to hadronic and leptonic final states, equal to the ratio of the total cross sections at the Z pole[8]. From the experimental point of view R_ℓ can be measured more precisely than individual partial widths since the uncertainty on the measurement of the total width drops out. In addition, as a ratio of cross sections it is also independent of the luminosity measurement. Figure 25 summarizes the results of the experiments. The combined value

$$R_\ell = 20.788 \pm 0.032 \tag{70}$$

has a precision of 0.15%.

[8] For the process $\mathrm{e^+e^-} \to \mathrm{e^+e^-}$ this applies only to the s-channel part.

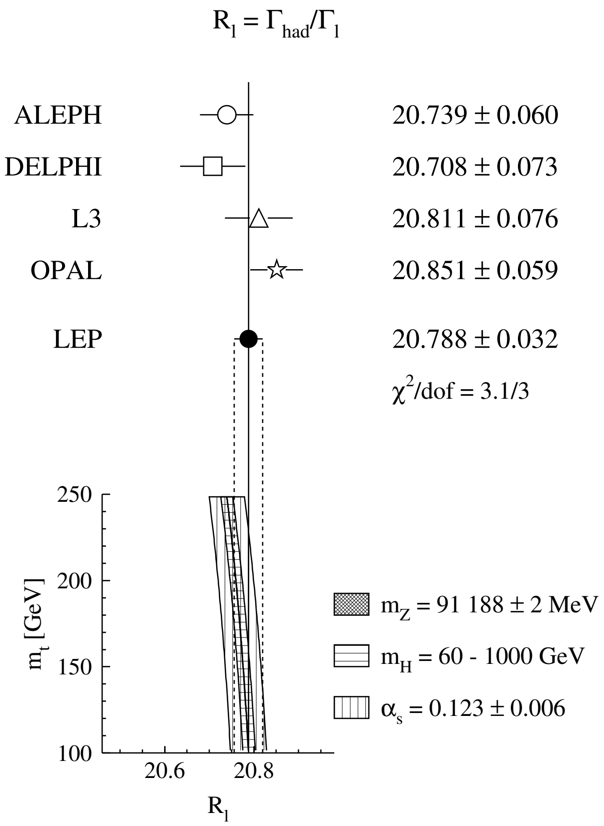

Figure 25: The ratio of the hadronic to leptonic width R_ℓ obtained by the LEP experiments from the fits imposing lepton universality compared to the Standard Model calculation.

Since the main part of the weak radiative corrections (see section 3.2) is universal to all Z decay channels the dependence on m_t and m_H cancels to first order in the Standard Model calculation of a partial width ratio. As can be seen from figure 25 R_ℓ varies by only $\pm 0.2\%$ for top and Higgs masses considered here. On the other hand the dependence on α_s is evident.

A value for α_s can be extracted from the R_ℓ using the parameterization [123]

$$R_\ell = 19.943 \left[1 + 1.060 \frac{\alpha_s}{\pi} + 0.90 \left(\frac{\alpha_s}{\pi} \right)^2 - 15 \left(\frac{\alpha_s}{\pi} \right)^3 \right] . \tag{71}$$

The combined LEP results on R_ℓ yields:

$$\alpha_s = 0.124 \pm 0.005 \pm 0.005. \tag{72}$$

The first error originates from the experimental precision of R_ℓ and the second reflects the theoretical uncertainties of electroweak and QCD calculations as well as the remaining dependence on the top quark and Higgs masses [123].

There is some more information about α_s contained in the measurement of the total width (see figure 20). A simultaneous fit to α_s and m_t in the Standard Model using the LEP results on cross sections and asymmetries is performed in section 9.1.

Both values for α_s are of similar precision and in good agreement with the results obtained from the analysis of event shape variables in hadronic Z decays [124]

$$\alpha_s(m_Z) = 0.123 \pm 0.006 \tag{73}$$

as well as with other α_s measurements at lower energies extrapolated to the Z mass [50].

The interest of determining the strong coupling from the total hadronic cross section is that it is largely independent of the details of hadronization in contrast to other methods like for instance the rate of 3-jet events [51]. The total cross section $e^+e^- \to$ hadrons has already been used by the experiments performed at lower energies to extract the strong coupling constant. A recent compilation and re-analysis of the experimental data in the range $20 \leq \sqrt{s} \leq 65$ GeV yields [125]

$$\alpha_s(35\ \mathrm{GeV}) = 0.146 \pm 0.030. \tag{74}$$

It can be converted into a value at $\sqrt{s} = m_Z$ using the running of α_s

$$\alpha_s(m_Z) = 0.124 \pm 0.021 \tag{75}$$

which is in good agreement with the LEP result.

6.4 The partial width $\mathrm{Z} \to \mathrm{b\bar{b}}$

Since the b-quark is the weak isospin partner of the top quark the Z decay into b-quarks deserves special attention among the hadronic decay channels. The $\mathrm{Zb\bar{b}}$ vertex contains weak radiative corrections involving the top quark which are unique to this channel (see figure 26). Top quark dependent vertex corrections are insignificant for other Z decays into quarks because the corresponding elements in the CKM matrix, V_{td} and V_{ts}, are small [20]. The couplings of the Z to the b-quark is modified and the top quark mass dependence of Γ_b is changed compared to other quarks (figure 27). As a consequence, the ratio

$$R_b = \Gamma_b/\Gamma_{had} \tag{76}$$

depends on the top quark mass but it is insensitive to α_s and the Higgs mass since those corrections are universal to all quarks and cancel. R_b is thus probing the top quark sector of the Standard Model.

There are several techniques used by the LEP experiments to identify b-quarks exploiting the relatively high mass of the b-quark (decay leptons with high transverse momentum, event shape variables) and the long lifetime of B-hadrons. See for instance [126, 127, 128] for an overview of tagging techniques used at LEP. Details about the analysis of the four LEP experiments can be found in references [129]–[135]. In general, tagging b-quarks by secondary vertices provides the best results.

Systematic uncertainties common to the four experiments and to the different tagging methods as well as the correlations between individual results are very important. They are studied in detail in reference [102] and the mean value obtained for the four LEP experiments, including preliminary 1993 and 1994 results, is [19]

$$R_b = 0.2205 \pm 0.0016. \tag{77}$$

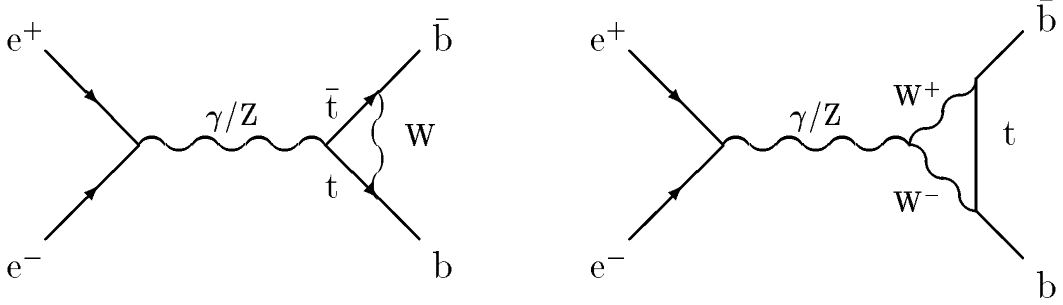

Figure 26: Weak correction diagrams to the $Zb\bar{b}$ vertex involving the top-quark.

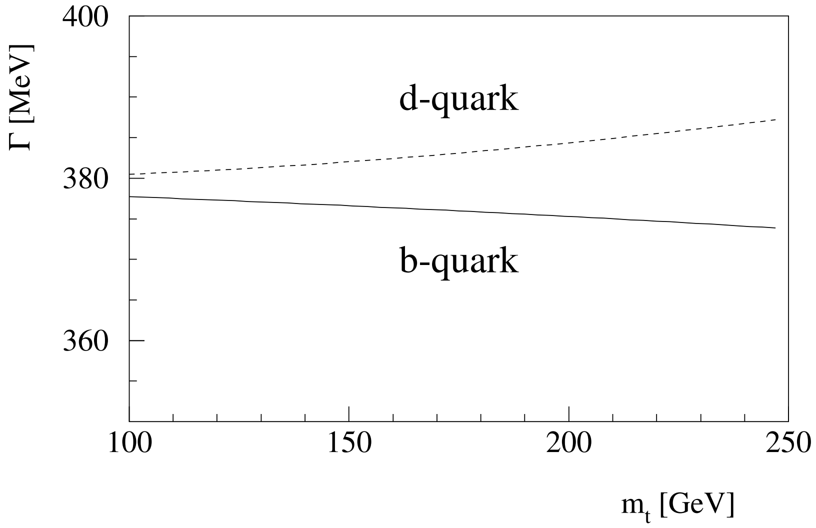

Figure 27: The dependence of the partial decay width $Z \to b\bar{b}$ compared to the partial decay width into d-quarks.

Here the ratio $R_c = \Gamma_c/\Gamma_{had}$ has been fixed to the Standard Model prediction, $R_c = 0.171$.

Figure 28 shows the best individual result obtained by each of the four experiments. Because not all information is contained in these values and because the errors are correlated in a complicated manner one cannot obtain the mean value from simply averaging these numbers. However, the results of the four experiments as well as those obtained from different tagging methods are consistent. The SLD experiment has measured this quantity, too, and obtains the consistent value $R_b = 0.2171 \pm 0.0054$ [137].

The comparison to the Standard Model calculation is also shown in figure 28. Evidently, the LEP measurement of R_b prefers a higher value than predicted. One observes a difference of 2.5 standard deviations comparing the measurement to the calculation for a top quark mass of 175 GeV or the lower limit obtained from the direct measurement of m_t (eq. 109):

$$(R_b)^{SM} \quad = \quad 0.2157 \qquad (m_t = 175 \text{ GeV})$$

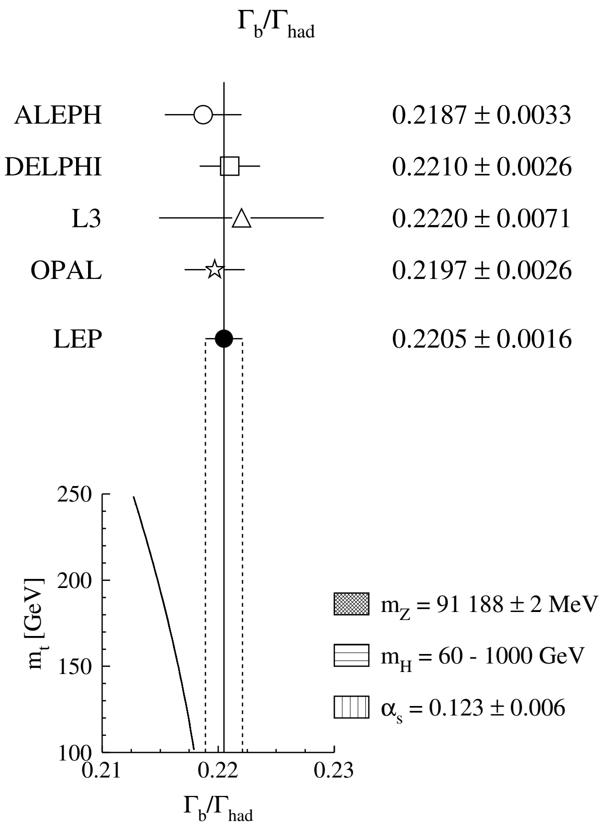

Figure 28: Measurements of the ratio $R_\mathrm{b} = \Gamma_\mathrm{b}/\Gamma_\mathrm{had}$ (fixing $R_\mathrm{c} = 0.171$) by the LEP experiments compared to the Standard Model calculation. The combined LEP value is the average over all b-tagging methods and experiments [19].

$$(R_\mathrm{b})^{\mathrm{SM}} \quad \leq \quad 0.2164 \qquad (m_\mathrm{t} \geq 156 \text{ GeV}) \tag{78}$$

The experimental result for R_b deviates even more from the theory if the partial decay width into c-quarks is no longer constrained to the Standard Model value. A common fit to b- and c-quark parameters (see appendix C) leads to

$$\begin{aligned} R_\mathrm{b} &= 0.2217 \pm 0.0017 \\ R_\mathrm{c} &= 0.1540 \pm 0.0074. \end{aligned} \tag{79}$$

Compared to the Standard Model expectation R_b comes out to be three standard deviations higher whereas R_c is two standard deviation smaller than expected.

It should be noted that if there was unknown physics modifying the special corrections to the $\mathrm{Zb\bar{b}}$ vertex and causing the increase of Γ_b above its Standard Model expectation this should also modify $R_\ell = \Gamma_\mathrm{had}/\Gamma_\ell$ since Γ_b contributes with more that 20% to Γ_had. However, this is not supported by experiment because the α_s value derived from R_ℓ is consistent with other independent determinations of α_s.

At the current level of precision no deviation from the Standard Model can be concluded from the single observable R_b. But if the experiments can further improve the identification techniques for b-quarks this measurement will become a powerful test of the Standard Model.

7 Measurement of asymmetries in $e^+e^- \to f\bar{f}$

In addition to the results obtained from the measurements of total cross sections $e^+e^- \to f\bar{f}$ presented in the previous sections, further information on electroweak parameters, in particular the couplings of the Z to fermions, is contained in the measurement of various asymmetries. As outlined in section 2.5 forward-backward and left-right asymmetries, as well as the tau polarization are experimental observables sensitive to different linear combinations of helicity amplitudes. The combination of these asymmetries and the total cross sections allow the precise determination of the vector and axial-vector couplings, $\bar{g}_V$ and $\bar{g}_A$, of charged leptons and heavy, bottom and charm, quarks.

Any of these observables can be interpreted as a measurement of the weak mixing angle $\sin^2\bar{\vartheta}_W$ (see section 8.1), or alternatively in the Standard Model framework as a value for the mass of the top quark.

7.1 Lepton forward-backward asymmetry below the Z resonance

The measurement of forward-backward asymmetries for muon and tau pairs, as well as for b- and c-quarks, has been already performed at e^+e^- colliders operating below the Z resonance (PEP, PETRA and TRISTAN). These measurements together with results on scattering of polarized electrons on deuterium [7] and the observation of atomic parity violation [138] provided the first experimental evidence for the interference of photon and Z exchange.

Appendix B contains a compilation of results on total cross sections and forward-backward asymmetries in $e^+e^- \to \mu^+\mu^-$ and $e^+e^- \to \tau^+\tau^-$ from experiments performed at lower energies. Clear evidence for γ–Z mixing is seen in the A_{FB} measurements. This is not visible in the total cross section of leptons where the experimental results up to energies of $\sqrt{s} = 60$ GeV are compatible with pure QED expectation[9]. Figures 29 and 30 compare the observed asymmetries in the reactions $e^+e^- \to \mu^+\mu^-$ and $e^+e^- \to \tau^+\tau^-$ with the Standard Model prediction in lowest order which is calculated from eq. 21 using $m_Z = 91\,188$ MeV, the weak mixing angle as calculated from the ratio of the vector boson masses, $\sin^2\vartheta_W = 0.226$, and the lowest order value for the axial-vector couplings, $g_A = -1/2$.

For the purpose of comparing these results to the measurements performed at LEP the results of the L3 experiments obtained in the 1993 scan of the Z resonance are added as an example to the plots. Similarly to the low energy points the L3 results are corrected for higher order QED effects (see appendix B).

Both figures demonstrate the perfect agreement of the data with the Standard Model over a large range of center-of-mass energies.

7.2 Lepton forward-backward asymmetry at the Z resonance

The experiments at LEP have measured the forward-backward asymmetry in the energy range 88–94 GeV for the three charged leptons. As the cross section around the Z resonance is very high these measurements are performed with unprecedented accuracy. The experimental precision achieved, in particular on the pole itself, allows

[9] However, electroweak interference effects are measurable in the total cross section $e^+e^- \to$ hadrons below the Z pole [139].

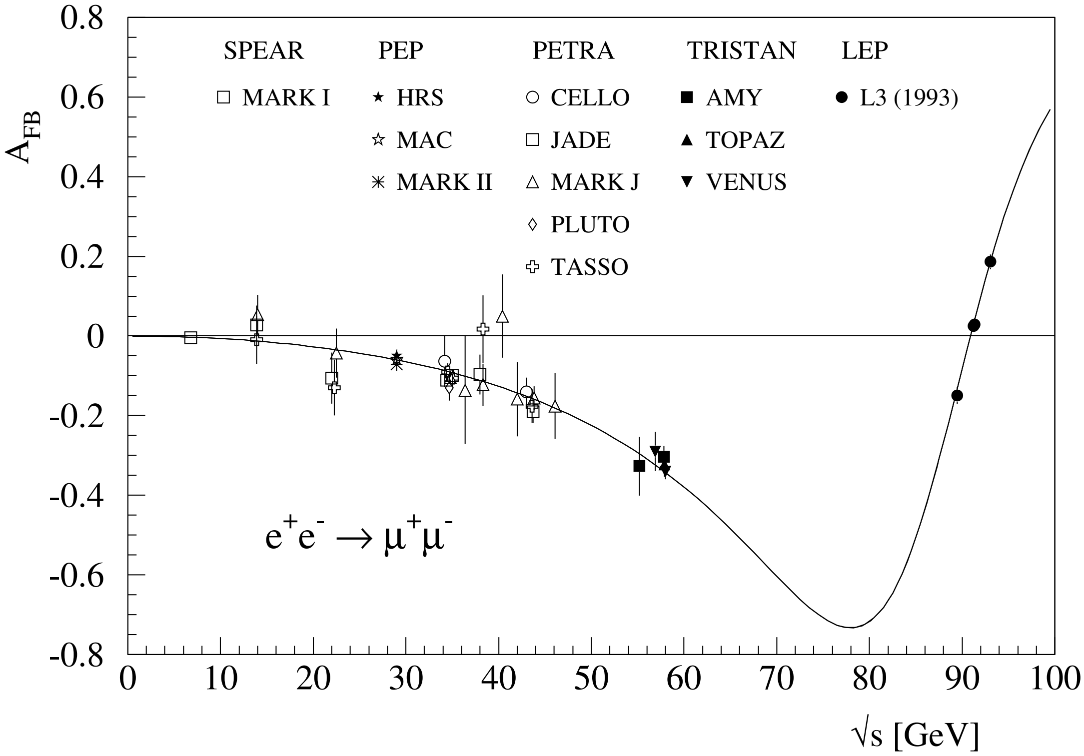

Figure 29: Muon pair forward-backward asymmetry A_{FB} as a function of the center-of-mass energy measured at e^+e^- colliders.

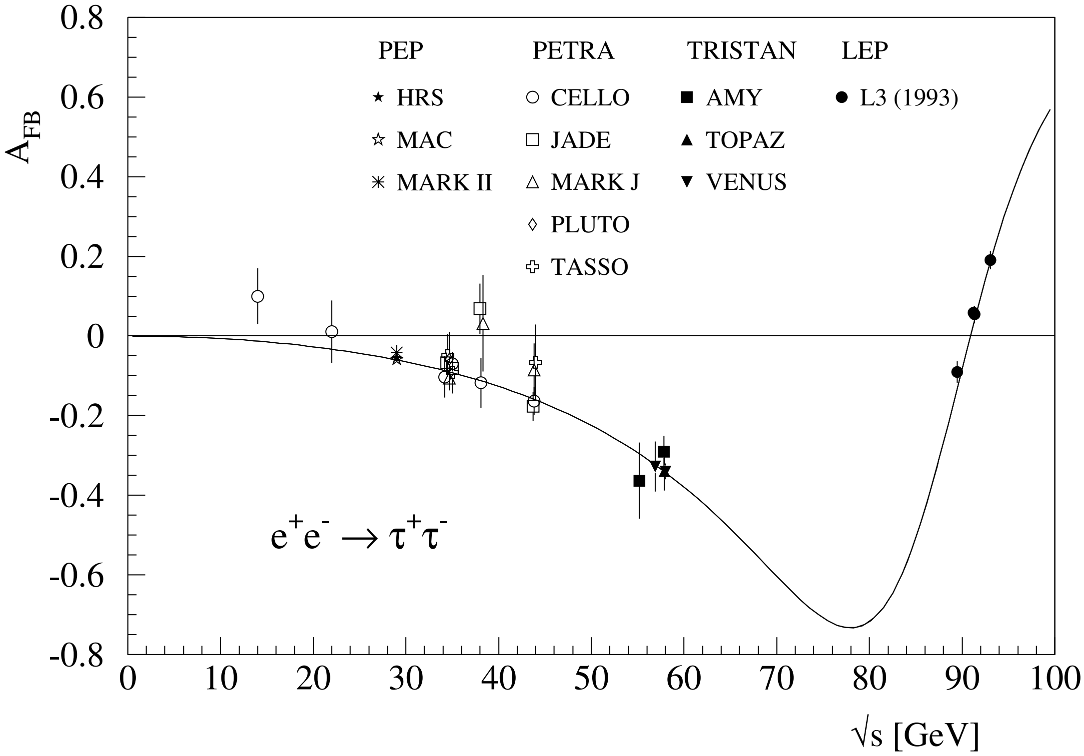

Figure 30: Same as figure 29 for tau pairs.

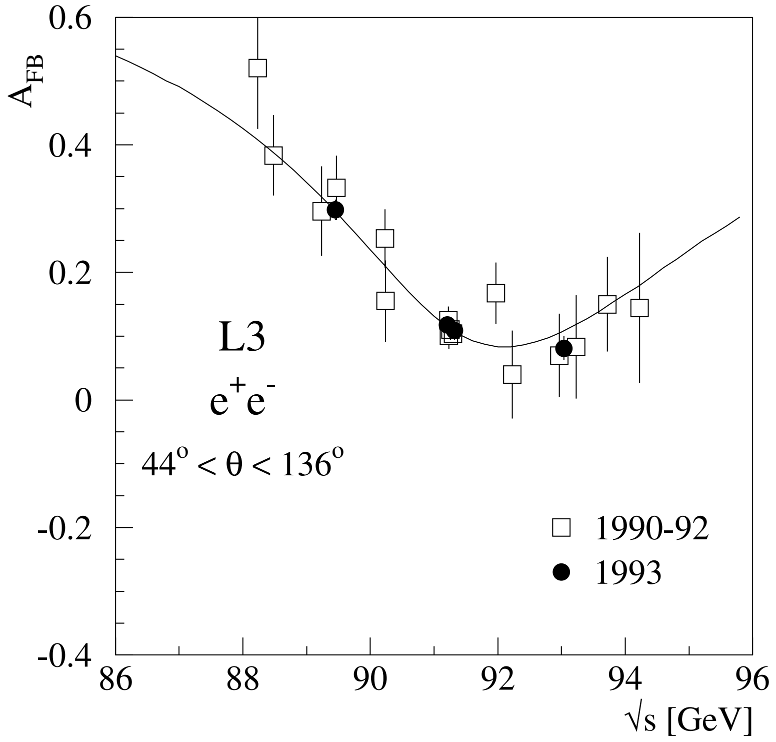

Figure 31: The forward-backward asymmetry in $e^+e^- \rightarrow e^+e^-$ measured by L3 compared to the fit to all cross sections and forward-backward asymmetries imposing lepton universality.

a precise determination of the Z couplings to charged leptons and of weak radiative corrections.

As an example figures 31, 32 and 33 show the lepton pair asymmetries observed by the L3 experiment as a function of the center-of-mass energy. Here the measurements are compared to the result of the fit to all total cross sections and forward-backward asymmetries, assuming lepton universality, in a similar way as it is done for the total cross section (see section 5.1). The forward-backward asymmetries are calculated from m_Z, Γ_Z and the effective couplings, $\bar{g}_A$ and $\bar{g}_V$, taking into account QED radiative corrections for the applied experimental cuts [64]. Since the mass and the total width of the Z are mainly determined by the measurement of the total hadronic cross section the excellent agreement found in the energy dependence of the leptonic forward-backward asymmetries is another, non-trivial confirmation of the Standard Model. Equivalent results are obtained by the other LEP collaborations.

To permit an unbiased analysis of the data the numbers quoted by the LEP experiments are the observed asymmetries corrected for experimental acceptances but not corrected for higher order radiation effects. As the radiative corrections depend on the experimental cuts, e.g. angular acceptance, acolinearity and minimum momentum, the A_{FB} results cannot be compared directly, neither between different experiments nor lepton flavors. Therefore, the LEP experiments extract in their fits to the measured total cross sections and forward-backward asymmetries the effective

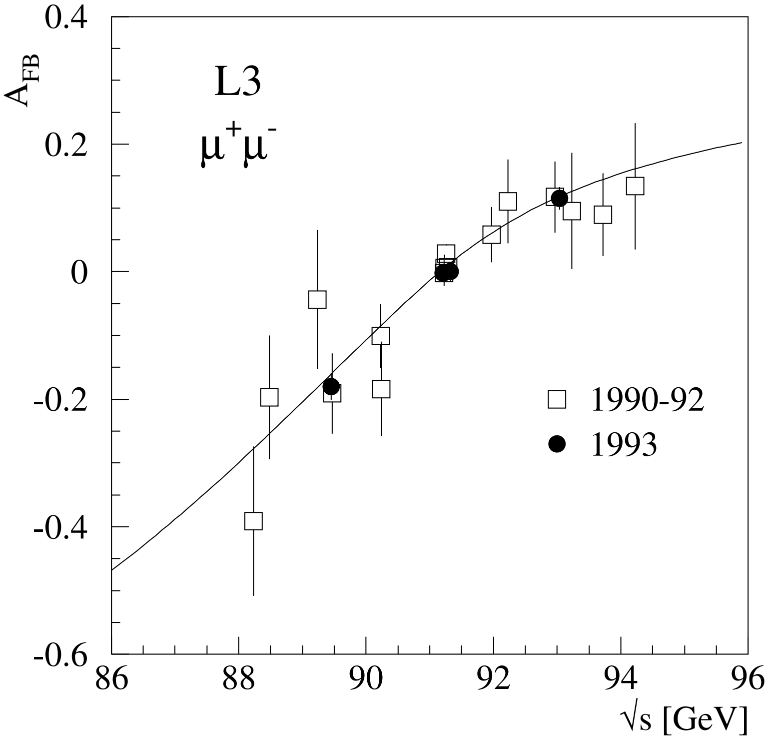

Figure 32: Same as figure 31 for $e^+e^- \rightarrow \mu^+\mu^-$.

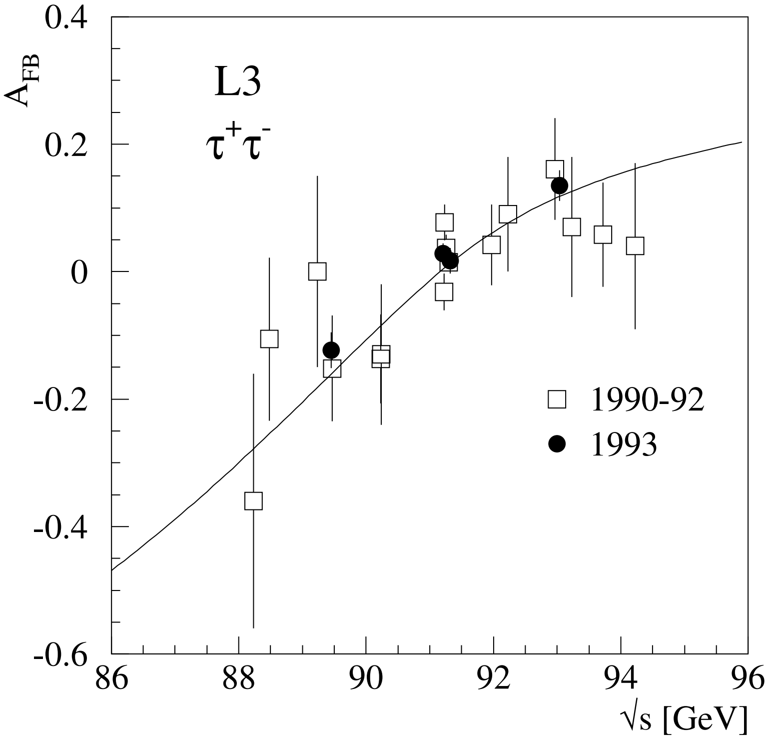

Figure 33: Same as figure 31 for $e^+e^- \rightarrow \tau^+\tau^-$.

coupling constants $\bar{g}_\mathrm{A}^\ell$ and $\bar{g}_\mathrm{V}^\ell$ ($\ell = \mathrm{e}, \mu, \tau$) and convert them into the bare peak asymmetry (see appendix A):

$$A_\mathrm{FB}^{0,\ell} = 3\,\frac{\bar{g}_\mathrm{V}^\mathrm{e}\,\bar{g}_\mathrm{A}^\mathrm{e}}{(\bar{g}_\mathrm{V}^\mathrm{e})^2 + (\bar{g}_\mathrm{A}^\mathrm{e})^2}\,\frac{\bar{g}_\mathrm{V}^\ell\,\bar{g}_\mathrm{A}^\ell}{(\bar{g}_\mathrm{V}^\ell)^2 + (\bar{g}_\mathrm{A}^\ell)^2}\,. \tag{80}$$

As in the case of the total cross section for the reaction $\mathrm{e^+e^-} \to \mathrm{e^+e^-}$ the contribution of the t-channel exchange and the s–t interference have to be accounted for as described in section 5.1. For small scattering angle the t-channel dominates and leads to a very high positive asymmetry. Even in the central part of the detectors where the $\mathrm{e^+e^-} \to \mathrm{e^+e^-}$ analysis is confined the asymmetry originating from Z exchange is severly modified resulting in a very different $\sqrt{s}$-dependence (see figure 31).

The results obtained on A_FB^0 from averaging over the three lepton flavors are shown in figure 34. Good agreement is found among the experiments. The combined value

$$A_\mathrm{FB}^0 = 0.0172 \pm 0.0012 \tag{81}$$

contains the common systematic error due to the LEP energy calibration (eq. 47). The comparison to the Standard Model calculation shows that the leptonic forward-backward asymmetries are sensitive to the top quark mass. It is remarkable that the preferred value of m_t is within errors in good agreement with the one obtained from the measurements of total cross sections (see section 5) which are experimentally completely independent observables.

7.3 Forward-backward asymmetries of heavy quarks

The forward-backward asymmetry of quark pairs are also studied in $\mathrm{e^+e^-}$ annihilation experiments. Due to the fractional charges of quarks their vector couplings to the Z are large which results in large forward-backward asymmetries on the Z pole (see eq. 21). One experimental observable is the asymmetry averaged over all five flavors, the quark charge asymmetry, which is deduced from the difference in charge flow in the forward and backward hemispheres of hadronic Z decays. For the results on quark charge asymmetries see references [140, 141, 142]. These measurements are interpreted in terms of the effective weak mixing angle $\sin^2\bar{\vartheta}_\mathrm{W}$ (see section 8.1).

Asymmetries of heavy quarks (c- and b-quarks) are measured individually through their decays into electrons and muons [143]–[146], from reconstructed $\mathrm{D}^{*\pm}$ mesons [147] or by tagging b-quarks by their displaced decay vertex and applying the charge flow method to sign the event direction [148]. Heavy quarks are identified in semileptonic decays through the, on average, high momentum and transverse momentum of the decay electrons and muons. The original quark direction is estimated by the thrust axis of the jet and the charge of the quark is inferred from the charge of the lepton.

The observed asymmetry derived from the polar angle distribution has to be corrected for the effect of $\mathrm{B_0} - \bar{\mathrm{B}}_0$ mixing

$$A_\mathrm{FB}^\mathrm{b} = \frac{1}{1 - 2\,\chi_\mathrm{B}}\,A_\mathrm{FB}^\mathrm{observed} \tag{82}$$

where χ_B is the mixing parameter giving the probability that a $\mathrm{B_0}$ converts to a $\bar{\mathrm{B}}_0$ before decaying and hence inverts the assignment of the direction of the b-quark originating from the Z decay. Experimentally χ_B is obtained from the rate of

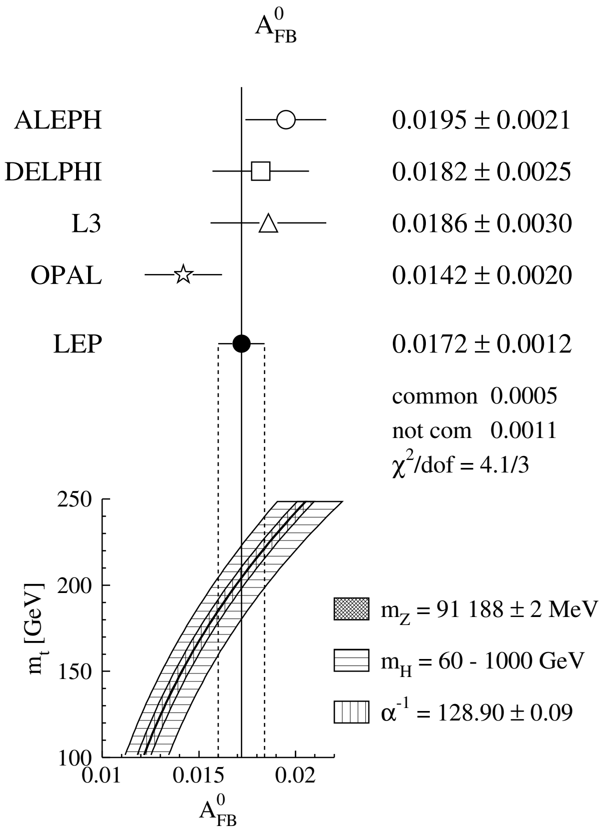

Figure 34: The leptonic pole asymmetry $A^0_{\rm FB}$ measured at LEP.

$e^+e^- \to b\bar{b}$ events where in both jets like sign leptons from b-decay are observed. A common fit to all LEP data a yields [19]

$$\chi_{\rm B} = 0.1149 \pm 0.0062. \tag{83}$$

Figures 35 and 36 compare the results on b- and c-quark forward-backward asymmetries obtained at e^+e^- colliders below the Z pole with the combined results of the LEP experiments (see appendix C). All b-quark asymmetries in figure 35 are corrected using the mixing parameter measured at LEP (eq. 83). As the LEP results given in table 25 (appendix C) are not corrected for QED effects they are shifted by the difference between the lowest order formula and the full Standard Model calculation including radiative corrections for the purpose of comparison. The measurements are well described by the Standard Model.

As in the case of the lepton asymmetries, the measurements of $A_{\rm FB}$ for b- and c-quarks are cast into a single number for the bare peak asymmetry. The combined results for the LEP experiments are obtained from a detailed analysis taking into account correlations among the quark species as well as errors common to the experiments [102, 19]. The results

$$\begin{aligned} A^{0,b}_{\rm FB} &= 0.0999 \pm 0.0031 & (A^{0,b}_{\rm FB})^{\rm SM} &= 0.100\,^{+0.023}_{-0.017} \\ A^{0,c}_{\rm FB} &= 0.0725 \pm 0.0058 & (A^{0,c}_{\rm FB})^{\rm SM} &= 0.072\,^{+0.018}_{-0.013} \end{aligned} \tag{84}$$

compare well with the Standard Model expectations. The experimental error of both

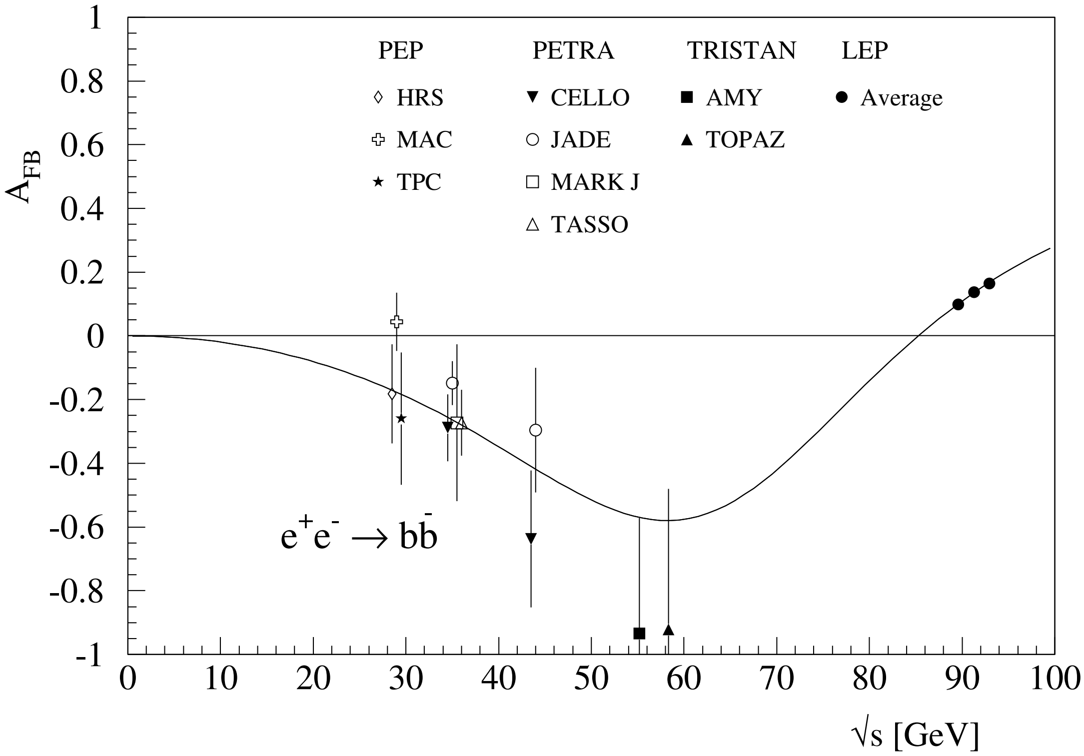

Figure 35: Forward-backward asymmetries in $e^+e^- \to b\bar{b}$ as function of the center-of-mass energy compared to the lowest order expectation. The measurements are corrected for $B_0 - \bar{B}_0$ mixing using the value for χ_B obtained at LEP (eq. 83).

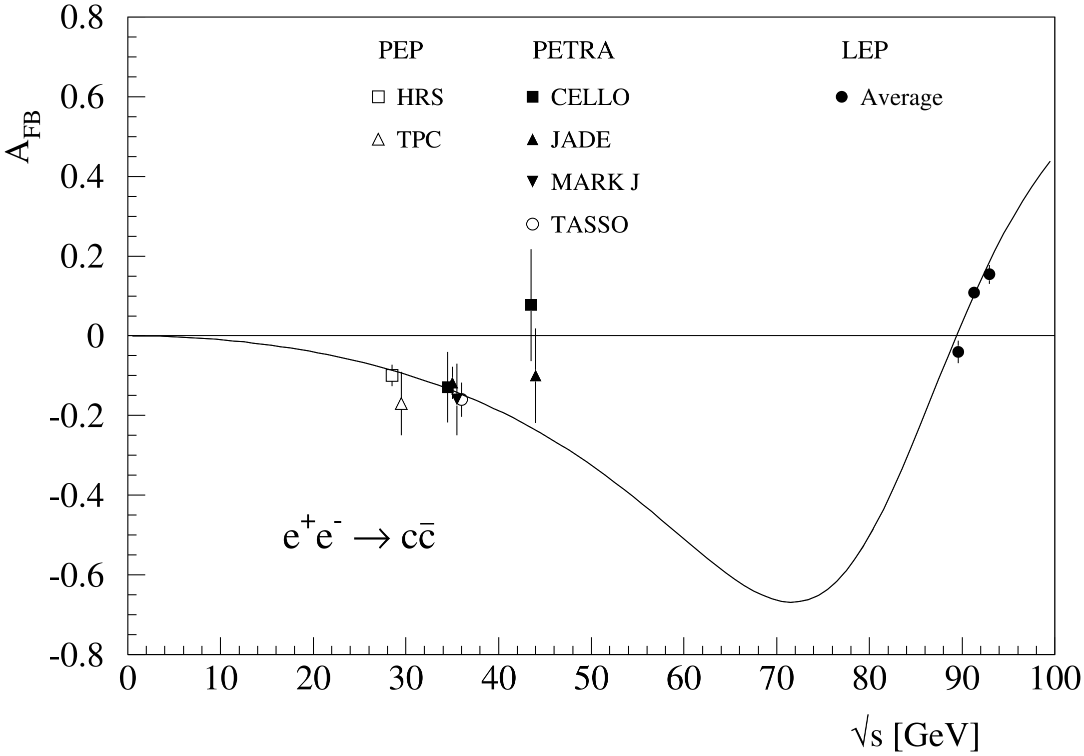

Figure 36: Same as figure 35 for $e^+e^- \to c\bar{c}$.

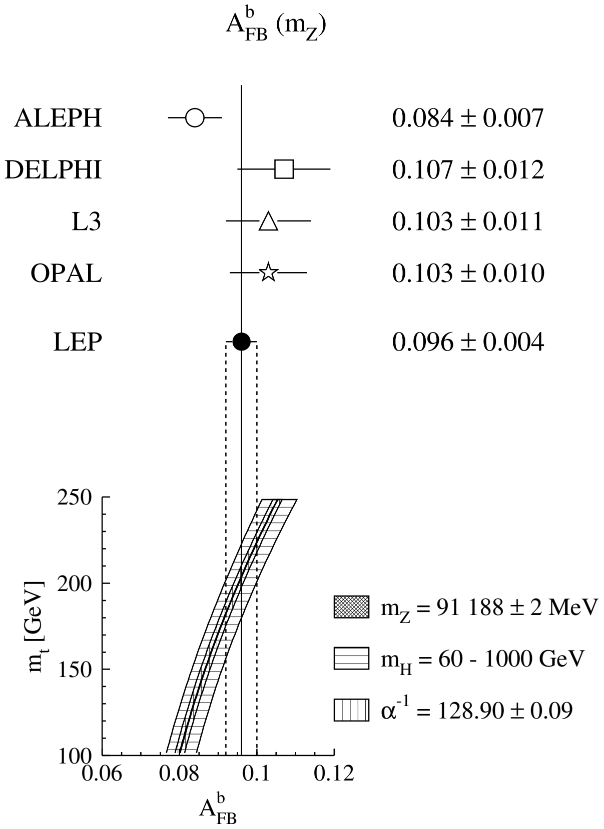

Figure 37: Measurements of the forward-backward asymmetries in $e^+e^- \to b\bar{b}$ at the Z pole. The LEP average is the result of the combined fit including all b-tagging techniques and experiments [19].

numbers is smaller than the uncertainty of the Standard Model calculation from the m_t variation. These measurements hence are sensitive to weak radiative corrections. In section 8.1 they will be compared in terms of $\sin^2\bar{\vartheta}_W$ to other asymmetry measurements.

Figure 37 shows a compilation of b-quark forward-backward asymmetries for $\sqrt{s} = m_Z$ measured at LEP. The quoted numbers of the four LEP experiments are the ones obtained from semileptonic b decays and the combined result emerges from the fit using all available measurements [19]. The Standard Model calculation is performed using ZFITTER and taking into account QCD corrections according to reference [149]. The sensitivity of the b-quark asymmetry measured at LEP to the mass of the top quark is comparable to the combined lepton forward-backward asymmetry.

7.4 Measurement of the tau polarization

Helicity states of final state fermions in e^+e^- collisions can only be observed in $e^+e^- \to \tau^+\tau^-$. Because of the short lifetime ($\tau = 0.296 \cdot 10^{-12}$ s) the tau leptons decay close to the interaction point before they reach active parts of the detector. This, however, allows the determination of the average tau helicity from the observed energy spectra of the decay products [150, 151]. This method cannot be applied for

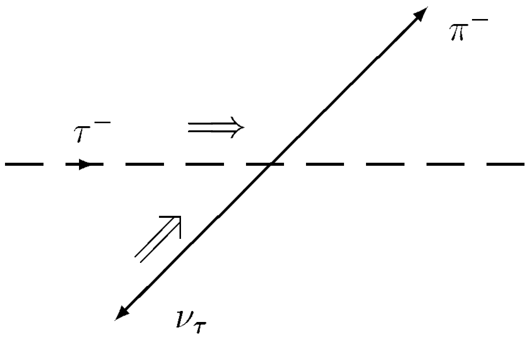

Figure 38: Tau decay into a charged pion and a neutrino in the tau rest frame.

quarks, i.e. b-quarks, as the formation of various baryons and mesons types with different spins washes out the correlation of the quark helicity and the energies of the fragmentation products. Also the acolinearity of the decay products of the tau pair is sensitive to the momentum distribution among the neutrinos and the charged decay products and hence can be used to measure the average polarization [152].

All main tau decay channels are exploited for the measurement of the tau polarization:

$$\begin{aligned} \tau^- &\rightarrow \mathrm{e}^- \bar{\nu}_\mathrm{e}\, \nu_\tau, \\ &\rightarrow \mu^- \bar{\nu}_\mu\, \nu_\tau, \\ &\rightarrow \pi^- \nu_\tau, \\ &\rightarrow \rho^- \nu_\tau, \\ &\rightarrow \mathrm{a}_1^- \nu_\tau \end{aligned} \tag{85}$$

and the corresponding charge conjugate reactions. The simplest case is the tau decay into a charged pion because it is a two-body decay involving only one neutrino and the spinless charged pion (figure 38). Assuming that the tau neutrino is always left-handed the pion preferentially escapes in the direction of the tau helicity. Hence, when boosted into the $\mathrm{e}^+\mathrm{e}^-$ center-of-mass frame, i.e. the detector frame, the pion receives on average more energy from the decay of a right-handed tau than from a left-handed tau (figure 39).

In the detector the sum of both spectra, weighted by the polarization asymmetry and smeared by the finite energy resolution, is observed. Figure 40 shows an example pion spectrum obtained by the L3 experiment. Also shown are the contributions of both helicities weighted by the fit result of the tau polarization.

The other tau decay channels are analyzed in a similar manner. However, due to the presence of two neutrinos in the purely leptonic tau decays the correlation of tau helicity and electron or muon energy is diluted. In the case of the decay $\tau^- \rightarrow \rho^-\nu_\tau$ some of the information lost due to the spin of the ρ^- can be restored by correlating the energies of the ρ^- decay products π^- and π^0 [153, 154]. Generally good agreement is observed among the different channels. See references [155]–[162] for details on the analysis.

Apart from small radiative corrections the tau polarization on the Z peak can be

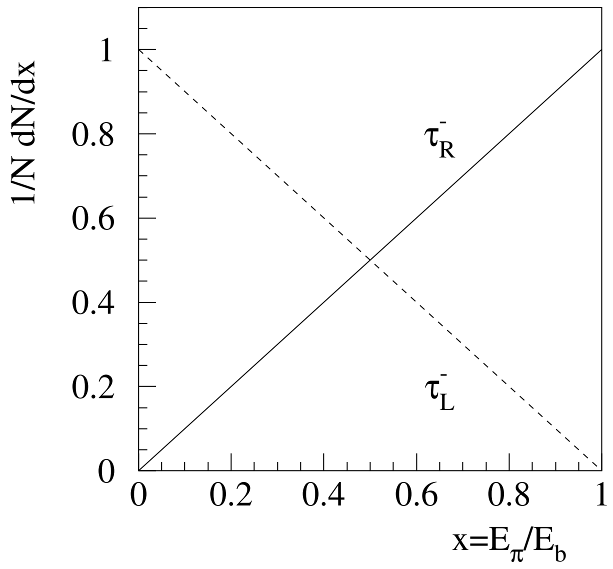

Figure 39: The expected energy spectra of pions from the decay of right- and left-handed taus in the e^+e^- center-of-mass frame.

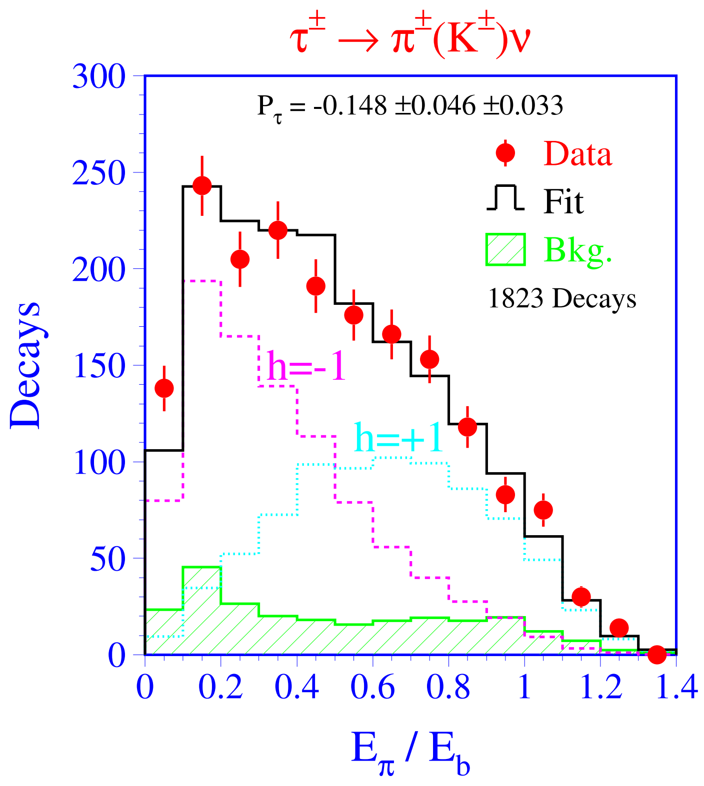

Figure 40: The energy spectrum of pions from the decay $\tau^- \to \pi^- \nu_\tau$ measured by L3 [159] together with the fitted contributions from right- and left-handed taus.

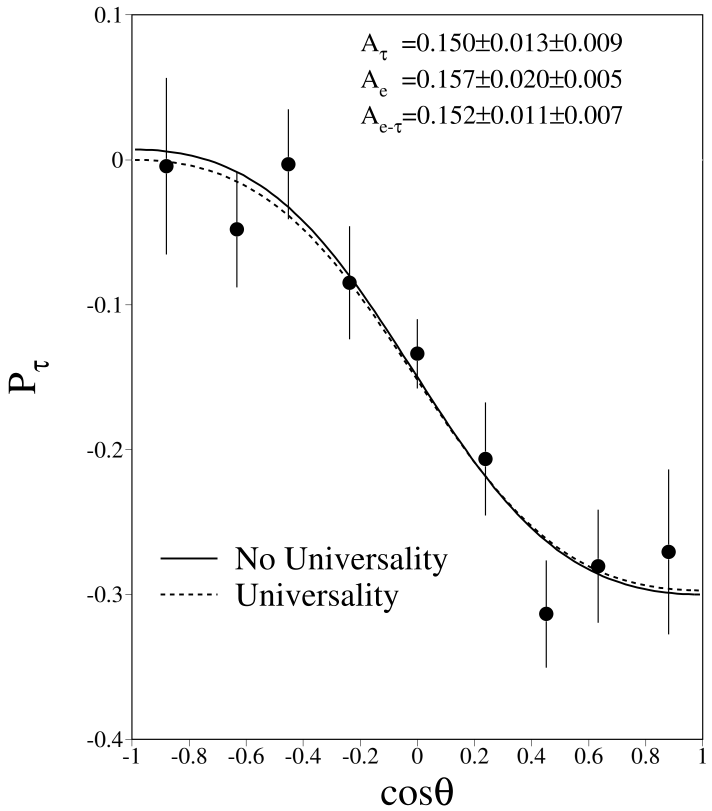

Figure 41: The tau polarization as a function of the scattering angle θ measured by L3 (data 1990-93) [160]. The solid (dashed) line shows the result of the fit without (with) imposing lepton universality.

written as [150]:

$$\begin{aligned} P_{\tau^-} &= \frac{\sigma^R_{\tau^-} - \sigma^L_{\tau^-}}{\sigma^R_{\tau^-} + \sigma^L_{\tau^-}} \\ &= -\frac{2\,\bar{g}^\tau_{\rm A}\,\bar{g}^\tau_{\rm V}}{(\bar{g}^\tau_{\rm A})^2 + (\bar{g}^\tau_{\rm V})^2} \;\equiv -A_\tau \end{aligned} \tag{86}$$

As discussed in section 2.5 additional information on electroweak couplings is contained in the angular dependence of the tau polarization:

$$P_{\tau^-}(\cos\theta) = -\frac{(1+\cos^2\theta)\,A_\tau + 2\cos\theta\,A_e}{(1+\cos^2\theta) + 2\cos\theta\,A_\tau A_e} \tag{87}$$

The forward-backward tau polarization asymmetry, the difference of the polarization in the forward and backward hemispheres, extracts the odd powers in $\cos\theta$ in eq. 87. In the limit of helicity conservation this determines the helicity state of the incoming electrons and hence is equivalent to the measurement of the left-right asymmetry $A_{\rm LR}$. Figure 41 shows the result of the L3 experiment. Since the electron and tau coupling constants can be obtained from one single measurement this provides an important test of lepton universality.

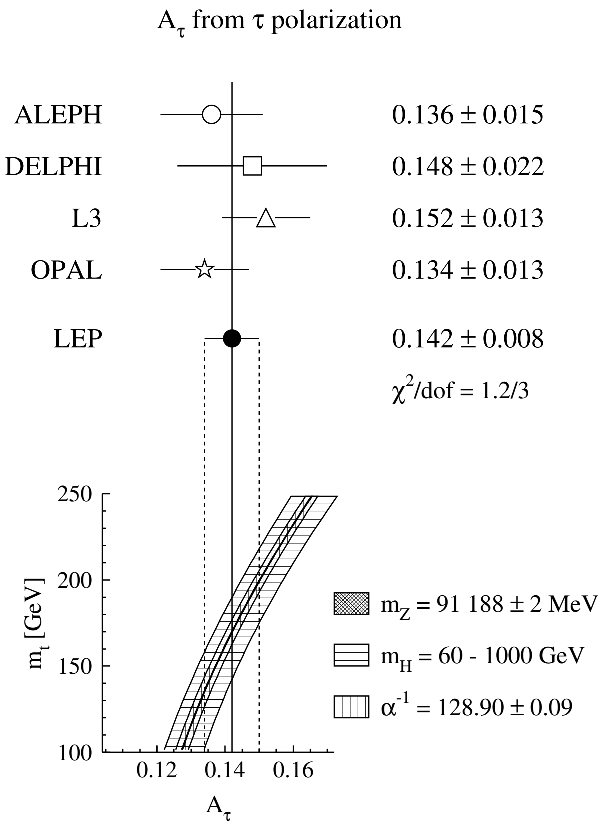

Figure 42: The results on tau polarization on the Z pole from the LEP experiments together with the combined result and the Standard Model calculation.

The results on A_τ and A_e from tau polarization at LEP are shown in figures 42 and 43. The experimental errors are assumed to be uncorrelated among the experiments. The LEP mean values are [19]:

$$\begin{aligned} A_\tau &= 0.142 \pm 0.008 \\ A_e &= 0.139 \pm 0.009. \end{aligned} \tag{88}$$

Again, both numbers are consistent with a top quark mass of about 175 GeV and thus are in agreement with all other electroweak observables at LEP.

7.5 Measurement of the left-right asymmetry at SLC

Similar to the asymmetry in the production of right- and left-handed taus in $e^+e^- \to \tau^+\tau^-$ at the Z pole, parity violation in weak interactions manifests itself also in the relative difference of the total cross section for right- and left-handed incoming electrons, the left-right asymmetry A_{LR} (see section 2.5). Because the measurement of A_{LR} needs the determination of neither the charge nor the helicity of the outgoing fermion all visible Z decays can be used. Hence, one can exploit the high pole cross section $e^+e^- \to$ hadrons to determine the couplings of the electron and results competitive to leptonic forward-backward asymmetry and tau polarization can be achieved with less integrated luminosity.

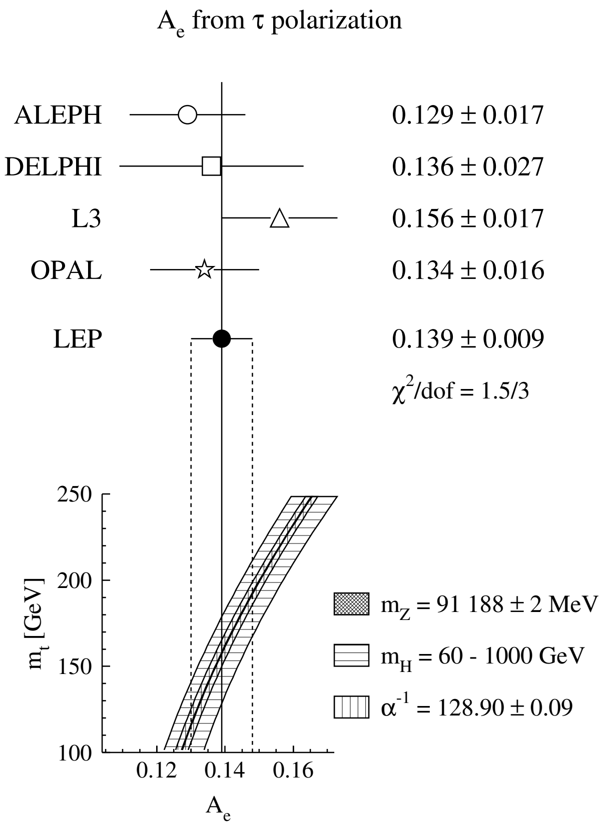

Figure 43: The results on forward-backward tau polarization on the Z pole from the LEP experiments together with the combined result and the Standard Model calculation.

However, the observation of A_{LR} requires longitudinal polarization of the initial state electrons. In e^+e^- storage rings such as LEP depolarizing effects accumulating over many turns of the particles around the ring make it very difficult to combine high luminosity and a high degree of polarization. Therefore, the measurement of A_{LR} has not yet been carried out at LEP. See for instance reference [163] for a discussion of this issue and future prospects.

Contrary to LEP the conditions for polarization experiments are very favourable at the SLC. Electrons and positrons pass only once through the arcs of the collider before interacting. Depolarizing effects such as imperfections of the magnets and beam-beam interactions do not pile up. The high degree of polarization obtained from the electron source [32] is hence essentially kept to the collision point.

The SLD [164] experiment at SLC has observed about 160 000 events $e^+e^- \to$ hadrons at the Z pole with an average degree of longitudinal polarization of the incoming electrons reaching $< P_e >= 77\%$ [165, 166]. From the observed number of hadronic events with left-handed ($N_{e_l^-}$) and right-handed ($N_{e_r^-}$) electron beams the left-right asymmetry is calculated:

$$A_{\mathrm{LR}} = \frac{1}{< P_e >} \frac{N_{e_l^-} - N_{e_r^-}}{N_{e_l^-} + N_{e_r^-}} \,. \tag{89}$$

After taking into account small radiative corrections and the contribution from the γ exchange the result obtained for the electron couplings is

$$A_{\rm e} \;=\; 2\,\frac{\bar{g}_{\rm V}^{\rm e}\,\bar{g}_{\rm A}^{\rm e}}{(\bar{g}_{\rm V}^{\rm e})^2+(\bar{g}_{\rm A}^{\rm e})^2} \quad = 0.1551 \pm 0.0040\,. \tag{90}$$

It should be noted that the left-right asymmetry measures, in a different experiment, the same physical quantity as the forward-backward tau polarization (eq. 88), namely the couplings of electrons to the Z. The apparent discrepancy of the two results (two standard deviations) must be of experimental nature and only future improved measurements can clarify this question.

Exploiting the longitudinal polarization at SLC and the tagging techniques for b-quarks the SLD experiment measures the left-right asymmetry as function of the scattering angle and determines $A_{\rm FB}^{\rm LR}$ for b-quarks (eq. 26):

$$A_{\rm FB}^{\rm LR,\,b} = \langle P_{\rm e} \rangle\, \frac{3}{4}\, A_{\rm b}\,. \tag{91}$$

Results are obtained from semi-leptonic b- and c-quark decays [167] and employing the charge flow technique in $\rm Z \to b\bar{b}$ events tagged by displaced b decay vertices [168, 166]. The combined results for the two quark species are

$$\begin{aligned} A_{\rm c} \;&=\; 2\,\frac{\bar{g}_{\rm V}^{\rm c}\,\bar{g}_{\rm A}^{\rm c}}{(\bar{g}_{\rm V}^{\rm c})^2+(\bar{g}_{\rm A}^{\rm c})^2} \quad = 0.57 \pm 0.10 \\ A_{\rm b} \;&=\; 2\,\frac{\bar{g}_{\rm V}^{\rm b}\,\bar{g}_{\rm A}^{\rm b}}{(\bar{g}_{\rm V}^{\rm b})^2+(\bar{g}_{\rm A}^{\rm b})^2} \quad = 0.861 \pm 0.053\,. \end{aligned} \tag{92}$$

This is in agreement with the Standard Model which predicts a very high degree of polarization in particular for b-quarks from Z decays:

$$\begin{aligned} A_{\rm c}^{\rm SM} \;&=\; 0.666^{+0.014}_{-0.011} \\ A_{\rm b}^{\rm SM} \;&=\; 0.934^{+0.002}_{-0.001}\,. \end{aligned} \tag{93}$$

8 The weak mixing angle and Z couplings to fermions

8.1 Determination of the effective weak mixing angle $\sin^2\bar{\vartheta}_{\rm W}$

A quantitative comparison of asymmetries can be performed in terms of the weak mixing angle. For the precision measurements performed at the Z resonance it is most convenient to adopt the definition of the effective weak mixing angle $\sin^2\bar{\vartheta}_{\rm W}$ by the ratio of the effective couplings (see section 3.2):

$$\frac{\bar{g}_{\rm V}^{\rm f}}{\bar{g}_{\rm A}^{\rm f}} = 1 - 4\,|Q_{\rm f}|\,\sin^2\bar{\vartheta}_{\rm W}\,. \tag{94}$$

The definition of $\sin^2\bar{\vartheta}_{\rm W}$ is in principle flavor dependent due to weak vertex corrections. The effect is demonstrated in table 10 which contains Standard Model calculations of $\sin^2\bar{\vartheta}_{\rm W}$ for various fermions. Since the most precise results are obtained from the charged leptons they are used to define $\sin^2\bar{\vartheta}_{\rm W}$. With the exception of b-quarks the difference compared to the charged leptons is found to be small compared to the experimental accuracy in these channels.

	$\sin^2\bar{\vartheta}_{\rm W}$	$\lvert\Delta \sin^2\bar{\vartheta}_{\rm W}\rvert$
$\nu\bar{\nu}$	0.23163	0.00036
$\ell^+\ell^-$	0.23199	—
$\rm u\bar{u}$	0.23189	0.00010
$\rm d\bar{d}$	0.23177	0.00022
$\rm c\bar{c}$	0.23189	0.00010
$\rm b\bar{b}$	0.23329	0.00306

Table 10: The effective weak mixing angle $\sin^2\bar{\vartheta}_{\rm W}$ calculated in the Standard Model for various fermions. The right column indicates the maximum difference found compared to charged leptons in the parameter range given in eq. 42.

The conversion of asymmetries into $\sin^2\bar{\vartheta}_{\rm W}$ is practically independent of assumptions about the Standard Model, in particular the ρ-parameter [169]. The measurements of the leptonic asymmetries (forward-backward, left-right and tau polarization) can be cast into A_ℓ only applying QED radiative corrections to the measurements and hence can be converted into $\sin^2\bar{\vartheta}_{\rm W}$ directly:

$$A_\ell = 2\,\frac{1-4\,\sin^2\bar{\vartheta}_{\rm W}}{1+(1-4\,\sin^2\bar{\vartheta}_{\rm W})^2} \tag{95}$$

The determination of $\sin^2\bar{\vartheta}_{\rm W}$ from the b-quark forward-backward asymmetry in principle depends on Standard Model assumptions to account for the special corrections to the $\rm Zb\bar{b}$ vertex (see figure 26). However, since $A_{\rm b} \gg A_{\rm e}$ the b-quark asymmetry $A_{\rm FB}^{\rm 0,b} = \frac{3}{4}\,A_{\rm e}\,A_{\rm b}$ is more sensitive to the electron couplings than to those of the b-quark and the dependence of $\sin^2\bar{\vartheta}_{\rm W}$ obtained from $A_{\rm FB}^{\rm b}$ on $m_{\rm t}$ is found to be numerically small. Ignoring the difference of $\sin^2\bar{\vartheta}_{\rm W}$ (see table 10) affects the calculation for the b-quark pole asymmetry by $\Delta A_{\rm FB}^{\rm 0,b} \ll 0.001$, i.e. much smaller than the current experimental precision (eq. 84). Therefore, all observables basically measure the effective mixing angle of leptons or, like the angular dependence of the left-right asymmetry for b-quarks (eq. 92), are not yet precise enough to be sensitive to the differences shown in table 10.

Extracting $\sin^2\bar{\vartheta}_{\rm W}$ from the measurement of the quark charge asymmetry is not independent of the Standard Model because it prescribes the quark flavor composition of hadronic Z decays to the Standard Model expectation. The result obtained at LEP [19]

$$\sin^2\bar{\vartheta}_{\rm W} = 0.2325 \pm 0.0013 \tag{96}$$

agrees well with other determinations, though.

Figure 44 summarizes the LEP averages on $\sin^2\bar{\vartheta}_{\rm W}$ obtained from the forward-backward asymmetries of leptons, b- and c-quarks, the tau polarization and its forward-backward asymmetry, and compares it to the measurement of the left-right asymmetry performed by the SLD experiment. Averaging the results of the six observables leads to

$$\sin^2\bar{\vartheta}_{\rm W} = 0.2314 \pm 0.0003 \tag{97}$$

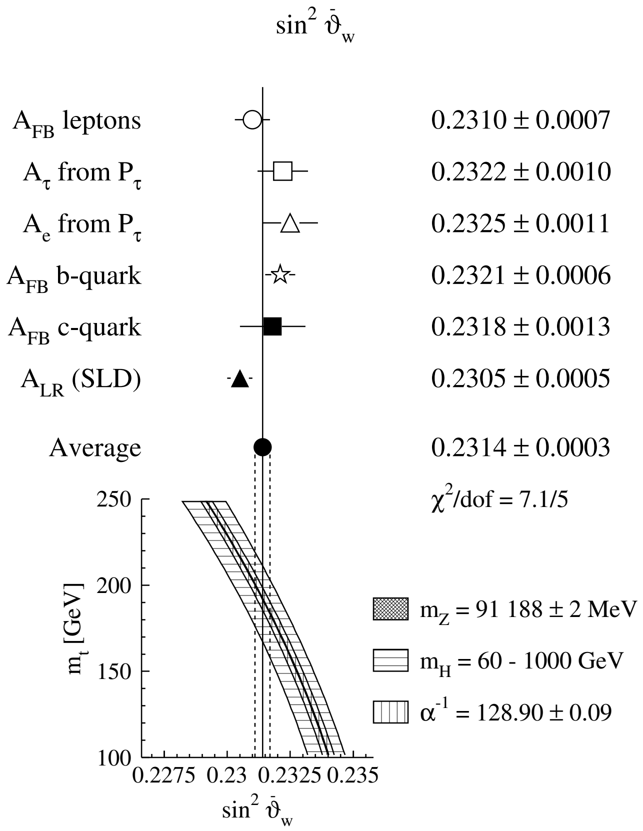

Figure 44: Comparison of the effective weak mixing angle $\sin^2\bar{\vartheta}_W$ obtained from asymmetry measurements at LEP and SLC together with the combined value and the Standard Model calculation for different Higgs masses and QED coupling constants $\alpha(m_Z)$.

with $\chi^2 = 7.1$ for five degrees of freedom. The main contribution to this χ^2 arises from the A_{LR} measurement at SLC which deviates from the average of the five measurements performed at LEP, $\sin^2\bar{\vartheta}_W = 0.2318 \pm 0.0004$ ($\chi^2 = 2.2$), by two standard deviations. Future improved determinations of A_{LR} and the other asymmetries will clarify this issue.

Both average values of $\sin^2\bar{\vartheta}_W$ are well compatible with a top quark mass of 180 GeV and the errors translates, for fixed m_H, to an estimate of $\Delta m_t \approx \pm 10$ GeV. Figure 44 also shows the dependence of the Standard Model calculation for $\sin^2\bar{\vartheta}_W$ on the QED coupling constant at the Z mass, $\alpha(m_Z)$. Varying this input parameter within its uncertainty (eq. 41) shifts the central value by $\Delta \sin^2\bar{\vartheta}_W \approx \pm 0.00023$ which is of the same order as the experimental error. The uncertainty on $\alpha(m_Z)$ is therefore a limiting factor for the interpretation of the measured $\sin^2\bar{\vartheta}_W$ in terms of Standard Model parameters like the top quark mass. On the other hand the uncertainty on $\alpha(m_Z)$ is not limiting the experimental precision on $\sin^2\bar{\vartheta}_W$. The QED corrections applied to obtain for instance A^0_{FB} from the measured forward-backward asymmetries do not depend much on the QED coupling constant at the mass of the Z.

The effective weak mixing angle can be obtained also from a Standard Model fit to the asymmetries used above and the measured total cross sections, or the total and partial width derived from the latter. Contrary to the asymmetries the widths are proportional to the square of the effective coupling constants (eq. 37) and hence depend on the ρ-parameter. To convert the measurements of the total and partial widths into $\sin^2\bar{\vartheta}_{\mathrm{W}}$ one therefore must assume the Standard Model relation between $\bar{\rho}$ and $\sin^2\bar{\vartheta}_{\mathrm{W}}$. The result of this fit (see section 9.1) is

$$\sin^2\bar{\vartheta}_{\mathrm{W}} = 0.2316 \pm 0.0003 \pm 0.0001 \tag{98}$$

where the second error reflects the variation of m_{H}. The error on $\alpha(m_{\mathrm{Z}})$ is also included in the result. This result is in good agreement with the more model-independent value obtained from the asymmetries alone which of course reflects again the good agreement of all total cross section and asymmetry measurements at LEP and SLC with the Standard Model using a common value for the top mass.

8.2 The effective vector and axial-vector coupling constants $\bar{g}_{\mathrm{V}}$ and $\bar{g}_{\mathrm{A}}$ for charged leptons

The vector and axial-vector coupling constants of electrons, muons and taus can be determined from the partial widths and the asymmetries exploiting their different dependence on the coupling constants. To obtain the combined result on $\bar{g}_{\mathrm{V}}$ and $\bar{g}_{\mathrm{A}}$ as well as the contour in the $\bar{g}_{\mathrm{V}}$-$\bar{g}_{\mathrm{A}}$ plane the results listed in table 17 (appendix A) and their correlations are used together with A_{e} and A_τ from the tau polarization and the measurement of A_{LR} by the SLD experiment. The leptonic partial widths are related to the effective couplings including final state QED and mass corrections as [64]:

$$\begin{aligned} \Gamma_\ell &= \frac{G_{\mathrm{F}}\, m_{\mathrm{Z}}^3}{6\sqrt{2}\,\pi}\sqrt{1-4\,\mu_\ell}\left(1+\frac{3}{4}\frac{\alpha}{\pi}\right)\left[\left((\bar{g}_{\mathrm{A}}^\ell)^2+(\bar{g}_{\mathrm{V}}^\ell)^2\right)(1+2\mu_\ell)-6(\bar{g}_{\mathrm{A}}^\ell)^2\mu_\ell\right] \\ \mu_\ell &= \left(\frac{m_\ell}{m_{\mathrm{Z}}}\right)^2 \end{aligned} \tag{99}$$

The results obtained for the three lepton species from LEP measurements are shown in table 11 together with the result imposing lepton universality. The numbers quoted in table 12 include also the measurement of A_{LR} performed at SLC (eq. 90).

	$\bar{g}_{\mathrm{A}}$	$\bar{g}_{\mathrm{V}}$
$\mathrm{e}^+\mathrm{e}^-$	-0.5011 ± 0.0005	-0.0368 ± 0.0018
$\mu^+\mu^-$	-0.5011 ± 0.0008	-0.0370 ± 0.0041
$\tau^+\tau^-$	-0.5015 ± 0.0009	-0.0371 ± 0.0018
$\ell^+\ell^-$	-0.5012 ± 0.0004	-0.0369 ± 0.0010

Table 11: The effective axial-vector and vector coupling constants $\bar{g}_{\mathrm{A}}$ and $\bar{g}_{\mathrm{V}}$ for charged leptons obtained from LEP cross section and asymmetry measurements.

Because of the small vector couplings the partial widths are essentially proportional to $\bar{g}_{\mathrm{A}}^2$ and the errors on the axial-vector couplings values reflect the errors on the partial widths as well as their correlations (see section 5.5). The experimental

	$\bar{g}_A$	$\bar{g}_V$
e^+e^-	-0.5010 ± 0.0005	-0.0385 ± 0.0009
$\mu^+\mu^-$	-0.5012 ± 0.0007	-0.0354 ± 0.0036
$\tau^+\tau^-$	-0.5015 ± 0.0009	-0.0369 ± 0.0018
$\ell^+\ell^-$	-0.5011 ± 0.0004	-0.0380 ± 0.0007

Table 12: Same as table 11 including the A_{LR} measurement of SLD.

error on the total width Γ_Z is one of the limiting factors in the measurement of the axial-vector coupling constant of leptons $\bar{g}_A^\ell$.

In the calculation leading to tables 11 and 12 the axial-vector coupling constant of the electron is constrained to negative values. The negative value of $\bar{g}_A^e$ has been experimentally established already from the combination of neutrino-electron scattering results and the forward-backward asymmetry measurements at PETRA and PEP [170, 171]. All other signs are unambiguously determined by the LEP and SLD measurements. Hence, lepton universality is confirmed in size and sign of the coupling constants to high accuracy by the experiments at the Z.

The test of lepton universality can be quantified by calculating the ratio of muon and tau to electron coupling constants obeying their correlations. From LEP (table 11) one obtains

$$\begin{array}{rclrcl} \bar{g}_A^\mu/\bar{g}_A^e & = & 1.0000 \pm 0.0018 & \bar{g}_V^\mu/\bar{g}_V^e & = & 1.01 \pm 0.14 \\ \bar{g}_A^\tau/\bar{g}_A^e & = & 1.0007 \pm 0.0020 & \bar{g}_V^\tau/\bar{g}_V^e & = & 1.01 \pm 0.07 \end{array} \tag{100}$$

and including the measurement of A_{LR} (table 12):

$$\begin{array}{rclrcl} \bar{g}_A^\mu/\bar{g}_A^e & = & 1.0004 \pm 0.0018 & \bar{g}_V^\mu/\bar{g}_V^e & = & 0.92 \pm 0.10 \\ \bar{g}_A^\tau/\bar{g}_A^e & = & 1.0009 \pm 0.0020 & \bar{g}_V^\tau/\bar{g}_V^e & = & 0.96 \pm 0.05 \end{array} \tag{101}$$

The numbers are all well compatible with unity and hence prove the universality of lepton couplings. In particular, the experimental accuracy on the ratios of axial-vector couplings is $\pm 0.2\%$. When including the A_{LR} result into the fit the muon and tau vector couplings come out to be different by about one standard deviation from electron coupling. Again, this reflects the apparent difference of the A_e measurements at LEP and SLC.

Figures 45 and 46 show the allowed contours (68% C.L.) in the $\bar{g}_A$-$\bar{g}_V$ plane for electrons, muons and taus. Good agreement is found for the three channels. The best measurements are obtained for the electron and for the tau whereas in $e^+e^- \to \mu^+\mu^-$ always the product of muon and electron couplings is measured. The polarization of muons from Z decay could be measured directly from the angular dependence of the left-right asymmetry, $A_{FB}^{LR,\mu}$, as it has been done for b- and c-quarks by the SLD experiment (see section 7.5) With 20 000 $\mu^+\mu^-$pairs a statistical precision of $\Delta\bar{g}_V^\mu = 0.004$ can be achieved from this measurement.

The contours are compared to Standard Model predictions for different top quark and Higgs masses again revealing the excellent agreement for a top mass of about 175 GeV. The uncertainty on $\alpha(m_Z)$ (see eq. 42) changes the prediction for the

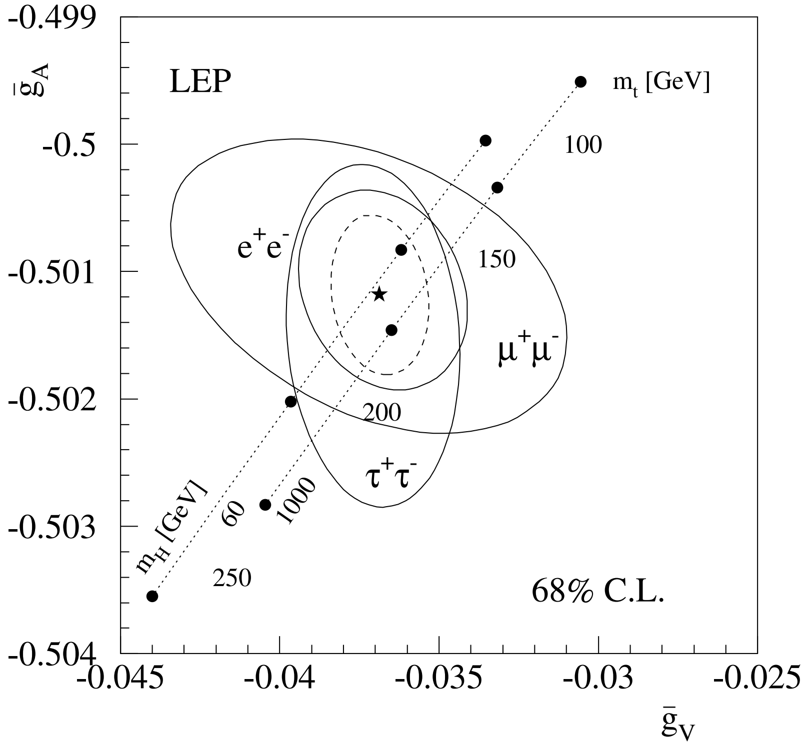

Figure 45: The contours (68% C.L.) in the $\bar{g}_{\rm A}$-$\bar{g}_{\rm V}$ plane for electrons, muons and taus obtained by the LEP experiments. The broken line is the combined contour for leptons and the star indicates the central value. The filled circles connected by dotted lines show the Standard Model predictions for different $m_{\rm t}$ and $m_{\rm H}$ values.

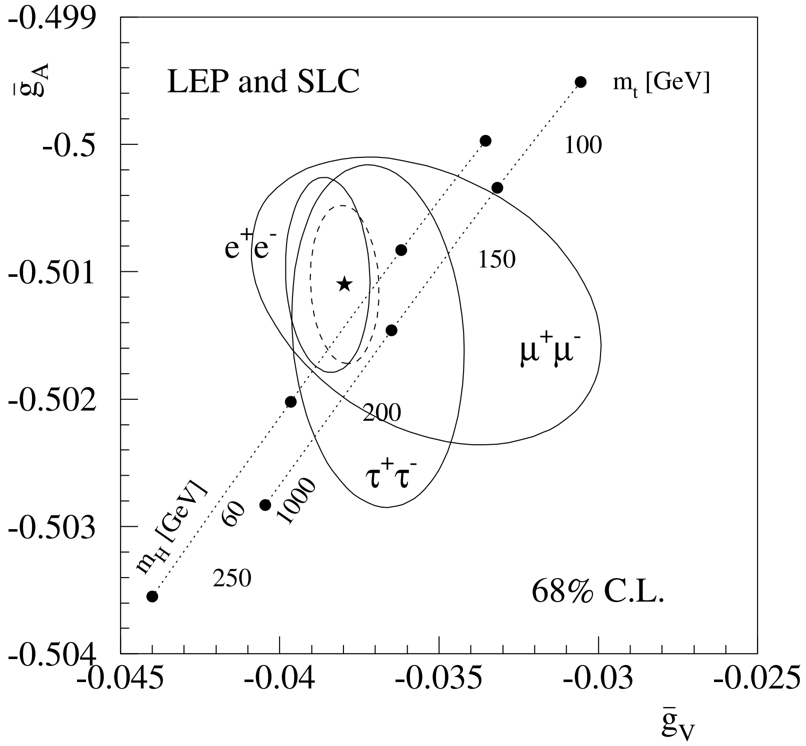

Figure 46: Same as figure 45 with the $A_{\rm LR}$ result from SLD included.

vector coupling constant by $\Delta\bar{g}_V^\ell = \pm 0.0005$ (not shown in the plot) while leaving $\bar{g}_A^\ell$ unchanged.

In neutrino-electron scattering experiments the vector and axial-vector coupling constants of the electron are measured at low momentum transfer ($Q^2 \approx 0.01$ GeV^2). The result of the CHARM II experiment obtained from muon-neutrino electron scattering [172]

$$\begin{aligned} g_A^e &= -0.503 \pm 0.006 \pm 0.016 \\ g_V^e &= -0.035 \pm 0.012 \pm 0.012 \end{aligned} \tag{102}$$

compares well to the measurements at the Z resonance.

8.3 The effective vector and axial-vector coupling constants $\bar{g}_V$ and $\bar{g}_A$ for heavy quarks

The coupling constants for b- and c-quarks can be derived from their measured forward-backward asymmetries and partial decay widths in the same way as the coupling constants of charged leptons. Belonging to different generations b- and c-quarks are representatives of different weak isospin states: $T_3 = -1/2$ and $T_3 = +1/2$, respectively. In this way the Standard Model assignment of vector and axial-vector coupling constants (eq. 11) can be experimentally verified also for quarks. As it is the weak isospin partner of the top quark the verification of the b-quark couplings and thus its isospin assignment provides indirect evidence for the existence of the top.

Forward-backward asymmetries and cross section of heavy quarks measured below the Z pole have been used in the past to obtain their coupling constants [173, 174]. Again, the experiments at the Z pole have largely improved the accuracy of these measurements.

	$\bar{g}_A$	$\bar{g}_V$
$b\bar{b}$	$-0.528\,^{+0.016}_{-0.013}$	$-0.313\,^{+0.023}_{-0.027}$
$c\bar{c}$	$+0.477 \pm 0.013$	$+0.176 \pm 0.015$

Table 13: The effective axial-vector and vector coupling constants for b- and c-quarks obtained from the combined LEP results, the SLD measurement of A_b and A_c and the forward-backward asymmetries measured at PEP, PETRA and TRISTAN experiments.

Table 13 shows the results for the axial-vector and vector coupling constants of b- and c-quarks. The numbers are obtained using the combined LEP results on b- and c-quarks (see appendix C) and their correlation. The results on forward-backward asymmetries below the Z pole (table 24) are included. These data determine the sign of $\bar{g}_A$ and solve the ambiguity in $\bar{g}_A$ and $\bar{g}_V$ which is present in the formulae for $\sqrt{s} = m_Z$. Also the SLD measurements of A_b and A_c (eq. 92) are added. The couplings of the electrons and the partial decay width of the Z into hadrons are constrained to the results of the fit for the leptonic coupling constants (table 12).

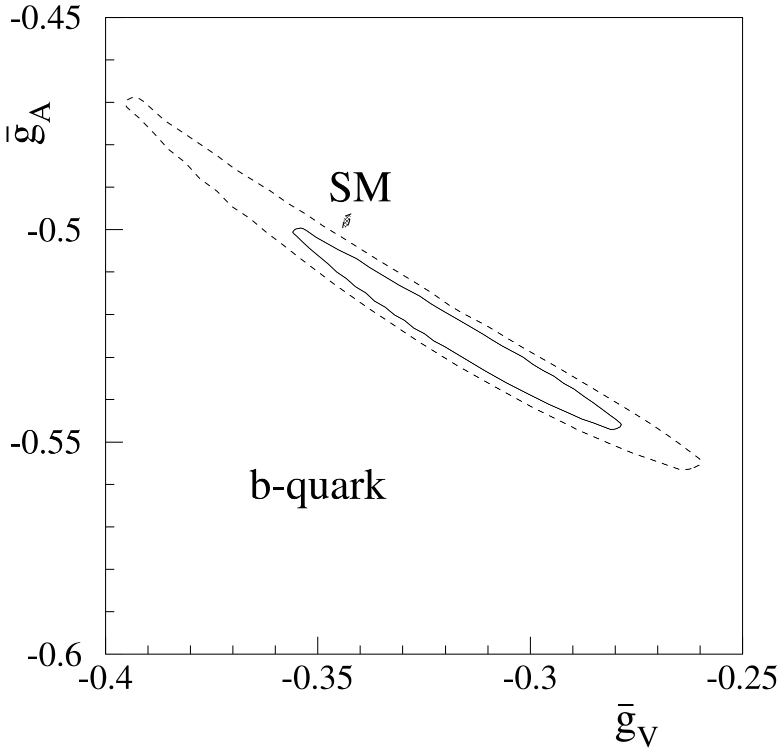

Figure 47: The 68% (solid line) and 95% C.L. (broken line) contours in the $\bar{g}_A$-$\bar{g}_V$ plane for b-quarks compared to the area allowed by the Standard Model (SM) for different m_t and m_H values.

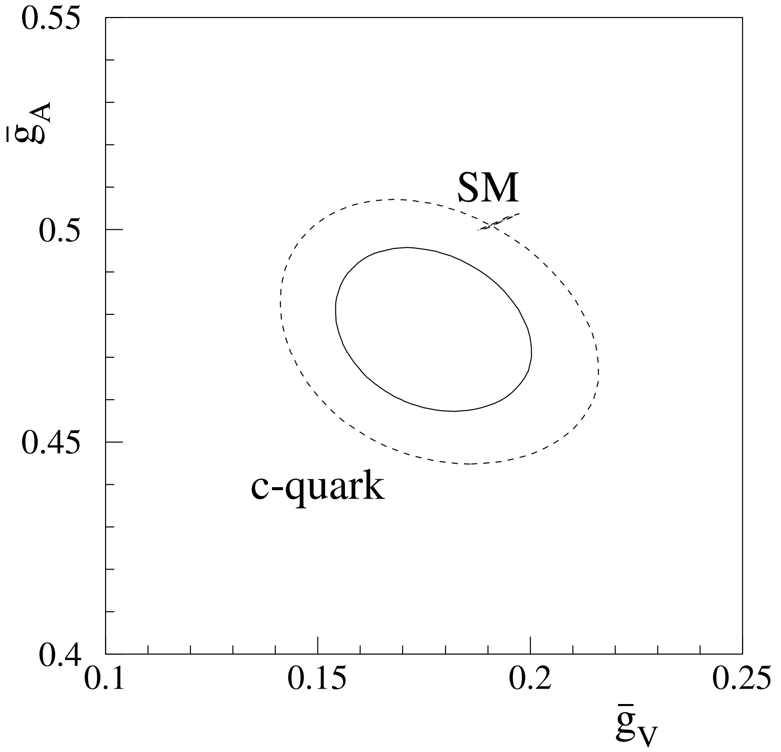

Figure 48: Same as figure 47 for c-quarks.

The contours in the $\bar{g}_V$-$\bar{g}_A$ plane are shown in figures 47 and 48. In both figures the area for $\bar{g}_A$ and $\bar{g}_V$ allowed in the Standard Model when varying the input parameters according to eq. 42 is indicated. The agreement with the experimental measurements is satisfactory and clearly supports the $T_3 = -1/2$ and $T_3 = +1/2$ hypothesis for b- and c-quarks, respectively. However, the discrepancies observed in Γ_b/Γ_{had} (see section 6.4), and also Γ_c/Γ_{had}, are again visible as a two or more standard deviation effects in the contours.

Contrary to the charged leptons the precision achieved in the quark couplings is not adequate to single out a preferred region for the top quark mass.

9 Interpretation of electroweak observables

9.1 The mass of the top quark

As has been demonstrated in the previous sections all experimental results obtained at the Z resonance with some reservations about the partial decay widths of b- and c-quarks are well described by the Standard Model using a common value for the mass of the top quark. Here all available measurements are used to derive the best estimate for m_t from the precision measurements of radiative corrections in the Standard Model framework. The experimental input used is the set of five parameters obtained from the total cross sections and lepton forward-backward asymmetries at LEP (table 14), the results of the tau polarization measurement (eq. 88) and the partial widths and forward-backward asymmetries of b- and c-quarks (table 25). The results from SLD (eq. 90 and eq. 92) are also added.

The result for the top quark mass is

$$m_t = 181\,^{+8}_{-9}\,^{+17}_{-20}(m_H)\ \text{GeV} \tag{103}$$

where the second error indicates the shift of the central value when varying the Higgs mass from 60 to 1000 GeV. This contribution to the uncertainty of the top mass estimate is larger than the experimental precision. The first error contains also the uncertainties introduced by the other Standard Model parameters, in particular the knowledge of the strong and QED coupling constants at the mass of the Z. Their uncertainties (eq. 42) contribute to approximately ± 3 GeV ($\Delta\alpha_s$) and ± 4 GeV ($\Delta\alpha(m_Z)$) to the error of the top mass estimate. In particular the precision of $\alpha(m_Z)$ plays a role due to the correlation of the running of α and the weak radiative corrections in Δr which is the quantity which most of the observables at the Z are sensitive to.

Releasing the constraint on the strong coupling constant one can fit simultaneously for m_t and α_s. The result obtained

$$\begin{aligned} m_t &= 181 \pm 9\,^{+17}_{-20}(m_H)\ \text{GeV} \\ \alpha_s &= 0.123 \pm 0.004 \pm 0.003 \end{aligned} \tag{104}$$

is consistent both with the top mass estimate from above and the value used for α_s obtained from the study of hadronic event shapes at the Z [124].

This value for α_s is also in agreement with the result obtained from the ratio of hadronic and leptonic widths alone (see section 6.3). The second error given for α_s contains the theoretical uncertainty in the calculation of the electroweak and QCD

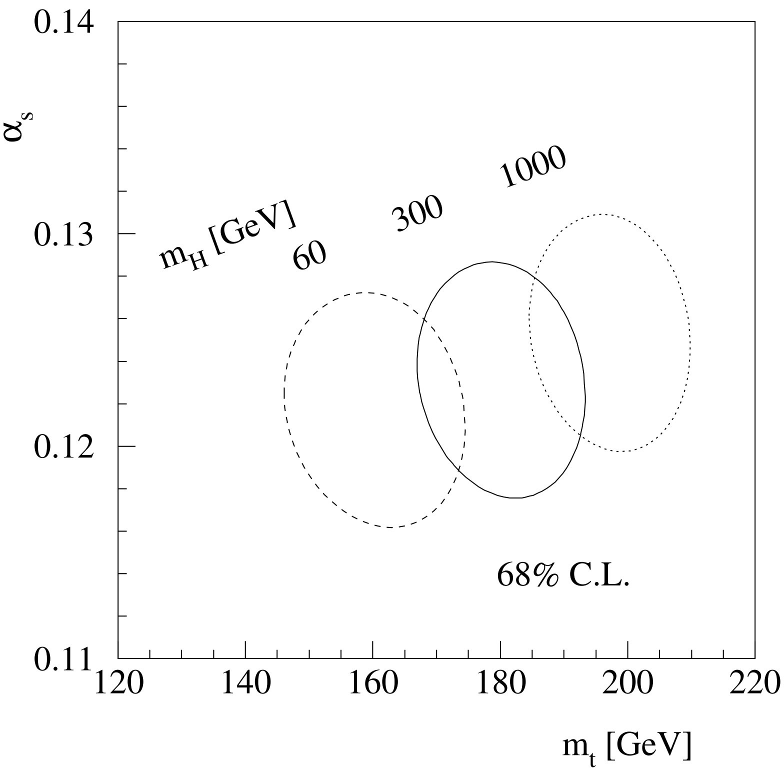

Figure 49: The 68% C.L. contour in the α_s–m_t plane obtained from a Standard Model fit assuming different values for the Higgs boson mass.

radiative corrections [123] and the shift of the central value when changing the Higgs boson mass. Figure 49 shows the 68% C.L. contour in the α_s and m_t plane which demonstrates the correlation between these two parameters as well as the dependence of the result on the unknown Higgs mass.

It should be noted that here an estimate for the mass of a particle is presented which is obtained from precision measurements of radiative corrections. As a matter of fact the top quark has been discovered recently at exactly the predicted mass by the two experiments at the FERMILAB $p\bar{p}$ collider [13]:

$$\begin{aligned} m_t &= 176 \pm 8 \pm 10 \text{ GeV} \qquad \text{(CDF)} \\ m_t &= 199\,^{+19}_{-21} \pm 22 \text{ GeV} \qquad \text{(D0).} \end{aligned} \tag{105}$$

This discovery is a striking success of the Standard Model since it proves that the major part of the weak radiative corrections (see section 3.2) does indeed originate from the large mass difference in the top-bottom weak isospin doublet. Non-trivial higher order diagrams like the vacuum polarization of heavy gauge bosons (figure 6) are thus experimentally established.

Leaving aside the unknown mass of the Higgs for a moment the mass of the top quark obtained in eq. 103 (and eq. 105) fixes the last unknown input parameter of the Standard Model. Hence it can be used to calculate any other quantity in the Standard Model framework. For instance, using the result of eq. 103 one obtains the following parameters:

$$
\begin{aligned}
\sin^2\bar{\vartheta}_W &= 0.2316 \pm 0.0003 \pm 0.0001 \\
\sin^2\vartheta_W &= 0.2233 \pm 0.0011 \,^{+0.0004}_{-0.0003} \\
m_W &= 80.36 \pm 0.06 \pm 0.02 \text{ GeV} \\
\Delta r &= 0.036 \,^{+0.004}_{-0.003} \pm 0.001
\end{aligned} \tag{106}
$$

The ignorance of m_H is the cause of the second error quoted. The $\sin^2\bar{\vartheta}_W$ value uses the information contained in the widths and thus depends on the Standard Model calculation of radiative corrections (see section 8.1).

The on-shell definition $\sin^2\vartheta_W$ has a larger error which is just an artifact reflecting its steeper m_t dependence demonstrated in figure 8. One can compare the LEP and SLC measurements in terms of $\sin^2\vartheta_W$ with neutrino-nucleon scattering experiments at low energies. The results of these experiments [175, 176, 177] yield an average value of [178]

$$\sin^2\vartheta_W = 0.2260 \pm 0.0048. \tag{107}$$

The good agreement with the result at the Z resonance demonstrates again that the Standard Model describes well all neutral current experiments from very low energies up to the Z mass.

The $W^\pm$ mass derived from the LEP measurements compares also very well with the direct measurements at the $p\bar{p}$ colliders [30]:

$$m_W = 80.23 \pm 0.18 \text{ GeV}. \tag{108}$$

Here it becomes evident that the combined result of electroweak observables at the Z resonance exceeds the precision on the direct mass measurement of the $W^\pm$ (see section 3.1).

The electroweak radiative corrections Δr determined in the Standard Model framework differ significantly from the 6% arising from the running of α (see section 3.3). This shows again that pure weak radiative corrections from a heavy top quark ($m_t > 100$ GeV) are necessary to describe the experimental results.

9.2 The mass of the Higgs boson

The precise measurements of electroweak observables at the Z and their interpretation in terms of weak radiative corrections led to a rather precise estimate for the mass of the top quark (eq. 103). Of course, this raises the question if the precise knowledge of Z parameters can be used similarly to derive a statement on the last missing Standard Model parameter: the mass of the Higgs boson.

As it has been demonstrated throughout this article the sensitivity of electroweak observables is much smaller for the Higgs mass as compared to the top quark mass since weak radiative corrections depend only logarithmically on m_H. From figure 45 (see also figure 51 below) it is very clear that the data constrain the range of allowed top masses in the Standard Model but that on the other hand the variation of Standard Model calculations in the range of reasonable Higgs masses is smaller than the current precision of the experimental input. As long as these data are used to constrain simultaneously both, m_t and m_H, no improvement of the experimental and theoretical limits on the Higgs boson (see section 2.2) is possible.

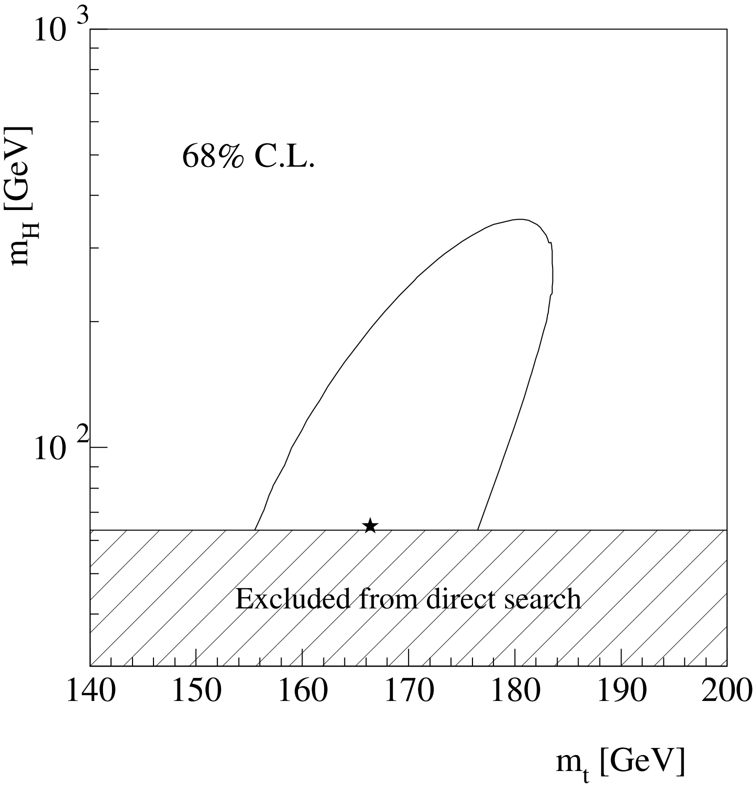

Figure 50: The 68% C.L. contour in the m_{H}–m_{t} plane obtained from a Standard Model fit constraining the top quark mass to the result of the direct measurement (eq. 109). The star indicates the central value of the fit. Higgs masses below 63.5 GeV are excluded by the result of the direct search [29].

However, one can now use the direct measurements of the top quark mass (eq. 105). Averaging the two results yields

$$m_{\mathrm{t}} = 180 \pm 12 \text{ GeV} \tag{109}$$

and with this additional constraint the 68% C.L. contour shown in figure 50 is obtained. The limit from the direct search for the Standard Model Higgs boson, $m_{\mathrm{H}} \geq 63.5$ GeV, is overlaid because the electroweak data cannot rule out the Higgs boson below this limit. The fit prefers a light Higgs with a central value of $m_{\mathrm{H}} = 65$ GeV. And with 95% probability a heavy Higgs boson ($m_{\mathrm{H}} > 536$ GeV) is excluded. See also the discussions in references [102, 19, 179].

However, the result of the b-quark partial width $R_{\mathrm{b}} = \Gamma_{\mathrm{b}}/\Gamma_{\mathrm{had}}$ (figure 27) has a rather large influence on this Higgs mass estimation. This measurement is insensitive to m_{H} but pulls the fit towards lower top quark masses and due to the correlation between the two parameters in Δr to lower m_{H} values. Leaving out R_{b} from the fit changes the central value to $m_{\mathrm{H}} = 129$ GeV and a Higgs mass of 1000 GeV cannot be excluded anymore from the remaining electroweak data.

In summary, one can state that the measurements of electroweak observables at LEP and SLC start to become sensitive to the Standard Model Higgs boson if the direct measurement of the top quark mass is included. With improved precision on both, the direct m_t measurement and the Z parameters, one might be able in near future to tell from figure 50 if the Standard Model Higgs boson is light or heavy. This would be an important experimental information for the plans for future accelerators intended to search for the Higgs boson.

9.3 The epsilon parameters

It has been shown in this article that the precision measurements of electroweak observables are all compatible with the Standard Model of electroweak interactions for a top mass $m_t \approx 175$ GeV and with any reasonable choice for the Higgs boson mass. But it is also very important to verify the validity of the Standard Model in a way as independently as possible of these two parameters. Several strategies have been proposed in the literature [180]. Here the parameterization of electroweak measurements in terms of ε parameters [181] is discussed. Two of these parameters, ε_1 and ε_3, are directly related to observables (leptonic partial width, lepton asymmetries) at LEP[10]. The aim is to disentangle the radiative corrections originating from top quark and Higgs masses:

$$\begin{aligned} \varepsilon_1 &= \Delta\rho \\ \varepsilon_3 &= c_0^2\,\Delta\rho + (c_0^2 - s_0^2)\,(\sin^2\bar{\vartheta}_W/s_0^2 - 1) \\ \text{with } s_0^2\,c_0^2 &= \frac{\pi\,\alpha(m_Z)}{\sqrt{2}\,G_F\,m_Z^2}. \end{aligned} \tag{110}$$

The first parameter (ε_1) is identical to the deviation of the ρ parameter from unity (see eq. 33) thus preserving the leading quadratic m_t dependence of weak radiative corrections in this parameter. The other, ε_3, is a linear combination of $\Delta\rho$ and the weak radiative corrections relating the definitions of the weak mixing angle (section 3.2). This linear combination is chosen such that the leading m_t^2-term of the weak radiative corrections drops out and only a mild m_t dependence remains in ε_3. The Standard Model calculations for various top quark and Higgs boson masses shown in figure 51 demonstrate this behaviour.

The result from the fit to the LEP cross section, lepton and b-quark forward-backward asymmetry and tau polarization data is shown as 68% and 95% C.L. contours. Again, it can be seen that the LEP data significantly constrain the mass of the top quark as discussed in the previous section. However, from the wide range of allowed ε_3 values it becomes clear that no statement on m_H from electroweak precision measurements alone can be made. The measurements have to be improved and, most importantly, the mass of the top quark must be measured as precisely as possible.

The fit shown in figure 51 severely constrains the allowed parameter space of extensions of the Standard Model like Technicolour [18], Supersymmetry [17] and new gauge groups. New physics would modify the expectations for these parameters. See for instance reference [182] for a detailed discussion.

9.4 Unification of coupling constants

Leaving aside gravitation there are two theories today which both together describe very successfully all interactions among elementary particles. The Standard Model

[10] Another parameter, ε_b, parametrizes the $Zb\bar{b}$ vertex corrections [181].

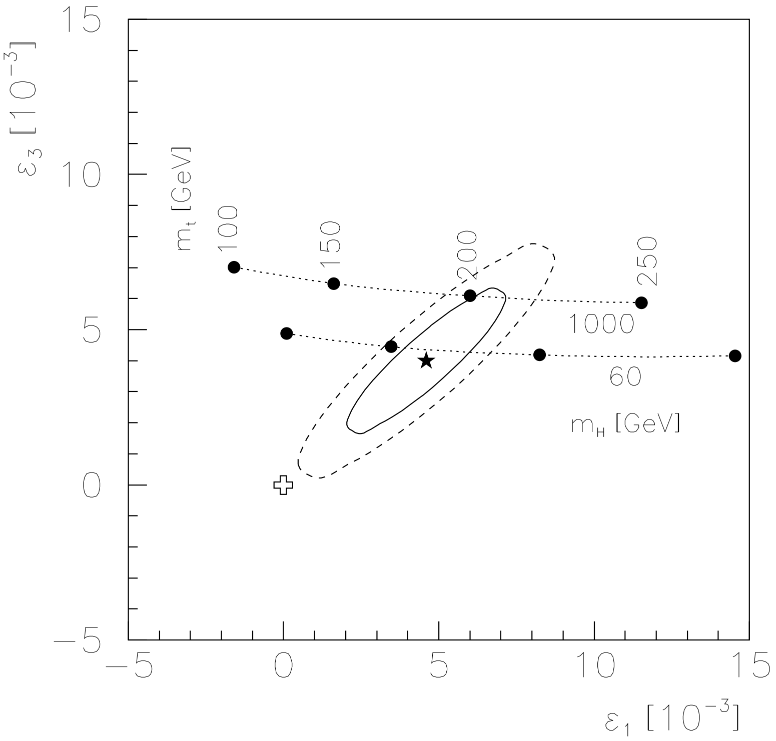

Figure 51: The contours in the ε_1 and ε_3 plane as obtained from the measurements of Γ_ℓ and $\sin^2\bar{\vartheta}_W$ at LEP and SLC. The solid line shows the 68%, the broken line the 95% C.L. contour and the star is the central value of the fit. The hollow cross indicates the Standard Model expectation without weak radiative corrections.

of electroweak interactions based on $SU(2)_L \times U(1)$ gauge symmetry accounts for all electroweak phenomena observed so far. Likewise strong interactions between quarks and gluons are described by QCD which is based upon SU(3) colour symmetry. However, both models are separated and there is no theoretical link between electroweak and strong interactions.

Naturally, the next step towards a more profound theoretical understanding of nature would be the unification of electroweak and strong interactions. Similar to the apparent distinction between electromagnetic and weak phenomena at energies well below the electroweak unification, i.e. the masses of the heavy gauge bosons, strong and electroweak phenomena are distinct at currently accessible energies. The appealing idea is that strong and electroweak interactions are described by a common symmetry beyond a certain energy, the grand unification (GUT) scale, and that this symmetry is broken at lower energies leading to the apparently very different behaviour of quarks and leptons. The SU(5) group is the simplest possible symmetry describing the unification of electroweak and strong interactions [16].

As the mass scale of the electroweak unification, the masses of the $W^\pm$ and Z bosons, were predictable from experiments at low energies there are observables at lower energies which can be exploited to constrain possible unification models as well as to derive limits on the energy scale. One of the predictions is the decay of the proton. The link between quarks and leptons requires heavy gauge bosons, X and Y, coupling to quark-lepton pairs with masses around the unification scale. Hence

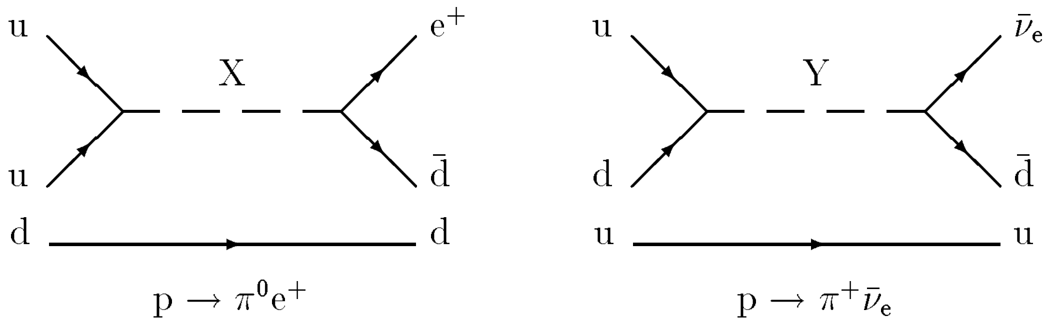

Figure 52: Examples of the proton decay in Grand Unification theories.

processes like the examples depicted in figure 52 are possible and lead to the decay of protons. Completely analogous to the decay of the muon from which the mass of the $W^{\pm}$ bosons can be derived (see section 3.1) the experimental limit on the proton lifetime

$$\tau_{\mathrm{p}} \geq 5 \cdot 10^{32} \text{ years} \tag{111}$$

implies a limit on the mass of the X and Y bosons and hence on the energy scale of grand unification [183, 20]

$$m_{\mathrm{X}} \geq 10^{15} \text{ GeV}. \tag{112}$$

Another consequence of the unification of strong and electroweak interactions would be that the coupling constants assigned to each symmetry group can be derived from one single coupling constant at the unification scale. Three independent coupling constants are needed for the three gauge groups which describe the interactions at the scale of electroweak unification: g and g' of $\mathrm{SU(2)_L} \times \mathrm{U(1)}$ (eq. 6) and α_s of QCD. For the discussion of grand unification they are usually parameterized as:

$$\begin{aligned} \alpha_1 &= \frac{5}{3}\frac{g'^2}{4\pi} = \frac{5}{3}\frac{\alpha}{\cos^2\vartheta_{\mathrm{W}}^2} \\ \alpha_2 &= \frac{g^2}{4\pi} = \frac{\alpha}{\sin^2\vartheta_{\mathrm{W}}^2} \\ \alpha_3 &= \alpha_s. \end{aligned} \tag{113}$$

Coupling constants are constant only at a given energy. They are energy, or equivalently, distance dependent through virtual corrections. The running of the QED coupling constant α discussed in section 3.3 is an example for the energy dependence of coupling constants.

The evolution of the coupling constants with the energy scale μ is governed by a set of non-linear differential equations, the renormalization group equations (RGE). In second order they can be written as [184]

$$\mu \frac{\partial \alpha_i^{-1}}{\partial \mu} = -\frac{1}{2\pi} b_i - \frac{1}{8\pi^2} \sum_j b_{ij}\alpha_j \qquad (i,j = 1,2,3). \tag{114}$$

The first and second order beta coefficients, b_i and b_{ij}, encode the particle spectrum of the theory and how the gauge couplings influence each other [185]. These coefficients hence depend on the number of fermion generations N_{g} and on the number of Higgs particles N_{H} in the model.

In the Standard Model these coefficients are [186]:

$$\begin{aligned} b_i &= \begin{pmatrix} 0 \\ -22/3 \\ -11 \end{pmatrix} + N_{\mathrm{g}} \begin{pmatrix} 4/3 \\ 4/3 \\ 4/3 \end{pmatrix} + N_{\mathrm{H}} \begin{pmatrix} 1/10 \\ 1/6 \\ 0 \end{pmatrix} \\ b_{ij} &= \begin{pmatrix} 0 & 0 & 0 \\ 0 & -136/3 & 0 \\ 0 & 0 & -102 \end{pmatrix} + N_{\mathrm{g}} \begin{pmatrix} 19/15 & 3/5 & 44/15 \\ 1/5 & 49/3 & 4 \\ 11/30 & 3/2 & 76/3 \end{pmatrix} \\ &+ N_{\mathrm{H}} \begin{pmatrix} 9/50 & 9/10 & 0 \\ 3/10 & 13/6 & 0 \\ 0 & 0 & 0 \end{pmatrix} \end{aligned} \tag{115}$$

The experiments at the Z resonance have significantly improved our knowledge of the coupling constants at the Z mass, $\alpha_i(m_{\mathrm{Z}})$. The measurements of α_{s} [124] and the weak mixing angle $\sin^2\vartheta_{\mathrm{W}}$ at LEP, together with the extrapolated QED coupling constant $\alpha(m_{\mathrm{Z}})$, fix the three coupling constants at m_{Z}. With the help of the RGE these coupling constants can then be calculated at any energy scale μ to test the hypothesis that they are equal at a certain point.

It should be noted here that the RGE as well as the beta coefficients depend on the renormalization scheme applied. The above cited relations are calculated in the modified minimal subtraction scheme ($\overline{\mathrm{MS}}$) [187]. The corresponding QED coupling constant and weak mixing angle determined in reference [188, 189], together with the α_{s} value given in eq. 73, will be used in the following:

$$\begin{aligned} \alpha(m_{\mathrm{Z}})^{-1} &= 127.9 \pm 0.2 \\ \sin^2\vartheta_{\mathrm{W}}^{\overline{\mathrm{MS}}}(m_{\mathrm{Z}}) &= 0.2334 \pm 0.0006. \end{aligned} \tag{116}$$

The value for $\sin^2\vartheta_{\mathrm{W}}^{\overline{\mathrm{MS}}}(m_{\mathrm{Z}})$ emerges from a fit using all Z, W and neutral-current data. The strong coupling constant α_{s} has the largest error and thus will determine the precision of the evolution of the coupling constants.

Solving the renormalization group equations [184] (eq. 114) using the beta coefficients for three generations and one Higgs boson leads to the evolution of the coupling constants shown in figure 53. The width of the bands represent the experimental error of the coupling constant at m_{Z}, propagated along the energy scale.

In the Standard Model the three coupling constants do not meet at one point and hence do not emerge from one common gauge group[11]. In addition, the coupling constants become of the same order already below the limit of 10^{15} GeV imposed by the lifetime of the proton. This has been already observed before the advent of LEP [190] but the precision measurements at the Z resonance rule out with much more significance the simplest model of grand unification.

[11] This could also be explained if one assumes that the common gauge group is broken in steps at different energies.

If one still wants to keep alive the idea of unifying electroweak and strong interactions new physics is required between the scale of the electroweak unification $\mathcal{O}(100\ \text{GeV})$ and the grand unification scale at $\mu \geq 10^{15}$ GeV. New particles cause additional virtual diagrams and consequently change the evolution of the coupling constants. This is reflected by a modification of the beta coefficients. For instance, in the minimal Supersymmetry Model [17] one obtains [186]

$$
\begin{aligned}
b_i &= \begin{pmatrix} 0 \\ -6 \\ -9 \end{pmatrix} + N_{\rm g} \begin{pmatrix} 2 \\ 2 \\ 2 \end{pmatrix} + N_{\rm H} \begin{pmatrix} 3/10 \\ 1/2 \\ 0 \end{pmatrix} \\
b_{ij} &= \begin{pmatrix} 0 & 0 & 0 \\ 0 & -24 & 0 \\ 0 & 0 & -54 \end{pmatrix} + N_{\rm g} \begin{pmatrix} 38/15 & 6/5 & 88/15 \\ 2/5 & 14 & 8 \\ 11/15 & 3 & 68/3 \end{pmatrix} \\
&+ N_{\rm H} \begin{pmatrix} 9/50 & 9/10 & 0 \\ 3/10 & 7/2 & 0 \\ 0 & 0 & 0 \end{pmatrix} .
\end{aligned} \tag{117}
$$

If one assumes a sharp threshold for supersymmetric particles at 1000 GeV the evolution of the coupling constants shown in figure 54 is obtained. It is calculated for three generations and two Higgs boson as required by the minimal supersymmetric model. Apparently the three couplings do match now at an energy beyond 10^{15} GeV. See reference [184, 189, 185] for detailed discussions.

Of course, figure 54 cannot be interpreted as a proof for the existence of Supersymmetry nor its energy scale. The assumption that all new particles have the same mass is too crude and the matching of three straight lines in one point is too weak as an argument. But the convergence of the coupling constants achieved by the introduction of new particles into the theory provides a strong indication that there is new physics between 100 and 10^{15} GeV and that the "Great Desert" does not exist.

10 Future tests of the Standard Model

The results on electroweak parameters obtained so far at LEP are much more precise than expected before the startup of LEP [191]. Further significant improvements are expected in the next years from running at the Z resonance.

The knowledge of the decay width of the Z into invisible particles $\Gamma_{\rm inv}$, or equivalently the number of neutrino families, is now limited by the theoretical precision of the cross section calculations for small angle Bhabha scattering (see section 6.1). Improved calculations are expected to be available soon and this will enhance the precision of this measurement already with the currently available data.

In 1994 LEP has delivered an integrated luminosity of 60 pb^{-1} to each of the four experiments at the Z pole. These data are only partially included as preliminary numbers in the results presented in this article [19]. Further enhancement of the specific luminosity is expected in 1995 from increasing the number of circulating bunches in the LEP ring (Bunch Train scheme [78, 79]). The expected large increase in the data samples will enable the experiments to further reduce the errors on electroweak observables, in particular improvements on forward-backward asymmetries

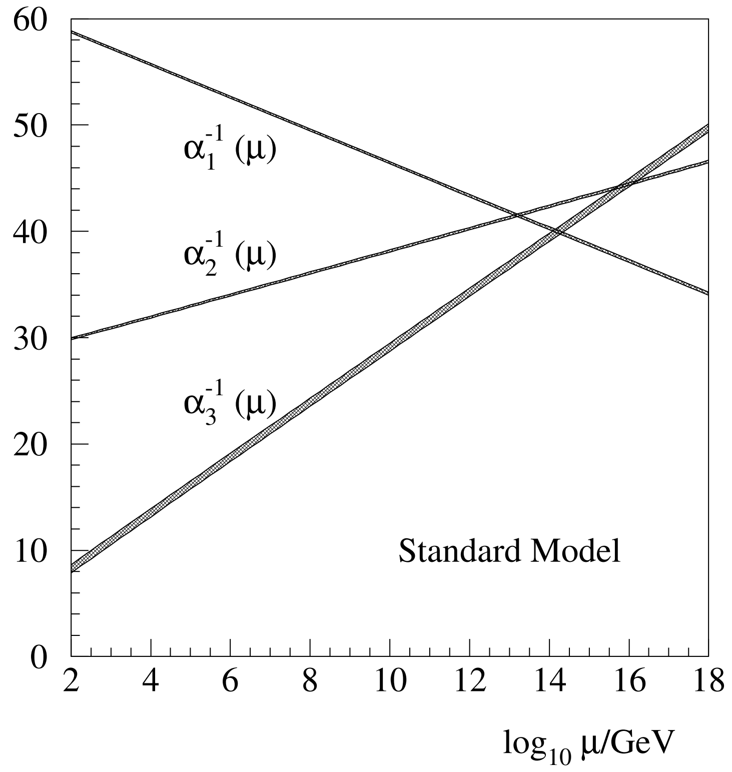

Figure 53: Running of coupling constants in the Standard Model.

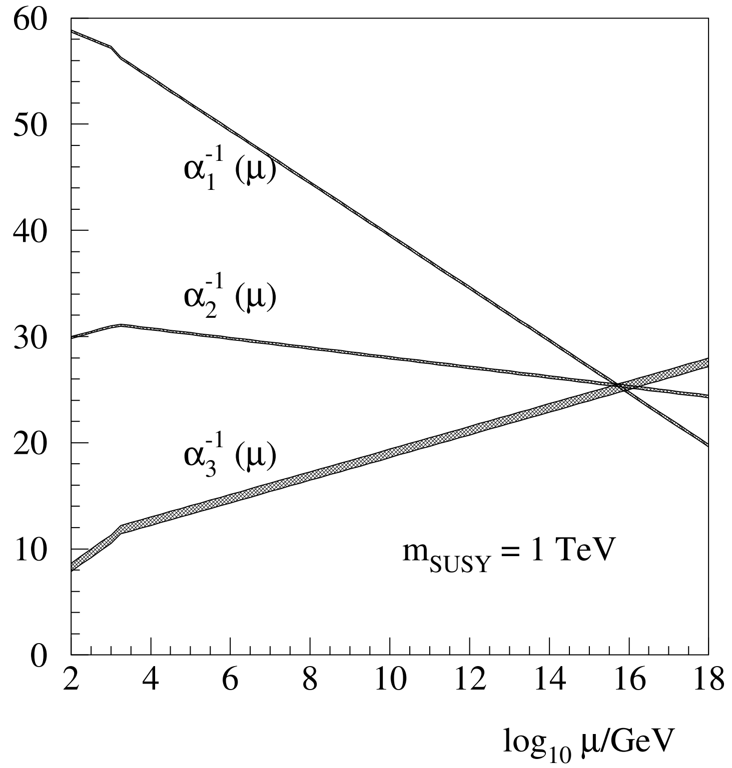

Figure 54: Running of coupling constants with Supersymmetry at 1 TeV.

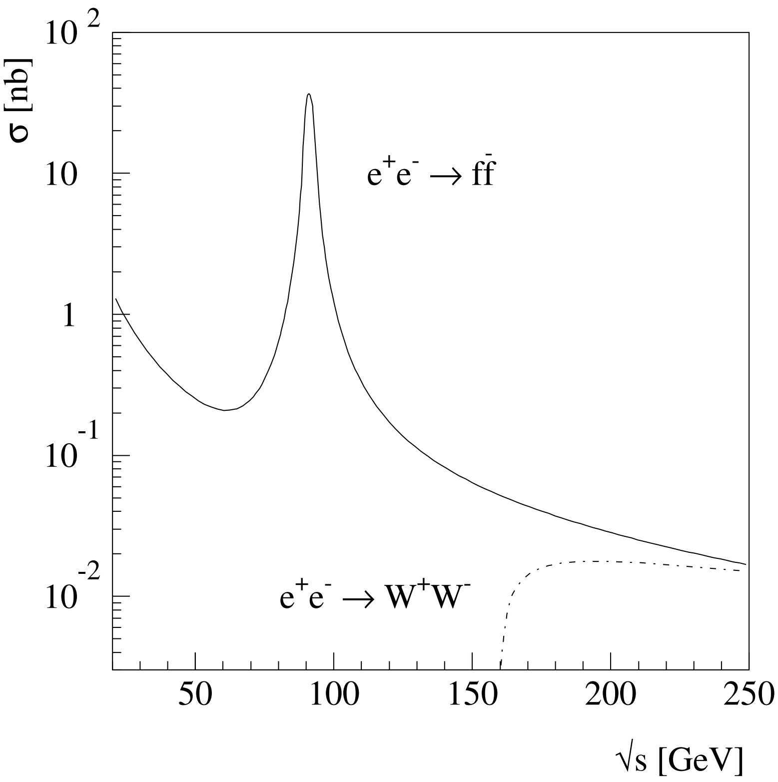

Figure 55: Lowest order cross section for $e^+e^- \to f\bar{f}$ and $W^\pm$ pair production as a function of the center-of-mass energy.

and tau polarization are expected. It is foreseen to perform another scan of the Z resonance with high luminosity at $\sqrt{s} \neq m_Z$ in 1995. This will lead to a significant improvement of the measurements of the mass and widths of the Z.

The measurement of the left-right asymmetry will be continued at the SLC. The aim is to collect one million Z decays which will allow a measurement of the effective weak mixing angle with a precision of $\Delta \sin^2\bar{\vartheta}_W = \pm 0.0002$ [192]. Together with the LEP results this will allow for better constraints on m_t and m_H from precision measurements of electroweak radiative corrections.

Other important experimental information will come from the experiments at the Tevatron. It is very important to measure the mass of the top quark as precisely as possible. This direct mass measurement can then be confronted with the top quark mass derived from the measurement of weak radiative corrections in order to constrain the mass of the Higgs boson and to verify if there is room for radiative corrections which do not originate from known particles and hence require new physics.

In 1996 after installation of superconducting radio frequency cavities the center-of-mass energy can be increased such that LEP will cross the threshold for $W^\pm$ pair production (LEP II). The goal is to deliver 500 pb^{-1} which amounts to about 10 000 W^+W^- pairs per experiment [193]. Figure 55 compares, in lowest order, the cross sections $e^+e^- \to f\bar{f}$ and $e^+e^- \to W^+W^-$ as function of the center-of-mass

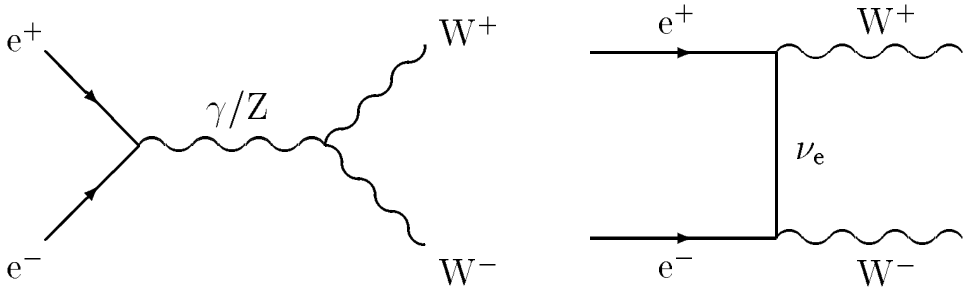

Figure 56: Lowest order Feynman diagrams for $e^+e^- \to W^+W^-$.

energy [194].

The mass of the $W^\pm$ will be determined to better than 50 MeV [195, 196] thus adding another precision measurement of an electroweak parameter. Comparing this precise direct measurement of m_W with the value derived from the electroweak observables at the Z will provide another consistency check of the Standard Model.

The process $e^+e^- \to W^+W^-$ proceeds in lowest order through three Feynman diagrams (figure 56). Each of these diagrams by itself violates unitarity, i.e. the cross section grows with energy. Only the interplay of the t-channel neutrino and the s-channel γ and Z exchange together with the right coupling strength at the γWW and ZWW vertices assure the decrease of the cross section and hence the renormalizibility of the Standard Model. See for instance reference [197] for a detailed discussion. At LEP II the $W^\pm$ couplings will be measured with a few percent accuracy from the measurement of the differential cross section. This should provide the first observation of the triple boson couplings γWW and ZWW and hence test the non-Abelian nature of the Standard Model.

The search for new particles will of course also profit from the increase of the center-of-mass energy. At LEP the limits for new particles are by now mostly determined by the available energy and not anymore by statistics. The most important remaining test of Standard Model is the existence of the Higgs boson. The range of Standard Model Higgs boson masses accessible for LEP II depends on the maximum center-of-mass energy [195]

$$m_H \leq \sqrt{s} - 100 \text{ GeV}. \tag{118}$$

This underlines the importance to aim for an energy as high as possible at LEP II in addition to a high luminosity. If the Higgs boson will not be discovered at LEP the final answer on its existence will be given at the Large Hadron Collider (LHC) [198] which is expected to cover the entire mass range up to $m_H = 1$ TeV [199].

11 Summary and Conclusions

The very successful operation of the LEP collider and the four experiments since 1989 has provided a wealth of experimental information on elementary particle physics. For reviews on LEP results see for instance [200, 201]. All phenomena studied by the experiments are well described by the Standard Model of electroweak interactions and, concerning strong interactions between quarks and gluons, by Quantum

Chromodynamics. In this article the aspects of the LEP results relevant for neutral current electroweak interactions are discussed.

The four LEP experiments have collected approximately 14 million hadronic and leptonic Z decays between 1989 and 1994. From the measurement of the total cross sections at energies close to m_{Z} and with the precise calibration of the LEP beam energy the mass of the Z, one of the fundamental input parameters of electroweak theory, is determined with very high precision:

$$m_{\mathrm{Z}} = 91\,188.4 \pm 2.2 \text{ MeV}. \tag{119}$$

Other Z parameters like the total and partial decay widths into hadrons and leptons are derived from the cross sections with a precision of $\mathcal{O}(10^{-3})$:

$$\begin{aligned} \Gamma_{\mathrm{Z}} &= 2496.3 \pm 3.2 \text{ MeV} \\ \Gamma_{\mathrm{had}} &= 1744.8 \pm 3.0 \text{ MeV} \\ \Gamma_{\ell} &= 83.93 \pm \ 0.14 \text{ MeV}. \end{aligned} \tag{120}$$

From these results the number of light neutrino families in the universe, which is not predicted by the Standard Model, is determined to be three. The exact result

$$N_\nu = 2.990 \pm 0.015\,^{+0.008}_{-0.005}\,(m_{\mathrm{t}}, m_{\mathrm{H}}, \alpha(m_{\mathrm{Z}})) \tag{121}$$

is compatible with an integer value and does not leave much room for the Z decaying into unknown particles.

From the total cross sections and the asymmetries the couplings of charged leptons and heavy quarks to the Z are derived. The coupling constants of electrons, muons and taus are found to be equal, supporting the Standard Model prediction of lepton universality. The combined values, from LEP and SLC experiments, for the effective coupling constants of leptons are:

$$\begin{aligned} \bar{g}_{\mathrm{A}}^{\ell} &= -0.5011 \pm 0.0004 \\ \bar{g}_{\mathrm{V}}^{\ell} &= -0.0380 \pm 0.0007\,. \end{aligned} \tag{122}$$

The observed deviation of the axial-vector coupling from the lowest order value $-1/2$ underlines the existence of weak radiative corrections and thus the need for a heavy top quark.

The coupling constants obtained for b- and c-quarks support the hypothesis of down- and up-type quarks. However, the current experimental results for the partial decay widths Γ_{b} and Γ_{c} are not in perfect agreement with the Standard Model. The observed discrepancy of about three standard deviations deserves special attention.

The effective weak mixing angle $\sin^2\bar{\vartheta}_{\mathrm{W}}$ is determined from the measurements of various asymmetries, forward-backward asymmetry of leptons and heavy quarks, tau polarization and the left-right asymmetry measured at SLC. All asymmetries measured at LEP in different reactions yield very consistent results. The apparent disagreement of the LEP and SLC result on $\sin^2\bar{\vartheta}_{\mathrm{W}}$, though, remains to be resolved. The mean value obtained at LEP and SLC

$$\sin^2\bar{\vartheta}_{\mathrm{W}} = 0.2314 \pm 0.0003 \tag{123}$$

severely constrains the allowed values for the top quark mass in the Standard Model.

Using all experimental information from LEP and SLC the mass of the top quark is derived in the Standard Model framework from the measurement of radiative corrections:

$$m_{\mathrm{t}} = 181\,^{+8}_{-9}\,^{+17}_{-20}(m_{\mathrm{H}})\ \mathrm{GeV} \tag{124}$$

This number is in excellent agreement with the mass measurements from top quark production at the Tevatron which yield a value of $m_{\mathrm{t}} = 180 \pm 12$ GeV. The observation of the top quark at the expected mass is a great success of the Standard Model as the precision measurements at the Z are predicting the mass of a particle through the measurement of higher order processes.

The results obtained at the Z pole can also be expressed in terms of the $\mathrm{W}^{\pm}$ mass:

$$m_{\mathrm{W}} = 80.36 \pm 0.06 \pm 0.02\ \mathrm{GeV} \tag{125}$$

Also this value is in excellent agreement with the direct measurement of the $\mathrm{W}^{\pm}$ mass at $\mathrm{p\bar{p}}$ colliders: $m_{\mathrm{W}} = 80.23 \pm 0.18$ GeV.

On the Higgs sector the LEP experiments have ruled out the entire mass range

$$0 \leq m_{\mathrm{H}} \leq 63.5\ \mathrm{GeV} \qquad (95\%\mathrm{C.L.}) \tag{126}$$

Using the mass of the top quark from its direct measurement the precision data of LEP and SLC will eventually allow to further constrain the Higgs boson mass in the Standard Model.

Further improvements in the measurements of electroweak parameters at the Z resonance are expected from the LEP and SLC experiments in the near future. The precise measurement of the $\mathrm{W}^{\pm}$ mass and the test of the three boson couplings at LEP II will provide additional important tests of the Standard Model. And the last missing particle of the Standard Model, the Higgs boson, will be searched for at LEP II up to a mass of approximately 90 GeV.

Despite its great success in describing all precision experiments at the Z pole and below it is likely that the Standard Model is not adequate for the physics at the 1 TeV scale and thus will have to be replaced by a new model when at the beginning of the next millenium this energy scale will become experimentally accessible.

12 Acknowledgements

I wish to express my gratitude to Albrecht Böhm for his continuous support and encouragement over one decade of collaboration. He interested me in the field of high energy physics and without his help this article would not have been written.

I acknowledge the efforts of all engineers and physicists who built, maintain and operate the LEP accelerator and the detectors. Without them the wealth of physics results would obviously not have been achieved. I would like to thank all my colleagues from L3 and the other LEP experiments for their marvellous work which I have described here. In particular, this article profited enormously from the work of the LEP Electroweak Working Group.

I would like to thank Samuel C.C. Ting for his leadership and the support of my work. I am indebted to all members of the L3 Lineshape Group for many stimulating discussions and all the things I learned from them.

I am grateful to John Field, Carlos Maña, Martin Pohl and Stephan Wynhoff for their careful reading of the manuscript and their fruitful comments, as well as to Jörg Wenninger who explained to me the details of the LEP energy calibration.

Since 1988 I am working as a visitor at the European Organization for Nuclear Research (CERN). I thank CERN for its hospitality and the German Bundesministerium für Bildung, Wissenschaft, Forschung und Technologie for supporting my stay.

Appendix

A Parametrisation of results from total cross sections and forward-backward asymmetries

For the purpose of comparing and averaging the results the four LEP experiments provide a set of nine parameters obtained from a fit to the measured total cross sections and leptonic forward-backward asymmetries [77]. Besides the mass and the total width of the Z these parameters are the lowest order hadronic peak cross section σ^0_{had}, the three ratios of the leptonic and hadronic Z width R_ℓ and the three lowest order peak forward-backward asymmetries $A^{0,\ell}_{\mathrm{FB}}$. They are defined by the partial widths and the effective vector and axial-vector couplings of the charged leptons:

$$\begin{aligned}
\sigma^0_{\mathrm{had}} &= \frac{12\,\pi}{m_{\mathrm{Z}}^2}\,\frac{\Gamma_{\mathrm{e}}\Gamma_{\mathrm{had}}}{\Gamma_{\mathrm{Z}}^2} \\
R_\ell &= \frac{\Gamma_{\mathrm{had}}}{\Gamma_\ell} \\
A^{0,\ell}_{\mathrm{FB}} &= 3\,\frac{\bar{g}^{\mathrm{e}}_{\mathrm{V}}\,\bar{g}^{\mathrm{e}}_{\mathrm{A}}}{(\bar{g}^{\mathrm{e}}_{\mathrm{V}})^2+(\bar{g}^{\mathrm{e}}_{\mathrm{A}})^2}\,\frac{\bar{g}^{\ell}_{\mathrm{V}}\,\bar{g}^{\ell}_{\mathrm{A}}}{(\bar{g}^{\ell}_{\mathrm{V}})^2+(\bar{g}^{\ell}_{\mathrm{A}})^2} = \frac{3}{4}\,A_{\mathrm{e}}A_\ell \qquad (\ell = \mathrm{e},\mu,\tau)
\end{aligned} \tag{127}$$

With the assumption of lepton universality the leptonic results are cast into a common ratio of hadronic to leptonic width R_ℓ and a common peak asymmetry $A^{0,\ell}_{\mathrm{FB}}$. Hence the number of parameters reduces to five.

The combined result of the four LEP experiment taking into account the remaining correlations and common errors for the nine and five parameter fit is shown in table 14. The symmetric correlation matrices for the two cases are shown in table 15 and 16. These numbers are taken from reference [19].

The advantage of this parameterization is that corrections like acceptances and QED effects which depend on the experimental setup and differ among the LEP detectors are taken into account. The fit results thus can be compared directly among the experiments. In addition, in this particular set the parameters are only weakly correlated among each other and thus well suited for averaging. The uncertainties common to all four LEP experiments (Δm_{Z}, $\Delta\Gamma_{\mathrm{Z}}$ and the theoretical part of the luminosity error) can be easily incorporated in the fit for the average LEP results. In particular, the hadronic pole cross section σ^0_{had} is the only parameter sensitive to the luminosity measurement.

On the other hand mapping all measured cross sections on only nine (or five) parameters results in loss of experimental information. For instance, as $A^{0,\ell}_{\mathrm{FB}}$ is symmetric in $\bar{g}_{\mathrm{V}}$ and $\bar{g}_{\mathrm{A}}$ there is an ambiguity in this quantities. This ambiguity is resolved by the energy dependence of forward-backward asymmetries measured at $\sqrt{s} \neq m_{\mathrm{Z}}$.

Table 17 shows the LEP averages for the hadronic and leptonic Z widths with and without imposing lepton universality. They are obtained from conversion of the parameter sets discussed above. From the correlation matrices (tables 18 and 19) the large correlation coefficients relating the measurements of the total and the partial widths can be seen.

	nine parameter non-universality	five parameter universality
m_{Z} [MeV]	$9\,188.5 \pm 2.2$	$91\,188.4 \pm 2.2$
Γ_{Z} [MeV]	$2\,496.3 \pm 3.2$	$2\,496.3 \pm 3.2$
σ^0_{had} [nb]	41.488 ± 0.078	41.488 ± 0.078
R_{e}	20.797 ± 0.058	
R_{μ}	20.796 ± 0.043	
R_{τ}	20.813 ± 0.061	
R_{ℓ}		20.788 ± 0.032
$A^{0,\mathrm{e}}_{\mathrm{FB}}$	0.0157 ± 0.0028	
$A^{0,\mu}_{\mathrm{FB}}$	0.0163 ± 0.0016	
$A^{0,\tau}_{\mathrm{FB}}$	0.0206 ± 0.0023	
$A^{0,\ell}_{\mathrm{FB}}$		0.0172 ± 0.0012

Table 14: The combined LEP result of the nine and five parameter fits to total cross sections and leptonic forward-backward asymmetries.

	m_{Z}	Γ_{Z}	σ^0_{had}	R_{e}	R_{μ}	R_{τ}	$A^{0,\mathrm{e}}_{\mathrm{FB}}$	$A^{0,\mu}_{\mathrm{FB}}$	$A^{0,\tau}_{\mathrm{FB}}$
m_{Z}	1.00	−0.08	0.02	0.03	−0.02	−0.01	0.02	0.07	0.04
Γ_{Z}		1.00	−0.12	−0.01	0.00	0.00	0.00	0.00	0.00
σ^0_{had}			1.00	0.08	0.12	0.08	0.01	0.00	0.00
R_{e}				1.00	0.08	0.03	−0.06	0.01	0.01
R_{μ}					1.00	0.06	0.00	0.01	0.00
R_{τ}						1.00	0.00	0.00	0.01
$A^{0,\mathrm{e}}_{\mathrm{FB}}$							1.00	−0.04	−0.02
$A^{0,\mu}_{\mathrm{FB}}$								1.00	0.07
$A^{0,\tau}_{\mathrm{FB}}$									1.00

Table 15: The correlation matrix of the combined nine parameter fit.

	m_{Z}	Γ_{Z}	σ^0_{had}	R_{ℓ}	$A^{0,\ell}_{\mathrm{FB}}$
m_{Z}	1.00	−0.08	0.02	0.00	0.08
Γ_{Z}		1.00	−0.12	−0.01	0.00
σ^0_{had}			1.00	0.15	0.01
R_{ℓ}				1.00	0.00
$A^{0,\ell}_{\mathrm{FB}}$					1.00

Table 16: The correlation matrix of the combined five parameter fit.

	nine parameter non-universality	five parameter universality
m_{Z} [MeV]	$91\,188.5 \pm 2.2$	$91\,188.4 \pm 2.2$
Γ_{Z} [MeV]	$2\,496.3 \pm 3.2$	$2\,496.3 \pm 3.2$
Γ_{had} [MeV]	$1\,745.3 \pm 3.6$	$1\,744.8 \pm 3.0$
Γ_{e} [MeV]	83.92 ± 0.17	
Γ_{μ} [MeV]	83.92 ± 0.23	
Γ_{τ} [MeV]	83.85 ± 0.29	
Γ_{ℓ} [MeV]		83.93 ± 0.14
$A_{\mathrm{FB}}^{0,\mathrm{e}}$	0.0157 ± 0.0028	
$A_{\mathrm{FB}}^{0,\mu}$	0.0163 ± 0.0016	
$A_{\mathrm{FB}}^{0,\tau}$	0.0206 ± 0.0023	
$A_{\mathrm{FB}}^{0,\ell}$		0.0172 ± 0.0012

Table 17: The LEP average for partial decay width of the Z as derived from a parameter transformation of table 14.

	m_{Z}	Γ_{Z}	Γ_{had}	Γ_{e}	Γ_{μ}	Γ_{τ}	$A_{\mathrm{FB}}^{0,\mathrm{e}}$	$A_{\mathrm{FB}}^{0,\mu}$	$A_{\mathrm{FB}}^{0,\tau}$
m_{Z}	1.00	−0.08	−0.01	−0.05	0.01	0.00	0.02	0.07	0.04
Γ_{Z}		1.00	0.54	0.58	0.40	0.32	0.00	0.00	0.00
Γ_{had}			1.00	0.05	0.66	0.54	−0.03	0.01	0.01
Γ_{e}				1.00	0.04	0.02	0.05	−0.01	−0.01
Γ_{μ}					1.00	0.39	−0.02	0.00	0.01
Γ_{τ}						1.00	−0.02	0.01	0.00
$A_{\mathrm{FB}}^{0,\mathrm{e}}$							1.00	−0.04	−0.02
$A_{\mathrm{FB}}^{0,\mu}$								1.00	0.07
$A_{\mathrm{FB}}^{0,\tau}$									1.00

Table 18: The correlation matrix for the partial widths (non-universality).

	m_{Z}	Γ_{Z}	Γ_{had}	Γ_{ℓ}	$A_{\mathrm{FB}}^{0,\ell}$
m_{Z}	1.00	−0.08	−0.03	−0.04	0.07
Γ_{Z}		1.00	0.65	0.71	0.00
Γ_{had}			1.00	0.56	0.00
Γ_{ℓ}				1.00	0.00
$A_{\mathrm{FB}}^{0,\ell}$					1.00

Table 19: The correlation matrix for the partial widths (lepton universality).

B Forward-backward asymmetries measured at e^+e^- collider experiments

The results on total cross sections and forward backward asymmetries in the reactions $e^+e^- \to \mu^+\mu^-$ and $e^+e^- \to \tau^+\tau^-$ obtained at e^+e^- colliders up to center-of-mass energy $\approx$ 60 GeV are listed in table 20 and table 21, respectively. The quantities $R_{\mu\mu}$ and $R_{\tau\tau}$ are defined as the ratio of the measured total cross section $\sigma_{\mu\mu}$ ($\sigma_{\tau\tau}$), corrected for higher order QED effects, and the lowest order QED expectation σ^0_{QED}:

$$R_{\mu\mu,\tau\tau} = \frac{\sigma_{\mu\mu,\tau\tau}}{\sigma^0_{\mathrm{QED}}} \tag{128}$$

$$\sigma^0_{\mathrm{QED}} = \frac{4\,\pi\alpha^2}{3\,s} = \frac{86.85}{s}\,\mathrm{nb\,GeV^2} \tag{129}$$

The forward-backward asymmetries quoted by the experiments are corrected for QED effects, too. They can be directly compared to the lowest order expression given in eq. 21.

In order to compare the low energy data to the LEP results the $\mu^+\mu^-$ and $\tau^+\tau^-$ asymmetries measured by one experiment (L3) are listed in tables 22 and 23. Here A_{FB} is the asymmetry obtained from a fit to the angular distribution of the events observed in the fiducial volume $|\cos\Theta| < 0.8$ using the function

$$\frac{\mathrm{d}\sigma}{\mathrm{d}\cos\theta} \propto 1 + \cos^2\theta + \frac{8}{3}A_{\mathrm{FB}}\cos\theta \tag{130}$$

derived from the lowest order differential cross section. The events used to determine the asymmetry are selected requiring an acolinearity angle $\xi \leq 15°$. Even in the presence of radiative corrections eq. 130 provides a very good approximation of the expected differential cross section in the polar angle range used. However, A_{FB} obtained this way contains QED radiative corrections as well as information on the weak corrections. It has to be compared to the full Standard Model calculation simulating the kinematical cuts and using a value for the top and Higgs mass:

$$A^{\mathrm{SM}}_{\mathrm{FB}}(\xi; m_{\mathrm{t}}, m_{\mathrm{H}}) = A^{\mathrm{SM}}_{\mathrm{FB}}(\xi; m_{\mathrm{t}}, m_{\mathrm{H}})\Big|_{|\cos\Theta|<0.8} \cdot \frac{1}{0.879}\,. \tag{131}$$

The factor 1/0.879 contains the extrapolation form $|\cos\Theta| < 0.8$ to the full angular acceptance according to eq. 130.

Also shown in table 22 and table 23 are the lowest order expectations from eq. 21, $A^{\mathrm{Born}}_{\mathrm{FB}}$, using as input values the mass of Z, $\sin^2\vartheta_{\mathrm{W}}$ as obtained from the ratio of the vector boson masses (see table 3) and the lowest order numbers for the coupling constants g_{A} and g_{V} (table 4).

The last column shows the experimental result, A'_{FB}, shifted by the difference of the full Standard Model calculation and the lowest order form. These asymmetries are hence corrected in the same way as it is done by the PEP, PETRA and TRISTAN experiments and thus allowing a direct comparison (see figures 29 and 30).

$e^+e^- \to \mu^+\mu^-$				
Experiment	$\sqrt{s}$ [GeV]	$N_{\mu\mu}$	$R_{\mu\mu}$	A_{FB} [%]
MARK I [202]	6.8	11 000		-0.4 ± 1.4
PEP				
HRS [203]	29.0	5 057	$0.990 \pm 0.017 \pm 0.030$	$-4.9 \pm 1.5 \pm 0.5$
MAC [204]	29.0	16 058	$1.01 \pm 0.01 \pm 0.03$	$-5.9 \pm 0.8 \pm 0.2$
MARK II [205]	29.0	5 312	$1.002 \pm 0.013 \pm 0.016$	-7.1 ± 1.7
PETRA				
CELLO [206, 207]	34.2	387	$0.91 \pm 0.05 \pm 0.05$	-6.4 ± 6.4
	43.0	1 039	$0.98 \pm 0.04 \pm 0.04$	$-14.1 \pm 3.7 \pm 1.0$
JADE [208, 209, 210]	13.9	458	$1.00 \pm 0.05 \pm 0.05$	$+2.7 \pm 4.9$
	22.0	264	$1.02 \pm 0.06 \pm 0.05$	-10.6 ± 6.4
	34.4	3 400	$0.99 \pm 0.02 \pm 0.05$	$-11.1 \pm 1.8 \pm 1.0$
	35.0	4 772	$0.984 \pm 0.019 \pm 0.020$	$-9.9 \pm 1.5 \pm 0.5$
	38.0	422		$-9.7 \pm 5.0 \pm 1.0$
	43.7	1 258	$0.98 \pm 0.04 \pm 0.05$	$-19.1 \pm 2.8 \pm 1.0$
MARK J [211, 212]	14.0	472	$1.04 \pm 0.05 \pm 0.03$	$+5.3 \pm 5.0 \pm 0.5$
	22.5	357	$1.02 \pm 0.05 \pm 0.03$	$-4.3 \pm 6.1 \pm 0.5$
	34.8	6 854	$0.99 \pm 0.01 \pm 0.03$	$-10.4 \pm 1.3 \pm 0.5$
	36.4	65	$1.08 \pm 0.13 \pm 0.03$	$-13.6 \pm 13.5 \pm 0.5$
	38.3	403	$1.07 \pm 0.05 \pm 0.03$	$-12.3 \pm 5.3 \pm 0.5$
	40.4	87	$0.93 \pm 0.10 \pm 0.03$	$+5.0 \pm 10.5 \pm 0.5$
	42.0	116	$1.04 \pm 0.09 \pm 0.03$	$-15.9 \pm 9.3 \pm 0.5$
	43.8	1 123	$0.99 \pm 0.03 \pm 0.03$	$-15.6 \pm 3.0 \pm 0.5$
	46.1	155	$0.96 \pm 0.08 \pm 0.03$	$-17.6 \pm 8.3 \pm 0.5$
PLUTO [213]	34.7	1 553	$0.94 \pm 0.03 \pm 0.04$	$-13.4 \pm 3.1 \pm 1.0$
TASSO [214, 215, 216]	13.9	341	1.05 ± 0.08	-1 ± 6
	22.3	268	1.06 ± 0.09	-13 ± 7
	34.5	2 673	$1.002 \pm 0.020 \pm 0.035$	$-9.1 \pm 2.3 \pm 0.5$
	35.0	2 563	$0.932 \pm 0.018 \pm 0.044$	$-10.6 \pm 2.2 \pm 0.5$
	38.3	173	$0.951 \pm 0.072 \pm 0.060$	$+1.7 \pm 8.5 \pm 0.5$
	43.6	612	$0.921 \pm 0.037 \pm 0.055$	$-17.6 \pm 4.3 \pm 0.5$
TRISTAN				
AMY [217, 218]	55.2	299	1.03 ± 0.07	$-32.7 \pm 7.4 \pm 5.0$
	57.8	1 899	$1.059 \pm 0.025 \pm 0.037$	$-30.3 \pm 2.7 \pm 0.8$
TOPAZ [219, 220]	57.9	880	$0.98 \pm 0.04 \pm 0.05$	$-32.2 \pm 3.1 \pm 1.1$
VENUS [221, 222]	56.9	447	$1.05 \pm 0.05 \pm 0.03$	$-29.0\,^{+5.0}_{-4.8} \pm 0.5$
	58.0	3 012	$0.98 \pm 0.02 \pm 0.03$	-34 ± 2

Table 20: Compilation of muon pair cross sections and forward-backward asymmetries measured in e^+e^- annihilation experiments below the Z resonance.

$e^+e^- \to \tau^+\tau^-$				
Experiment	$\sqrt{s}$ [GeV]	$N_{\tau\tau}$	$R_{\tau\tau}$	A_{FB} [%]
PEP				
HRS [223, 224]	29.0		$1.044 \pm 0.014 \pm 0.030$	$-4.4 \pm 1.4 \pm 0.5$
MAC [225]	29.0	10 153	$0.98 \pm 0.01 \pm 0.034$	$-5.5 \pm 1.2 \pm 0.5$
MARK II [205]	29.0	3 714	$0.996 \pm 0.016 \pm 0.028$	-4.2 ± 2.0
PETRA				
CELLO [226, 227]	14.0	234	$1.09 \pm 0.07 \pm 0.06$	$+10.0 \pm 7.0$
	22.0	186	$1.02 \pm 0.08 \pm 0.04$	$+1.1 \pm 7.8$
	34.2	434	$1.03 \pm 0.05 \pm 0.07$	-10.3 ± 5.2
	35.0	3 032	$0.98 \pm 0.02 \pm 0.02$	$-7.0 \pm 1.9 \pm 0.9$
	38.1	260	$0.99 \pm 0.06 \pm 0.04$	$-11.8 \pm 6.2 \pm 2.7$
	43.8	824	$0.99 \pm 0.03 \pm 0.04$	$-16.3 \pm 3.5 \pm 1.3$
JADE [208, 209, 210]	13.9		$1.29 \pm 0.24 \pm 0.04$	
	22.0		$1.16 \pm 0.16 \pm 0.04$	
	34.6	1 998		$-6.7 \pm 2.5 \pm 1.0$
	35.0	3 238	$1.012 \pm 0.021 \pm 0.023$	$-8.1 \pm 2.0 \pm 0.6$
	38.0	336		$+6.8 \pm 6.3 \pm 1.0$
	43.7	913		$-17.7 \pm 3.6 \pm 1.0$
MARK J [211, 228]	14.0	79	$1.13 \pm 0.14 \pm 0.07$	
	22.4	92	$1.02 \pm 0.12 \pm 0.06$	
	34.7	1 401	$1.00 \pm 0.03 \pm 0.05$	$-10.6 \pm 3.1 \pm 1.0$
	38.3	90	$1.00 \pm 0.11 \pm 0.05$	$+3.2 \pm 12.1 \pm 1.0$
	43.8	287	$0.97 \pm 0.06 \pm 0.05$	$-8.5 \pm 6.6 \pm 1.0$
PLUTO [229]	34.6	419	$0.89 \pm 0.05 \pm 0.08$	$-5.9 \pm 6.8 \ ^{+0.0}_{-2.5}$
TASSO [214, 230]	13.9	63	$1.05 \pm 0.14 \ ^{+0.06}_{-0.11}$	
	22.3	46	$1.01 \pm 0.15 \ ^{+0.06}_{-0.11}$	
	34.5	608	$1.03 \pm 0.05 \ ^{+0.06}_{-0.11}$	$-4.9 \pm 5.3 \ ^{+1.3}_{-1.2}$
	35.0	476	$1.036 \pm 0.050 \pm 0.068$	$-9.2 \pm 5.2 \pm 1.0$
	44.0	117	$1.011 \pm 0.097 \pm 0.079$	$-6.6 \pm 9.5 \pm 1.0$
TRISTAN				
AMY [217, 218]	55.2	216	1.25 ± 0.12	$-36.3 \pm 9.6 \pm 5.0$
	57.8	1 149	$1.087 \pm 0.033 \pm 0.027$	$-29.1 \pm 4.0 \pm 1.9$
TOPAZ [219, 220]	57.9	572	$1.04 \pm 0.04 \pm 0.05$	$-33.9 \pm 4.9 \pm 1.0$
VENUS [221, 222]	56.9	283	$1.03 \pm 0.06 \pm 0.04$	$-32.8 \ ^{+6.4}_{-6.2} \pm 0.5$
	58.0	1 971	$0.99 \pm 0.02 \pm 0.03$	-29 ± 2

Table 21: Same as table 20 for $e^+e^- \to \tau^+\tau^-$.

$e^+e^- \to \mu^+\mu^-$						
	$\sqrt{s}$ [GeV]	$N_{\mu\mu}$	$A_{\rm FB}$	$A_{\rm FB}^{\rm SM}$	$A_{\rm FB}^{\rm Born}$	$A'_{\rm FB}$
L3 1993	91.319	5 181	$0.000 \pm 0.015 \pm 0.001$	0.010	0.039	0.029
	89.452	2 704	$-0.180 \pm 0.021 \pm 0.001$	−0.163	−0.133	−0.150
	91.206	8 953	$-0.002 \pm 0.011 \pm 0.001$	0.001	0.029	0.025
	93.036	3 623	$0.115 \pm 0.018 \pm 0.001$	0.115	0.186	0.186

Table 22: Forward-backward asymmetry in $e^+e^- \to \mu^+\mu^-$ as measured by the L3 experiment in 1993 (preliminary result), $A_{\rm FB}$, together with the Standard Model expectation, $A_{\rm FB}^{\rm SM}$, using the input parameters given in eq. 42, the lowest order calculation, $A_{\rm FB}^{\rm Born}$, and the experimental value corrected for the difference of the latter two, $A'_{\rm FB}$.

$e^+e^- \to \tau^+\tau^-$						
	$\sqrt{s}$ [GeV]	$N_{\tau\tau}$	$A_{\rm FB}$	$A_{\rm FB}^{\rm SM}$	$A_{\rm FB}^{\rm Born}$	$A'_{\rm FB}$
L3 1993	91.319	3 889	$0.025 \pm 0.021 \pm 0.004$	0.010	0.039	0.054
	89.452	1 936	$-0.121 \pm 0.027 \pm 0.004$	−0.163	−0.133	−0.091
	91.206	6 436	$0.030 \pm 0.016 \pm 0.004$	0.001	0.029	0.058
	93.036	2 669	$0.119 \pm 0.023 \pm 0.004$	0.115	0.186	0.190

Table 23: Same as table 22 for $e^+e^- \to \tau^+\tau^-$.

C Results on b- and c-quarks

Table 24 is a compilation of b- and c-quark asymmetries at e^+e^- colliders below the Z resonance. The b-quark asymmetries are not corrected for $B_0 - \bar{B}_0$ mixing.

Table 25 list the result of a combined fit to b- and c-quark results obtained by the four LEP experiments. The numbers are taken from reference [231, 19] where the fitting procedure is described in detail.

		$e^+e^- \to b\bar{b}$	$e^+e^- \to c\bar{c}$
Experiment	$\sqrt{s}$ [GeV]	A_{FB}	A_{FB}
HRS [232]	29	-0.14 ± 0.12	-0.099 ± 0.027
MAC [233]	29	$+0.034 \pm 0.070 \pm 0.035$	
TPC [234]	29	-0.20 ± 0.16	-0.17 ± 0.08
CELLO [173]	35	-0.222 ± 0.081	-0.129 ± 0.088
	43	-0.491 ± 0.165	$+0.077 \pm 0.140$
JADE [174]	35	$-0.114 \pm 0.053 \pm 0.033$	$-0.118 \pm 0.041 \pm 0.038$
	44	$-0.228 \pm 0.151 \pm 0.035$	$-0.100 \pm 0.119 \pm 0.042$
MARK J [235]	35.3	-0.21 ± 0.19	-0.16 ± 0.09
TASSO [236]	35	-0.21 ± 0.08	-0.160 ± 0.043
AMY [237]	55.2	$-0.72 \pm 0.28 \pm 0.13$	
TOPAZ [238]	58.3	$-0.71 \pm 0.34\,^{+0.07}_{-0.08}$	

Table 24: Compilation of b- and c-quark forward-backward asymmetries measured in e^+e^- annihilation experiments below the Z resonance. The b-quark asymmetries are not corrected for $B_0 - \bar{B}_0$ mixing.

R_b	0.2217 ± 0.0017
R_c	0.1540 ± 0.0074
$BR(b \to \ell)$	0.1111 ± 0.0023
$BR(b \to c \to \ell^+)$	0.0777 ± 0.0037
$\bar{\chi}_b$	0.1149 ± 0.0062
A_{FB}^b (89.55 GeV)	0.055 ± 0.014
A_{FB}^c (89.55 GeV)	-0.079 ± 0.028
A_{FB}^b (91.26 GeV)	0.0945 ± 0.0031
A_{FB}^c (91.26 GeV)	0.0684 ± 0.0060
A_{FB}^b (92.94 GeV)	0.113 ± 0.012
A_{FB}^c (92.94 GeV)	0.089 ± 0.024

Table 25: The results of a combined fit to b- and c-quark measurements of the four LEP experiments [231].

List of Figures

List of Tables

References

[1] S.L. Glashow, Nucl. Phys. **A 22** (1961) 579;
S. Weinberg, Phys. Rev. Lett. **19** (1967) 1264;
A. Salam, "Elementary Particle Theory", Ed. N. Svartholm, Stockholm, "Almquist and Wiksell" (1968), 367.

[2] N. Cabbibo, Phys. Rev. Lett. **10** (1963) 531.

[3] S.L. Glashow, J. Iliopoulos and L. Maiani, Phys. Rev. **D 2** (1970) 1285.

[4] J.J. Aubert et al., Phys. Rev. Lett. **33** (1974) 1404;
J.E. Augustin et al., Phys. Rev. Lett. **33** (1974) 1406;
C. Bacci et al., Phys. Rev. Lett. **33** (1974) 1408.

[5] F.J. Hasert et al., Phys. Lett. **B 46** (1973) 121;
J. Blietschau et al., Nucl. Phys. **B 114** (1976) 189;
H. Faissner et al., Phys. Rev. Lett. **41** (1978) 213.

[6] UA1 collaboration, G. Arnison et al., Phys. Lett. **B 122** (1983) 103;
UA2 collaboration, M. Banner et al., Phys. Lett. **B 122** (1983) 476;
UA1 collaboration, G. Arnison et al., Phys. Lett. **B 126** (1983) 398;
UA2 collaboration, P. Bagnaia et al., Phys. Lett. **B 129** (1983) 130;
UA1 collaboration, G. Arnison et al., Phys. Lett. **B 129** (1983) 273.

[7] C.Y. Prescott et al., Phys. Lett. **B 77** (1978) 347;
C.Y. Prescott et al., Phys. Lett. **B 84** (1979) 524.

[8] J.G. Branson, Procs. of the International Symposium on Lepton Photon Interactions at High Energies, Bonn (1981), ed. W. Pfeil;
A. Böhm, Procs. of the International Europhysics Conference on High Energy Physics, Brighton (1983), eds. J. Guy and C. Costain;
G. Herten, Procs. of the International Europhysics Conference on High Energy Physics, Brighton (1983), eds. J. Guy and C. Costain.

[9] F.A. Berends and A. Böhm in "High Energy Electron-Positron Physics", eds. A. Ali and P. Söding, World Scientific, Singapore (1988).

[10] SLAC Linear Collider Conceptual Design Report, Preprint SLAC-PUB-229, SLAC, 1980.

[11] L. Camilleri et al., "Physics with Very High Energy e^+e^- Colliding Beams", Preprint CERN/76-18, CERN, 1976.

[12] CDF collaboration, F. Abe et al., Phys. Rev. Lett. **73** (1994) 225;
CDF collaboration, F. Abe et al., Phys. Rev. **D 50** (1994) 2966.

[13] CDF collaboration, F. Abe et al., Phys. Rev. Lett. **74** (1995) 2626;
D0 collaboration, S. Abachi et al., Phys. Rev. Lett. **74** (1995) 2632.

[14] P.W. Higgs, Phys. Lett. **12** (1964) 132;
P.W. Higgs, Phys. Rev. Lett. **13** (1964) 508;
P.W. Higgs, Phys. Rev. **145** (1966) 1156;
F. Englert, R. Brout, Phys. Rev. Lett. **13** (1964) 321.

[15] M. Gell-Mann, Acta Phys. Austriaca, Suppl. **IX** (1972) 733;
H. Fritzsch and M. Gell-Mann, 16^{th} International Conference on High Energy Physics, Batavia, 1972; eds. J.D. Jackson and A. RRoberts, National Accelerator Laboratory (1972);
H. Fritzsch, M. Gell-Mann and H. Leutwyler, Phys. Lett. **B 47** (1973) 365;
D.J. Gross and F. Wilczek, Phys. Rev. Lett. **30** (1973) 1343;
D.J. Gross and F. Wilczek, Phys. Rev. **D 8** (1973) 3633;
H.D. Politzer, Phys. Rev. Lett. **30** (1973) 1346;
G. 't Hooft, Nucl. Phys. **B 33** (1971) 173.

[16] H. Georgi, S.L. Glashow, Phys. Rev. Lett. **32** (1974) 438;
A.J. Buras et al., Nucl. Phys. **B 135** (1978) 66.

[17] P. Fayet, Phys. Lett. **B 64** (1976) 159;
P. Fayet, Phys. Lett. **B 69** (1977) 489;
P. Fayet and S. Ferrara, Phys. Rep. **32 C** (1977) 249;
H.P. Nilles, Phys. Rep. **110** (1984) 1;
H. Haber and G. Kane, Phys. Rep. **117** (1985) 75.

[18] S. Weinberg, Phys. Rev. **D 13** (1976) 974;
S. Weinberg, Phys. Rev. **D 19** (1979) 1277;
L. Susskind, Phys. Rev. **D 20** (1979) 2619;
E. Fahri and L. Susskind, Phys. Rep. **74** (1981) 277.

[19] The LEP Electroweak Working Group, "A Combination of Preliminary LEP Electroweak Results for the 1995 Summer Conferences", ALEPH 95-093, DELPHI 95-137, L3 1814 and OPAL TN312, CERN PPE preprint in preparation.

[20] Particle Data Group, "Review of Particle Properties", Phys. Rev. **D 50** (1994) 1173.

[21] B.C. Barish and R. Stroynowski, Phys. Rep. **157** (1988) 1.

[22] D0 collaboration, S. Abachi et al., Phys. Rev. Lett. **72** (1994) 2138.

[23] L.M. Krauss, Procs. of the XXVI International Conference on High Energy Physics, Dallas (1992), ed. J.R. Sanford.

[24] M. Kobayashi and M. Maskawa, Prog. Theor. Phys. **49** (1963) 652.

[25] R.G.H. Robertson, Procs. of the XXVI International Conference on High Energy Physics, Dallas (1992), ed. J.R. Sanford.

[26] G. Altarelli, "Neutrino Masses: A Theoretical Introduction", International Symposium on Neutrino Telescopes, Venice, February 1994, Preprint CERN-TH/7315-94, CERN, 1994.

[27] M. Veltman, Acta Phys. Polon. **B 8** (1977) 475;
B.W. Lee, C. Quigg, H.B. Thacker, Phys. Rev. **D 16** (1977) 1519.

[28] G. Altarelli, "The Standard Electroweak Theory and its Experimental Tests", Preprint CERN-TH/6867-93, CERN, 1993.

[29] P. Giacomelli, "The Search for the Standard Model Higgs Boson: Results at LEP 100 and Prospects for LEP 200", Preprint CERN-PPE/93-18;
J. Schwindling, Procs. of the International Europhysics Conference on High Energy Physics, Marseille (1993), eds. J. Carr and M. Perrottet;
A. Sopczak, Nucl. Phys. B, Proc. Suppl. **37 C** (1995) 168.

[30] C.K. Jung, Procs. of the XXVII International Conference on on High Energy Physics, Glasgow (1994), eds. P.J. Bussey and I.G. Knowles.

[31] R. Kleiss, "Electroweak Interaction", Lectures given at CERN, 1990 (unpublished).

[32] N. Phiney, Int. J. Mod. Phys. A, Proc. Suppl. **2 A**, 45 (1993);
T. Maruyama et al., Phys. Rev. **B 46** (1992) 4261;
J. Frisch et al., SLAC-PUB-6165, April 1993.

[33] D.A. Ross and J.C. Taylor, Nucl. Phys. **B 51** (1973) 125.

[34] E.R. Cohen and B.N. Taylor, Rev. Mod. Phys. **59** (1987) 1121;
E.R. Cohen and B.N. Taylor, Inst. Stand. Technol. **95** (1990) 497.

[35] R.E. Behrends, R.J. Finkelstein, A. Sirlin, Phys. Rev. **101** (1956) 866.

[36] A. Sirlin, Phys. Rev. **D 22** (1980) 971;
A. Sirlin, Phys. Rev. **D 29** (1984) 89;
W.J. Marciano and A. Sirlin, Phys. Rev. **D 29** (1984) 945.

[37] G. Burgers and F. Jegerlehner in "Z Physics at LEP I", eds. G. Altarelli, R. Kleiss and C. Verzegnassi, CERN Report CERN 89-08 (1989), Vol. 1, p. 55.

[38] W. Hollik, Fortschr. Phys. **38** (1990) 165.

[39] F. Jegerlehner, in "Testing the Standard Model - Proceedings of the 1990 Theoretical Advanced Study Institue in Elementary Particle Physics", Boulder, Colorado, June 1990, ed. M. Cvetic and P. Langacker, World Scientific, Singapore, (1991), p. 476.

[40] M. Veltman, Nucl. Phys. **B 123** (1977) 89;
M.S. Chanowitz et al., Phys. Lett. **B 78** (1978) 1;
M. Consoli, S. Lo Presti, L. Maiani, Nucl. Phys. **B 223** (1983) 474;
J. Fleischer, F. Jegerlehner, Nucl. Phys. **B 228** (1983) 1.

[41] M. Consoli and W. Hollik in "Z Physics at LEP I", eds. G. Altarelli, R. Kleiss and C. Verzegnassi, CERN Report CERN 89-08 (1989), Vol. 1, p. 7.

[42] R. Barbieri and L. Maiani, Nucl. Phys. **B 224** (1983) 32;
L. Alvarez-Gaumé, J. Polchinski and M.B. Wise, Nucl. Phys. **B 221** (1983) 495.

[43] F. Jegerlehner, Prog. Part. and Nucl. Physics, **27**, 1991, 1.

[44] S. Eidelman and F. Jegerlehner, "Hadronic contributions to $(g-2)$ of the leptons and to the effective fine structure constant $\alpha(m_Z)$", Preprint PSI-PR-95-01, Paul Scherrer Institut, 1995.

[45] H. Burkhardt, Talk given at the XXX Rencontres de Moriond, 1995, to appear in the proceedings.

[46] M.L. Swartz, "Reevaluation of the Hadronic Contribution to $\alpha(m_Z^2)$", Preprint SLAC-PUB-6710, SLAC, 1994, submitted to Phys. Rev.

[47] A.D. Martin and D. Zeppenfeld, "A determination of the QED coupling at the Z pole", Preprint MAD/PH/855, University of Wisconsin, Madison, 1994.

[48] F. Berends in "Z Physics at LEP I", eds. G. Altarelli, R. Kleiss and C. Verzegnassi, CERN Report CERN 89-08 (1989), Vol. 1, p. 89.

[49] D. Bardin et al.., "Reports of the Working Group on Precision Calculations for the Z Resonance", CERN Report CERN 95-03 (1995);
see also G. Passarino, Procs. of the XXVII International Conference on on High Energy Physics, Glasgow (1994), eds. P.J. Bussey and I.G. Knowles.

[50] S. Bethke, "Hadron Physics in Electron-Positron Annihilation", Preprint HD-PY 93/7, Universität Heidelberg, 1993.

[51] T. Hebbeker, Phys. Rep. **217** (1992) 69.

[52] G. Marchesini and B. Webber, Nucl. Phys. **B 310** (1988) 461;
G. Marchesini et al., Comp. Phys. Comm. **67** (1992) 465.

[53] T. Sjöstrand, Comp. Phys. Comm. **39** (1986) 347;
T. Sjöstrand and M. Bengtsson, Comp. Phys. Comm. **43** (1987) 367;
T. Sjöstrand, "PHYTHIA 5.6 JETSET 7.3 Physics and Manual", Preprint CERN-TH 6488/92, CERN (1992).

[54] S. Jadach, B.F.L. Ward and Z. Wąs, Comp. Phys. Comm. **66** (1991) 276.

[55] W. Beenaker, F.B. Berends and S.C. van der Marck, Nucl. Phys. **B 349** (1991) 323.

[56] J.H. Field, Phys. Lett. **B 323** (1994) 432.

[57] H. Anlauf et al., Comput. Phys. Commun. **79** (1994) 466.

[58] G. Montagna et al., Nucl. Phys. **B 401** (1993) 3;
G. Montagna et al., Comp. Phys. Comm. **76** (1993) 328.

[59] R. Brun et al.,"GEANT 3", CERN DD/EE/84-1 (Revised), September 1987.

[60] H.Fesefeldt, RWTH Aachen, Preprint PITHA 85/02 (1985).

[61] S. Jadach et al., Phys. Rev. **D 40** (1989) 3582;
S. Jadach et al., Phys. Lett. **B 268** (1991) 253;
S. Jadach et al., Comp. Phys. Comm. **70** (1992) 305.

[62] M. Böhm, A. Denner and W. Hollik, Nucl. Phys. **B 304** (1988) 687;
F.A. Berends, R. Kleiss and W. Hollik, Nucl. Phys. **B 304** (1988) 712.

[63] S. Jadach et al., Phys. Lett. **B 353** (1995) 349;
S. Jadach et al., Phys. Lett. **B 353** (1995) 362.

[64] D. Bardin et al., FORTRAN package ZFITTER, Preprint CERN-TH 6443/92;
D. Bardin et al., Z. Phys. **C 44** (1989) 493;
D. Bardin et al., Nucl. Phys. **B 351** (1991) 1;
D. Bardin et al., Phys. Lett. **B 255** (1991) 290.

[65] M. Martinez et al., Z. Phys. **C 49** (1991) 645;
S. Jadach et al., Phys. Lett. **B 280** (1992) 129.

[66] F. James, CERN Program Library Long Writeup D506 MINUIT, CERN, 1993.

[67] M. Bourquin et al., European Comittee for Future Accelerators, General meeting on LEP, Villars-sur-Ollon, ECFA 81-54, 1981.

[68] ALEPH Collab., D. Decamp et al., Nucl. Inst. Meth. **A 294** (1990) 121.

[69] DELPHI Collab., P. Aarnio et al., Nucl. Inst. Meth. **A 303** (1991) 233.

[70] L3 Collab., B. Adeva et al., Nucl. Inst. Meth. **A 289** (1990) 35.

[71] OPAL Collab, K. Ahmet et al., Nucl. Inst. Meth. **A 305** (1991) 275.

[72] High-Luminosity Options for LEP, ed. J.M. Jowett, CERN 91-02, CERN, 1991.

[73] Proceedings of the 3rd Workshop on LEP performance, ed. J. Poole, CERN-SL/93-19, CERN, 1993.

[74] LEP Collaborations: ALEPH, DELPHI, L3 and OPAL, Phys. Lett. **B 276** (1992) 247.

[75] The Working Group on LEP Energy and the LEP Collaborations: ALEPH, DELPHI, L3 and OPAL, Phys. Lett. **B 307** (1993) 187.

[76] L. Rolandi, Procs. of the XXVI International Conference on High Energy Physics, Dallas (1992), ed. J.R. Sanford.

[77] The LEP collaborations: ALEPH, DELPHI, L3, OPAL and the LEP Electroweak Working Group, "Updated Parameters of the Z Resonance from Combined Preliminary Data of the LEP Experiments", Preprint CERN-PPE/93-157, CERN, 1993.

[78] E. Keil, CERN-SL/92-55(AP);
E. Keil, Proceedings of the third workshop on LEP performance, CERN-SL/93-16 (1993) 459;
W. Herr, Proceedings of the fourth workshop on LEP performance, CERN-SL/94-06 (1994) 323.

[79] T. Camporesi et al., "Report from the Bunch Train Working Group", CERN-LEPC/94-13 (1994).

[80] LEP Polarization Collaboration,L. Arnaudon et al., Phys. Lett. **B 284** (1992) 431.

[81] Working Group on LEP Energy, L. Arnaudon et al., "The Energy Calibration of LEP in 1991", Preprint CERN-PPE/92-125, CERN, 1992.

[82] Working Group on LEP Energy, L. Arnaudon et al., “The Energy Calibration of LEP in 1992“, Preprint CERN-SL/93-21, CERN, 1993.

[83] M. Sokolov and I.M. Ternov, Sov. Phys. Dokl. **8** (1964), 1203.

[84] V. Bargmann, L. Michel and V.L. Telegdi, Phys. Rev. Lett. **10** (1959) 435.

[85] M. Placidi and R. Rossmanith, Nucl. Inst. Meth. **A 274** (1989) 79.

[86] R. Assmann et al., “Polarization Studies at LEP in 1993“, Preprint CERN-SL/94-08, CERN, 1994.

[87] L. Arnaudon et al., Z. Phys. **C 66** (1995) 45.

[88] Working Group on LEP Energy, R. Assmann et al., Z. Phys. **C 66** (1995) 567.

[89] ALEPH Collab., D. Decamp et al., Z. Phys. **C 53** (1992) 1.

[90] ALEPH Collab., D. Buskulic et al., Z. Phys. **C 60** (1993) 71.

[91] ALEPH Collab., D. Buskulic et al., Z. Phys. **C 62** (1994) 539.

[92] DELPHI Collab., P. Abreu et al., Nucl. Phys. **B 367** (1991) 511.

[93] DELPHI Collab., P. Abreu et al., Nucl. Phys. **B 417** (1994) 3.

[94] DELPHI Collab., P. Abreu et al., Nucl. Phys. **B 418** (1994) 403.

[95] L3 Collab., B. Adeva et al., Z. Phys. **C 51** (1991) 179.

[96] L3 Collab., O. Adriani et al., Physics Reports **236** (1993) 1.

[97] L3 Collab., M.Acciarri et al., Z. Phys. **C 62** (1994) 551.

[98] OPAL Collab, G. Alexander et al., Z. Phys. **C 52** (1991) 175.

[99] OPAL Collab, P.D. Acton et al., Z. Phys. **C 58** (1993) 219.

[100] OPAL Collab, R. Akers et al., Z. Phys. **C 61** (1994) 19.

[101] D. Bédérède et al., ”SICAL - a high precision silicon-tungsten luminosity calorimeter for ALEPH”, Preprint CERN-PPE/95-017, CERN, 1995, submitted to Nucl. Inst. Meth.

[102] The LEP Electroweak Working Group, ”Combined Preliminary Data on Z Paramters from the LEP Experiments and Constraints on the Standard Model”, Preprint CERN-PPE/94-187, CERN, 1994.

[103] D. Schaile, Fortschr. Phys. **42** (1994) 429.

[104] D.Y. Bardin et al., Phys. Lett. **B 206** (1988) 539.

[105] S. Willenbrock and G. Valencia, Phys. Lett. **B 259** (1991) 373;
R.G. Stuart, Phys. Lett. **B 262** (1991) 113;
A. Sirlin, Phys. Rev. Lett. **67** (1991) 2127.

[106] L3 Collab., O. Adriani et al., Phys. Lett. **B 315** (1993) 494.

[107] G. Isidori, Phys. Lett. **B 314** (1993) 139.

[108] M. Grünewald and S. Kirsch, "A possible modification of a LEP energy scan for an improved determination of Z-boson parameters", Preprint CERN-PPE/93-188, CERN, 1993.

[109] TOPAZ collaboration, K. Miyabayashi et al., Phys. Lett. **B 347** (1995) 171.

[110] L3 collaboration, Paper contributed to the 1995 International Conference on High Energy Physics, Brussels, Belgium, and the 17$^{\mathrm{th}}$ International Symposium on Lepton-Photon Interactions, Beijing, China, July 1995.

[111] M. Martinez and B. Pietrzyk, Phys. Lett. **B 324** (1994) 492.

[112] L. Trentadue in "Z Physics at LEP I", eds. G. Altarelli, R. Kleiss and C. Verzegnassi, CERN Report CERN 89-08 (1989), Vol. 1, p. 129.

[113] S. Jadach, Procs. of the XXIX Rencontres de Moriond, Méribel les Allues, France (1994), ed. J. Trân Thanh Vân;
L. Trentadue, Procs. of the XXIX Rencontres de Moriond, Méribel les Allues, France (1994), ed. J. Trân Thanh Vân.

[114] ALEPH Collab., D. Decamp et al., Phys. Lett. **B 231** (1989) 519.

[115] DELPHI Collab., P. Aarnio et al., Phys. Lett. **B 231** (1989) 539.

[116] L3 Collab., B. Adeva et al., Phys. Lett. **B 231** (1989) 509.

[117] OPAL Collab, M.Z. Akrawy et al., Phys. Lett. **B 231** (1989) 530.

[118] MARK II Collab., G.S. Abrams et al., Phys. Rev. Lett. **63** (1989) 2173.

[119] G. Raven, "Measurement of the Reaction $e^+e^- \to \nu\bar{\nu}\gamma$ at LEP", Talk given at the Lake Louise Winter Institute, February 1995, to appear in the proceedings, Preprint NIKHEF-H/95-010, NIKHEF, 1995.

[120] ALEPH Collab., D. Buskulic et al., Phys. Lett. **B 313** (1993) 520.

[121] OPAL Collab., R. Akers et al., Z. Phys. **C 65** (1995) 47.

[122] C. Luci private communication.

[123] T. Hebbeker et al., Phys. Lett. **B 331** (1994) 165.

[124] S. Banerjee, "α_s Measurements from Event Shape Data using Z Data", Procs. of the International Europhysics Conference on High Energy Physics, Marseille (1993), eds. J. Carr and M. Perrottet.

[125] D. Haidt, in "Precision Tests of the Standard Model", ed. P. Langacker, World Scientific (1993);
S. Catani, Procs. of the International Europhysics Conference on High Energy Physics, Marseille (1993), eds. J. Carr and M. Perrottet;
S. Bethke, Procs. of the XXVI International Conference on High Energy Physics, Dallas (1992), ed. J.R. Sanford.

[126] A. De Angelis, Nucl. Phys. B, Proc. Suppl. **37 C** (1995) 106.

[127] S. de Jong, "Heavy Quark Electroweak Results from Z Decay", 8èmes Rencontres de Physique de la Vallée d'Aoste, La Thuile, Italy, 1994, ed. M. Greco.

[128] T. Behnke and D.G. Charlton, "Electroweak Measurements using Heavy Quarks at LEP", Preprint CERN-PPE/95-11, CERN, 1995, submitted to Physica Scripta.

[129] ALEPH Collab., D. Buskulic et al., Phys. Lett. **B 313** (1993) 549.

[130] ALEPH Collab., D. Buskulic et al., Phys. Lett. **B 313** (1993) 535.

[131] DELPHI Collab., P. Abreu et al., "Measurement of the $\Gamma_{b\bar{b}}/\Gamma_{had}$ branching ratio of the Z by double hemisphere tagging", Preprint CERN-PPE/94-131, CERN, 1994, submitted to Z. Phys.

[132] DELPHI Collab., P. Abreu et al., Z. Phys. **C 66** (1995) 323.

[133] L3 Collab., O. Adriani et al., Phys. Lett. **B 307** (1993) 237.

[134] OPAL Collab., P. D. Acton et al., Z. Phys. **C 60** (1993) 579.

[135] OPAL Collab, R. Akers et al., Z. Phys. **C 60** (1993) 199.

[136] OPAL Collab., R. Akers et al., Z. Phys. **C 65** (1994) 47.

[137] SLD collaboration, "A Measurement of R_b Using Lifetime Double Tag", paper contributed to the EPS conference, Brussels, Belgium, July 1995.

[138] M.A. Bouchiat et al., Phys. Lett. **B 117** (1982) 358;
M.C. Noecker et al., Phys. Rev. Lett. **61** (1988) 310;
M.A. Bouchiat and L. Pottier, Science **234** (1986), 1203.

[139] G. D'Agostini, W. de Boer and G. Grindhammer, Phys. Lett. **B 229** (1989) 160.

[140] ALEPH Collab., D. Decamp et al., Phys. Lett. **B 259** (1991) 377.

[141] DELPHI Collab., P. Abreu et al., Phys. Lett. **B 277** (1992) 371.

[142] OPAL Collab, P.D. Acton et al., Phys. Lett. **B 294** (1992) 436.

[143] ALEPH Collab., D. Buskulic et al., Z. Phys. **C 62** (1994) 179.

[144] DELPHI Collab., P. Abreu et al., Phys. Lett. **B 276** (1992) 536.

[145] L3 Collab., M.Acciarri et al., Phys. Lett. **B 335** (1994) 542.

[146] OPAL Collab, R. Akers et al., Z. Phys. **C 60** (1993) 601.

[147] DELPHI Collab., P. Abreu et al., Z. Phys. **C 66** (1994) 341.

[148] ALEPH Collab., D. Buskulic et al., Phys. Lett. **B 335** (1994) 99.

[149] A. Djouadi, B. Lampe and P.M. Zerwas, "A Note on the QCD Corrections to Forward-Backward Asymmetries of Heavy-Quark Jets in Z Decays", Preprint DESY 94-201, DESY, 1994.

[150] S. Jadach and Z. Wąs in "Z Physics at LEP I", eds. G. Altarelli, R. Kleiss and C. Verzegnassi, CERN Report CERN 89-08 (1989), Vol. 1, p. 235.

[151] Y.S. Tsai, Phys. Rev. **D 4** (1971) 2821.

[152] R. Alemany et al., Nucl. Phys. **B 379** (1992) 3.

[153] K. Hagiwara, A.D. Martin and D. Zeppenfeld, Phys. Lett. **B 235** (1990) 198.

[154] A. Rougé, Z. Phys. **C 48** (1990) 75.

[155] ALEPH Collab., D. Buskulic et al., Z. Phys. **C 59** (1993) 369.

[156] ALEPH Collab., D. Buskulic et al., "Improved Tau Polarisation Measurement", Preprint CERN-PPE/95-23, CERN, 1994, submitted to Z. Phys.

[157] DELPHI Collab., P. Abreu et al., Z. Phys. **C 55** (1992) 555.

[158] DELPHI Collab., P. Abreu et al., Z. Phys. **C 67** (1995) 183.

[159] L3 Collab., O. Adriani et al., Phys. Lett. **B 294** (1992) 466.

[160] L3 Collab., M. Acciarri et al., Phys. Lett. **B 341** (1994) 245.

[161] OPAL Collab, G. Alexander et al., Phys. Lett. **B 266** (1991) 201.

[162] OPAL Collab., R. Akers et al., Z. Phys. **C 65** (1995) 1.

[163] A. Blondel in "Precision Tests of the Standard Model", ed. P. Langacker, World Scientific (1993).

[164] SLD Collab., K. Abe et al., "The SLD Design Report", Preprint SLAC report No. 273, SLAC, 1984.

[165] SLD Collab., K. Abe et al., Phys. Rev. Lett. **73** (1994) 25.

[166] C. Baltay, Talk given at the XV International Conference on Physics in Collisions, Krakow, Poland, June 1995, to appear in the proceedings.

[167] SLD Collab., K. Abe et al., Phys. Rev. Lett. **74** (1995) 2895.

[168] SLD Collab., K. Abe et al., Phys. Rev. Lett. **74** (1995) 2890.

[169] L3 Collab., O. Adriani et al., Phys. Lett. **B 309** (1993) 451.

[170] DESY-Journal 81-3, December 1981.

[171] J. Panman and S.L. Wu, Procs. of the International Symposium on Lepton Photon Interactions at High Energies, Hamburg (1987), eds. W. Bartel and R. Rückl.

[172] CHARM II collaboration, P. Vilain et al., Phys. Lett. **B 335** (1994) 246.

[173] CELLO collaboration, H.J. Behrend et al., Z. Phys. **C 47** (1990) 333.

[174] JADE collaboration, E. Elsen et al., Z. Phys. **C 46** (1990) 349.

[175] CCFR collaboration, C.G. Arroyo et al., Phys. Rev. Lett. **72** (1994) 3452.

[176] CDHS collaboration, H. Abramowicz et al., Phys. Rev. Lett. **57** (1986) 298; CDHS collaboration, A. Blondel et al., Z. Phys. **C 45** (1990) 361.

[177] CHARM collaboration, J.V. Allaby et al., Phys. Lett. **B 177** (1986) 446; CHARM collaboration, J.V. Allaby et al., Z. Phys. **C 36** (1987) 611;.

[178] P. Langacker and J. Erler in [20].

[179] G. Montagna et al., Phys. Lett. **335** (1994) 484.

[180] M.E. Peskin and T. Takeuchi, Phys. Rev. Lett. **65** (1990) 964.

[181] G. Altarelli, R. Barbieri and S. Jadach, Nucl. Phys. **B 369** (1992) 3 and Nucl. Phys. **B 376** (1992) 444;
G. Altarelli, R. Barbieri and F. Caravaglios, Nucl. Phys. **B 405** (1993) 3.

[182] G. Altarelli, Procs. of the International Europhysics Conference on High Energy Physics, Marseille (1993), eds. J. Carr and M. Perrottet;
G. Altarelli, "Status of Precision Tests of the Electroweak Theory", CERN-TH/7319-94 (1994).

[183] W. de Boer, Prog. Part. Nucl. Phys. **33** (1994) 201.

[184] U. Amaldi, W. de Boer and H. Fürstenau, Phys. Lett. **B 260** (1991) 447.

[185] J.L. Lopez, D.V. Nanopoulos and A. Zichichi, Prog. Part. Nucl. Phys. **33** (1994) 303.

[186] M.B. Einhorn and D.R.T. Jones, Nucl. Phys. **B 196** (1982) 475.

[187] W.A. Bardeen et al., Phys. Rev. **D 18** (1978) 3998.

[188] G. Degrassi, S. Fanchiotti and A. Sirlin, Nucl. Phys. **B 351** (1991) 49.

[189] P. Langacker and N. Polonsky, Phys. Rev. **D 47** (1993) 4028.

[190] U. Amaldi et al., Phys. Rev. **D 36** (1987) 1385.

[191] G. Altarelli in "Physics at LEP", eds. J. Ellis and R. Peccei, CERN Report CERN 86-02 (1986), Vol. 1, p. 1.

[192] M. Woods, "Measurement of $A_{\rm LR}$ in $e^+e^- \to Z$ by the SLD Collaboration", Procs. of the XXIX Rencontres de Moriond, Méribel les Allues, France (1994), ed. J. Trân Thanh Vân.

[193] Proceedings of the ECFA Workshop on LEP 200, eds. A. Böhm and W. Hoogland, CERN 87-02 (1987).

[194] W. Alles, Ch. Boyer and A.J. Buras, Nucl. Phys. **B 119** (1977) 125.

[195] D. Treille in “Precision Tests of the Standard Model“, ed. P. Langacker, World Scientific (1993).

[196] L. Camilleri, “The Measurement of m_W at LEP 200“, Presentation at the LEPC meeting, November 1992.

[197] W. Beenaker and A. Denner, “Standard Model Predictions for W-Pair Production in Electron-Positron Collisions“, Preprint DESY 94-051, DESY, 1994.

[198] “Design Study of the Large Hadron Collider (LHC)“, The LHC Study Group, CERN 91-03 (1991).

[199] D. Treille, Report on Progress in Physics **57** (1994) 1137.

[200] S.C.C. Ting, “New Results from LEP Experiments“, Preprint CERN-PPE/93-34, CERN, 1993.

[201] J.E. Augustin, “LEP Physics”, Preprint CERN-PPE/93-83, CERN, 1993.

[202] MARK I collaboration, T. Himel et al., Phys. Rev. Lett. **41** (1978) 449.

[203] HRS collaboration, M. Derrick et al., Phys. Rev. **D 31** (1985) 2352.

[204] MAC collaboration, W.W. Ash et al., Phys. Rev. Lett. **55** (1985) 1831.

[205] MARK II collaboration, M.E. Levi et al., Phys. Rev. Lett. **51** (1983) 1941.

[206] CELLO collaboration, H.J. Behrend et al., Z. Phys. **C 14** (1982) 283.

[207] CELLO collaboration, H.J. Behrend et al., Phys. Lett. **B 191** (1987) 209.

[208] JADE collaboration, W. Bartel et al., Z. Phys. **C 26** (1985) 507.

[209] JADE collaboration, W. Bartel et al., Z. Phys. **C 30** (1986) 371.

[210] JADE collaboration, S. Hegner et al., Z. Phys. **C 46** (1990) 547.

[211] MARK J collaboration, B. Adeva et al., Phys. Rev. **D 38** (1988) 2665.

[212] J. Mnich, PITHA 87/19, RWTH Aachen (1987).

[213] PLUTO collaboration, Ch. Berger et al., Z. Phys. **C 21** (1983) 53.

[214] TASSO collaboration, R. Brandelik et al., Phys. Lett. **B 110** (1982) 173.

[215] TASSO collaboration, M. Althoff et al., Z. Phys. **C 22** (1984) 13.

[216] TASSO collaboration, W. Braunschweig et al., Z. Phys. **C 40** (1988) 163.

[217] AMY collaboration, A. Bacala et al., Phys. Lett. **B 218** (1989) 112.

[218] AMY collaboration, C. Velissaris et al., Phys. Lett. **B 331** (1994) 227.

[219] TOPAZ collaboration, I. Adachi et al., Phys. Lett. **B 208** (1988) 318.

[220] TOPAZ collaboration, B. Howell et al., Phys. Lett. **B 291** (1992) 206.

[221] VENUS collaboration, K. Abe et al., Z. Phys. **C 48** (1990) 13.

[222] M. Miura, "Study of $\mu^+\mu^-$ and $\tau^+\tau^-$ Production in VENUS", Presentation at the 2nd Workshop on TRISTAN Physics at High Luminosities, KEK, November 1993.

[223] S. Abachi et al., ANL-HEP-CP-86-55, paper contributed to the 23rd International Conference on High Energy Physics, Berkeley (1986).

[224] HRS collaboration, S. Abachi et al., Phys. Rev. **D 40** (1989) 902.

[225] MAC collaboration, E. Fernandez et al., Phys. Rev. Lett. **54** (1985) 1620.

[226] CELLO collaboration, H.J. Behrend et al., Phys. Lett. **B 114** (1982) 282.

[227] CELLO collaboration, H.J. Behrend et al., Phys. Lett. **B 222** (1989) 163.

[228] E. Deffur, Ph.D. thesis, RWTH Aachen (1988).

[229] PLUTO collaboration, Ch. Berger et al., Z. Phys. **C 28** (1985) 1.

[230] TASSO collaboration, W. Braunschweig et al., Z. Phys. **C 43** (1989) 549.

[231] The LEP Electroweak Heavy Flavours Working Group and the SLD Heavy Flavour Group, "Combined LEP and SLD Electroweak Heavy Flavour Results for Summer 1995 Conferences", Internal Note: ALEPH 95-091, DELPHI 95-115, L3 1813, OPAL TN313 and SLD PN39.

[232] HRS collaboration, C.R. Ng et al., ANL-HEP-PR-88-11;
HRS collaboration, P. Baringer et al., Phys. Lett. **B 206** (1988) 551.

[233] MAC collaboration, H.R. Band et al., Phys. Lett. **B 218** (1989) 369.

[234] TPC collaboration, H. Aihara et al., Phys. Rev. **D 31** (1985) 2719;
TPC collaboration, H. Aihara et al., Z. Phys. **C 27** (1985) 39;
TPC collaboration, H. Aihara et al., Phys. Rev. **D 34** (1986) 1945.

[235] MARK J collaboration, B. Adeva et al., Phys. Rep. **109** (1984) 131.

[236] TASSO collaboration, W. Braunschweig et al., Z. Phys. **C 48** (1990) 433.

[237] AMY collaboration, H. Sagawa et al., Phys. Rev. Lett. **63** (1989) 2341.

[238] TOPAZ collaboration, A. Shimonaka et al., Phys. Lett. **B 268** (1991) 457.